Arkadiusz Bubak

Liquid Argon Time Projection Chambers in the studies of rare events (phenomena) in particle physics and astrophysics

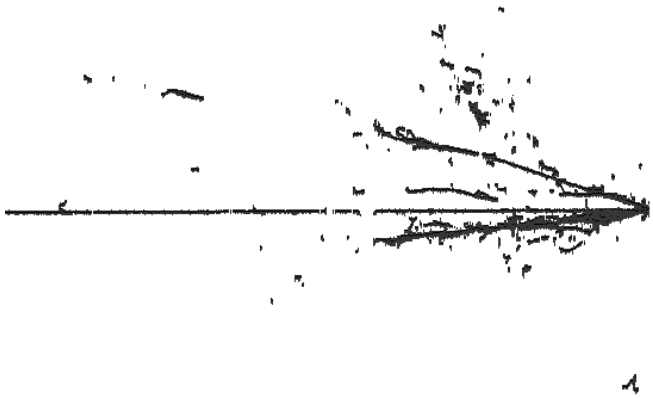

Chorzów 2018

Liquid Argon Time Projection Chambers in the studies of rare events (phenomena) in particle physics and astrophysics

Arkadiusz Bubak

Chorzów 2018

Referee: prof. dr. hab. Henryk Czyż

Polish title: Ciekłoargonowe komory projekcji czasu wykorzystywane w badaniach rzadkich przypadków (zjawisk) w fizyce cząstek i astrofizyce

Printed by: Drukarnia Advert
Krakowska 21
41-503 Chorzów Poland
http://www.advertdruk.pl
Phone: +48 32 244 58 97

ISBN 978-83-64804-82-3

First edition, Chorzów 2018

Cover design by the author (ICARUS: ν_μCC from CNGS. Run 11838, event 9697)
Typeset by the author with the LaTeX Documentation System

Abstract

Over the past few decades, the worldwide neutrino scientific community has demonstrated a tremendous amount of interest in the use of Liquid Argon Time Projection Chambers (LAr-TPCs) as detectors for rare events (phenomena e.g. neutrinos or WIMPs interaction). LAr-TPCs operating principle is based on the measure of the ionization energy loss of any charged particle (dE/dx), in order to reconstruct the particle's trajectory, momentum, range and consequently type of the particle. In the following pages I present the liquid argon technology, advantages and disadvantages of the various LAr-TPC concepts, constructions and principle of the operation of various types of LAr-TPC detectors and what can be achieved with the use of this technology. The achievements are shown on the example of the largest ever built LAr-TPC detector: ICARUS T600. The ICARUS T600 detector, with its 760 tons of LAr (476 t of active mass) had been successfully in operation in the underground Laboratori Nazionali del Gran Sasso in Italy (LNGS [1]) since 2010, concluding its long operation run in 2013. During this period, the data from the the CERN to Gran Sasso neutrino beam (CNGS [2]) and cosmic rays had been collected. Its excellent calorimetric resolution and topology reconstruction capabilities permit the performance of a wide physics program, which goes from nucleon decay to the study of the oscillation of the neutrinos from the CNGS beam. Among the studies carried out on the beam events, a sensitive search for anomalous electron-neutrino appearance and muon-neutrino disapearance was performed. The electron-neutrino appearance study aimed at experimental verification or exclusion of the neutrino anomalies suggested by the LSND signal [3]. The problem of superluminal propagation of the CNGS neutrinos from CERN to LNGS, suggested by the experiment OPERA [4], was also verified. This monograph also covers various aspects related to the work of the ICARUS T600 detector, starting with the use of the liquid argon, as a medium in which the particles interact, through physical achievements to the future of the ICARUS T600 detector at the Fermilab National Accelerator Laboratory (FNAL [5]) in the frame of Short-Baseline Neutrino Program (SBN) [6].

Streszczenie

W ciągu kilku ostatnich dekad, neutrinowa społeczność naukowa, wykazała olbrzymie zainteresowanie wykorzystaniem techniki ciekłoargonowej i ciekłoargonowymi komorami projekcji czasu (LAr-TPC) do badania rzadkich zdarzeń (np. oddziaływanie neutrin czy WIMPów). Działanie ciekłoargonowych komór projekcji czasu polega na pomiarze śladów naładowanych cząstek oddziałujących w ciekłym argonie, pomiarze strat energii w wyniku jonizacji ośrodka (dE/dx) oraz identyfikacji oddziałujących i powstałych cząstek. W pracy tej przedstawiona została technika ciekłoargonowa, zalety i wady różnych koncepcji detektora ciekłoargonowego, ich konstrukcja i zasada działania, przykłady możliwych zastosowań i wyniki jakie można osiągnąć stosując ciekłoargonową komorę projekcji czasu. To ostatnie pokazane jest na przykładzie największego zbudowanego do tej pory ciekłoargonowego detektora projekcji czasu: ICARUSa T600 (760 t LAr, 476 t czynnej masy). Detektor ICARUS T600 z powodzeniem pracował w podziemnym laboratorium w Gran Sasso we Włoszech (LNGS - Laboratori Nazionali del Gran Sasso [1]) od 2010

do 2013 roku. Podczas jego eksploatacji zebrano dane będące wynikiem oddziaływania, w ciekłym argonie, neutrin wyprodukowanych w ośrodku CERN i przesłanych do Gran Sasso (wiązka CNGS [2]). Przeprowadzono także badania oddziaływań neutrin atmosferycznych. Doskonała rozdzielczość kalorymetryczna i rekonstrukcyjna detektora pozwoliła na szeroki program badawczy, od rozpadu nukleonu do badania oscylacji neutrin z wiązki CNGS. Wśród badań przeprowadzonych z wykorzystaniem wiązki neutrin możemy wyróżnić trzy główne: (1) weryfikacja zjawiska nadświetlności neutrin sugerowanej przez eksperyment OPERA [4], (2) dokładne badanie znikania neutrin mionowych oraz (3) anomalne pojawianie się neutrin elektronowych. Celem tego ostatniego była eksperymentalna weryfikacja lub wykluczenie nieprawidłowości w liczbie obserwowanych neutrin elektronowych, sugerowany przez eksperyment LSND [3]. W pracy zostały także opisane różne aspekty związane z pracą detektora ICARUS T600, począwszy od zastosowania ciekłego argonu jako medium w którym oddziałują cząstki, przez osiągnięcia z zakresu fizyki, do przyszłości detektora w ośrodku Fermilab National Accelerator Laboratory (FNAL [5]) i jego udział w programie badawczym z krótką bazą (SBN [6]).

Contents

Introduction iii

1 LAr technology 1
1.1 Introduction of LAr technology . . . 1
1.2 The advantages and disadvantages of LAr-TPC technology . . . 2
1.3 Principle of operation . . . 4
1.4 Various LAr-TPC concepts . . . 4
1.4.1 Large scale and modular LAr-TPCs . . . 5
1.4.2 Single and dual phase LAr-TPCs . . . 7
1.5 Selected past, present and future LAr-TPC experiments . . . 8
1.5.1 ArgoNeuT - forerunner of low energy neutrinos . . . 10
1.5.2 LArIAT . . . 10
1.5.3 CAPTAIN . . . 11
1.5.4 SBND, MicroBooNE and ICARUS . . . 11
1.5.4.1 SBND . . . 11
1.5.4.2 MicroBooNE . . . 12
1.5.5 MODULAr . . . 12
1.5.6 DUNE . . . 12
1.5.6.1 DUNE far detector . . . 13
1.5.6.1.1 WA105 . . . 13
1.5.6.1.2 ProtoDUNE - NP02, NP04 . . . 14
1.5.6.2 DUNE Near Detector . . . 15
1.5.7 ArgonCube . . . 16
1.5.8 LAGUNA-LBNO, GLACIER . . . 17
1.5.8.1 GLACIER . . . 18
1.5.9 Okinoshima 100-kt . . . 19
1.5.10 ArDM . . . 20
1.5.11 DarkSide detectors . . . 20
1.5.12 WARP, WArP . . . 21
1.5.13 ARIADNE . . . 22
1.5.14 LANNDD . . . 23
1.5.14.1 Mini-LANNDD T40 . . . 24

2 ICARUS T600 - a single phase Liquid Argon TPC 27
2.1 Detector overview . . . 28

2.2 The dimensions of the ICARUS T600 detector . . . 29
2.3 Cryogenic plant . . . 30
2.4 Purification of LAr and ionizing electrons lifetime . . . 31
2.5 Trigger system of the ICARUS T600 detector . . . 33
2.5.1 Photomultiplier Tube system . . . 33
2.5.2 S-Daedalus system . . . 35
2.6 ICARUS T600 overhauling at CERN (WA104/NP01) . . . 35

3 CNGS muon-neutrino beam 37
3.1 CNGS beam at CERN . . . 37
3.2 The underground Gran Sasso laboratory . . . 41

4 Physics results of the ICARUS T600 experiment 43
4.1 Neutrino time of flight measurements . . . 43
4.1.1 The CNGS bunched beam for the ν_μ time of flight measurements . 45
4.1.2 Time synchronization between CERN and LNGS . . . 45
4.1.3 Distance between CERN and LNGS . . . 47
4.2 ICARUS search for an LSND-like effect with CNGS beam . . . 48
4.3 Search for the atmospheric $\nu_{\mu,e}$ interactions in the ICARUS T600 detector 52
4.3.1 The atmospheric ν_μ and ν_e classification algorithm . . . 54
4.3.2 The atmospheric ν_e classification algorithm . . . 55
4.4 CNGS neutrino study . . . 56
4.4.1 Measurement of muon momentum via Multiple Coulomb Scattering 57
4.4.2 The seven identified ν_e events from CNGS beam . . . 60
4.4.3 The 2482 CNGS subsample data analysis . . . 64
4.4.4 Correction for undetected/non contained hadronic part . . . 66
4.4.5 ν_μCC vertex reconstruction . . . 69
4.4.6 Reconstruction of the muon-neutrino energy E_{ν_μ} . . . 70
4.4.7 Search for ν_μ disappearance with the ICARUS T600 detector . . . 71
4.4.7.1 Expected ν_μ events . . . 73

5 Current status of the ICARUS T600 detector 75

Conclusions 78

A The Famous Pauli letter 81

B A new concept for ν detectors: LAr-TPC 85

Acknowledgements 86

Bibliography 89

Introduction

Neutrino physics has opened a new and broad window into phenomena beyond the Standard Model and the short and long-baseline neutrino experiments may allow further insight into neutrino physics.

The Liquid Argon Time Projection Chamber (LAr-TPC) technology is the first important alternative to the scintillation and water Cherenkov detectors used in neutrino experiments. The last one, with its kiloton water/ice mass, has for years been one of the key choices for studying neutrinos. The usage of the drifting ionizing electron, in an electric field in pure LAr, for both, (1) the spacial track reconstruction and (2) energy calorimetric measurement was originally proposed in 1977 by C. Rubbia [7].

Taking into account the three-dimensional track reconstruction and calorimetric measurement the LAr-TPC can be considered as a continuously sensitive electronic bubble chamber. But contrary to traditional bubble chambers, this detection technique can be scaled to larger masses and therefore can be successfully employed to register rare events effectively, like neutrino interactions and nucleon decay.

Currently there are various experiments exploiting LAr detection technique and LAr-TPC detectors. Among them one can distinguish: (1) single and double phase detectors, (2) small (with liters of LAr) and large (with tons of LAr), (3) with and without magnetic field surrounding the detector and (4) with single and modular time projection chamber. In chapter 1 of this monograph a short characterization of issues related to the liquid argon technology is presented together with a brief introduction to detectors which either used or still use the LAr-TPC detection technique. The biggest ever built single phase, modular LAr-TPC detector is the ICARUS T600 [8] with the cryostat containing 760 tons (476 tons of active mass) of LAr. The ICARUS stands for **I**maging **C**osmic **A**nd **R**are **U**nderground **S**ignal. This detector is described in detail and its example shows the possibilities of particle detection by the exploiting the LAr technique as well as the achieved physical results.

The ICARUS T600 is a result of many years of R&D studies performed by the ICARUS Collaboration, with laboratory and industrial prototypes of growing mass. The idea of the ICARUS detector arose in Italy, as the result of a combined effort of the ICARUS Collaboration and Instituto Nazionale di Fisica Nucleare (INFN [9]). This effort has led, through many stages of prototyping and interaction with industries, to the final result i.e. the T600 detector.

In 2013 the ICARUS T600 LAr-TPC completed its successful, continuous three year operation at the Laboratori Nazionali del Gran Sasso (LNGS [1]) underground lab-

oratory, where it was exposed to both, the 'CERN[1] to Gran Sasso' neutrino beam (CNGS [10]) and cosmic rays. The achieved physics and technical results proved the maturity of the LAr-TPC technique and therefore will have an impact on future neutrino and astroparticle physics experiments. The currently realized at Fermi National Accelerator Laboratory (FNAL, Fermilab [5]), Short-Baseline Neutrino Program (SBN [6]) with three LAr-TPC detectors (SBND [11], MicroBooNE [12] and ICARUS T600) and considered multi-kt DUNE LAr-TPC detector at the Sanford Underground Research Facility (SURF) [13] serve as a good example.

The main physics results obtained during the three years run at LNGS can be described as: (1) measurement of the non-superluminal neutrino velocity (section 4.1), (2) search for anomalies in the ν_e appearance from the CNGS ν_μ beam confirming the absence of anomalous oscillations (section 4.2), (3) measurements of neutrinos from astrophysical sources (section 4.3) and (4) study of ν_μ disappearance in the CNGS beam (section 4.4). The first mentioned result was triggered by the surprising outcome reported in 2011 by the OPERA experiment [4], whereas the second fell in line with longstanding the LSND experiment anomaly [3], implying the existence of new sterile neutrino flavor with additional mass-squared difference.

In addition to the physical results the ICARUS Collaboration has also obtained respectable technical achievements. The main are: (1) the solutions for the argon purification and recirculation permitting to reach impressive LAr purity and extremely high electron lifetime exceeding 15 ms (section 2.4) and (2) precise reconstruction of neutrino interactions within a very broad energy range (from hundreds of MeV to tens of GeV) leading to different and complicated event topologies (sections 4.3 and 4.4).

Furthermore, some technical aspects related to the ICARUS T600 detector's activity are also given in this monograph. Chapter 2 contains description of the ICARUS T600 - single phase LAr-TPC detector, where separate sections are devoted to: (1) technical detail of the ICARUS T600 detector (sections 2.1 and 2.2), (2) cryogenic plant (section 2.3), (3) argon purification and electron lifetime (section 2.4), (4) trigger systems (section 2.5) and (5) overhauling and refurbishing within CERN Neutrino Platform (CENF [14]), in a frame of WA104/NP01 program [15] (section 2.6). In chapter 3, ν_μ beam propagation from CERN to Gran Sasso and the underground laboratory at the Gran Sasso are described. The main physical results of the ICARUS T600 experiment can be found in chapter 4.

Chapter 5 concerns the present and future use of the ICARUS T600 within the SBN program at FNAL which is followed by conclusions.

[1] CERN stands for European Organization for Nuclear Research (French: Organisation européenne pour la recherche nucléaire). The name CERN derived from french Conseil Européen pour la Recherche Nucléaire. The term CERN is also used to refer to the laboratory.

Carlo Rubbia[2] foreword

I have initiated the systematic study of cryogenic liquids when professor in Pavia in the late nineties, after some initial preliminary studies when I was at Harvard with Elena Aprile and her (then) husband Giboni and a few others.

This has required our new and very successful development of the purification technology to the continuative level of several parts per trillion against other chemically active gases. My major participants in Pavia have been Calligarich, Montanari, Vignoli and several others.

Our success has opened the lines of practical experimentation with both Argon and Xenon, initially in Pavia with table top type detectors.

The program has then been devoted at the LNGS/INFN laboratory with ICARUS liquid Ar and with liquid Xe. WARP and presently XENON, the last driven by Elena Aprile who had also initially followed such technology. A neutrino beam was provided from CERN.

The LAr technology is presently developed both at CERN with the "Platform" where ICARUS had been provisionally transferred and in the US where ICARUS is now been moved; later with the huge future DUNE program, all starting with the FermiLab accelerators.

The Xe line is also presently being pursued by several US teams.

Carlo Rubbia, February 22nd, 2018

[2]The originator of the LAr-TPC and the Nobel Prize winner in Physics (1984). Spokesperson of the ICARUS Collaboration.

Chapter 1

LAr technology

1.1 Introduction of LAr technology

The existence of neutrinos was postulated for the first time by Wolfgang Pauli in 1930 to explain how beta decay could conserve energy, momentum and angular momentum (spin) (see appendix A). However due to their elusive behavior neutrinos were not discovered until 1956 [16], when Clyde Lorrain Cowan and Frederick Reines finally found a particle that fitted to the properties of the particle proposed by Pauli. The discovered neutrinos (to be specific anti-neutrinos) were produced in a nuclear reactor and then by interacting with protons in two tanks of water led to the creation of neutrons and positrons. The last ones (i.e. positrons) after annihilation with an electron created a pair of gamma rays detected by liquid scintillators which sandwiched the water tank. The obtained results were not conclusive and required further investigations. The researchers mentioned above decided to use cadmium chloride for the detection of neutrons. The gammas produced during neutron absorption in cadmium, delayed with respect to gammas from the positron annihilation, convinced the researchers that the interacting particle is a neutrino. The second neutrino flavor (muon-neutrino) was discovered in 1962 by Leon Lederman, Melvin Schwartz and Jack Steinberger [17]. The third one, the tau-neutrino, was first deduced after discovery of the τ particle in a series of experiments between 1974 and 1977 by Martin Lewis Perl and others at the Stanford Linear Accelerator Center (SLAC). Finally it was "directly" discovered in July 2000 by the DONUT experiment [18]. A detailed description of the path towards the discovery of neutrinos can be found in [19, 20].

One of the first apparatus used for neutrino detection was the Water Cherenkov detector. This technology could be scaled to a very large size. Nevertheless, due to the comparatively high energy threshold of the Water Cherenkov detectors, details of the interactions, particularly of low-momentum recoil protons or soft pions are not visible. The reconstruction of the high-multiplicity events also poses a challenge, as the multiple overlapping Cherenkov rings are difficult to sort out. Simultaneously the gas TPCs were developed by Dave Nygren following Georges Charpak's idea, with the first large-scale implementation PEP-4 detector [21] at SLAC, which started to operate in 1980.

In the late 60's the potential of liquefied noble gases as detection media to build detec-

tors with high spatial resolution was recognized [22]. The Liquid Argon Time Projection Chamber (LAr-TPC[1]) was proposed by C. Rubbia in 1977 [7], as a powerful detection technique to provide a three dimensional (3D) imaging of any ionizing event.

Currently, there is worldwide interest in exploiting this technology, with the goal of deploying multi-kiloton LAr-TPCs in the far-detector locations, as part of long-baseline neutrino oscillation and nucleon decay search programs.

Table 1.1: The selected physical parameters of gaseous argon. Adapted from [23].

Parameter	Value
Atomic number	18
Molecular weight	39.948 g/mol
Natural concentration	0.934% of air
Melting point	83.4 K at 1 atm
Boiling point	87.3 K at 1 atm
Triple point	83.8 K at 0.687 bar
Latent heat (1 atm)	160.81 kJ/kg
Dielectric constant	1.5
Electric breakdown	1.2–1.4 MV/cm
dE/dx for m.i.p.	2.12 MeV/cm
Ionization energy W_e $(E = \infty)$	23.6 eV
Excitation energy W_γ $(E = 0)$	19.5 eV
Radiation length X_0	14 cm
γ pair production length $(9/7)X_0$	18 cm
Molière radius	9.28 cm
Nuclear interaction length λ_{int}	84 cm
Critical energy	30 MeV

1.2 The advantages and disadvantages of LAr-TPC technology

The LAr-TPCs are an exciting class of detectors designed for registration of rare events, like neutrino interactions or nucleon decay. They offer good detection efficiency, excellent background rejection, bubble chamber quality images and very good particle identification. Liquid argon, as was pointed out in the pioneer work [24], is a medium that satisfies calorimetric requirements better than many other materials, allowing for the reconstruction of particle's deposited energy. These characteristics made LAr-TPCs a very promising choice for neutrino physics experiments.

The advantage of LAr-TPCs is their high resolution in spatial reconstruction of the ionizing tracks and low energy threshold (albeit higher than a liquid scintillator), which allow for highly detailed reconstruction of neutrino events. Moreover LAr-TPCs provide a complete 3D image of the interaction final state particles over a wide range of energies with an efficient background rejection and a good energy reconstruction. In addition, the noble element allowing the ionization electrons to drift through it is relatively cheap. The principal disadvantage is that they cannot to be constructed as large as water Cherenkov detectors: the DUNE far detector [26] will be only about one-tenth of the

[1]The original abbreviation proposed by C. Rubbia was LAPC [7]. See appendix B.

Table 1.2: The selected physical parameters of liquid argon. Adapted from [25].

Parameter	Value
Mean Energy Loss (minimum ionizing particle)	$\langle dE_{m.i.p.}/dx \rangle = 1.519\,\mathrm{MeVcm^2/g}$
Average Energy for (e^-, Ar^+ pair production)	$W_{LAr} = 23.6\,\mathrm{eV}$
Mean Electron Number/cm [at 0.5 kV/cm] (m.i.p.)	$N_e/\mathrm{cm} \simeq 6 \cdot 10^4\,\mathrm{e^-/cm}$
Ar_2^* excited dimer states (M-band)	Singlet $^1\Sigma_u$; Triplet $^3\Sigma_u$
Decay γ Energy	$\langle E_\gamma \rangle = 9.7\,\mathrm{eV}$
Decay γ Spectrum	$\langle \lambda_{scint} \rangle = 128\,\mathrm{nm}$; $\sigma_{scint} \simeq 3\,\mathrm{nm}$
Decay Time constant	$\tau_S \sim 4 \div 6\,\mathrm{ns}$; $\tau_T \sim 1.2 \div 1.6\,\mu\mathrm{s}$
Decay Intensity Ratio (m.i.p.)	$I_S/I_T = 0.3$ (23%/77%)
Average Energy for γ production	$W' = 19.5\,\mathrm{eV}$
Photon Yield [at 0-field] (ideal)	$Y_\gamma = 5.1 \cdot 10^4\ \gamma/\mathrm{MeV}$
Photon Yield [at 0-field] (m.i.p.)	$Y_\gamma = 4.1 \cdot 10^4\ \gamma/\mathrm{MeV}$
Photon Yield [at 0.5 kV/cm] (m.i.p.)	$Y_\gamma = 2.4 \cdot 10^4\ \gamma/\mathrm{MeV}$
Mean Photon Number/cm [at 0.5 kV/cm] (m.i.p.)	$N_\gamma/cm \simeq 5 \cdot 10^4\ \gamma/\mathrm{cm}$
Rayleight scattering length (at 128 nm, 89 K)	$L_R = 90\,\mathrm{cm} \pm 25\%$
Attenuation length (ultra high purity)	∞
Refractive index at 128 nm	1.38
Rayleight scattering length	$\lambda_0 = 90\,\mathrm{cm}$
Cherenkov photons per cm (110-600 nm)	1430 γ/cm
Electron Mobility (boiling point)	$500\,\mathrm{cm^2/C \cdot s}$
Electron Drift Velocity [at 0.5 kV/cm](89 K)	$1.55\,\mathrm{mm}/\mu\mathrm{s}$
Electron Diffusion Coefficient (89 K)	$4.8\,\mathrm{cm^2/s}$
Nuclear collision length	53.2 cm
Absorption length	80.9 cm
Minimum dE/dx	2.11 MeV/cm
Radiation length	14 cm
Liquid density	
at 83.7 K	$1392.8\,\mathrm{kg/m^3}$
at 90 K	$1383.0\,\mathrm{kg/m^3}$

mass of Hyper-Kamiokande [27], when both are completed. Another drawback is that LAr must be kept extremely pure for the electrons to drift towards the anode wires without attaching to impurities. In highly purified liquid argon ionization electrons can be practically transported undistorted by a uniform, hundred kV, electric field over distances of the order of meters. The issues related to the purity of argon can be partially solved by the usage of dual phase LAr-TPC with less stringent constraints on the liquid argon purity.

In fact, LAr and water Cherenkov technologies are highly complementary. One gives a higher target mass, the other greater precision. At low energies, for solar and supernova neutrinos, water Cherenkov detectors see mostly electron-anti-neutrinos (from inverse beta decay, $\overline{\nu}_e + p \rightarrow e^+ + n$) whereas LAr detectors see mostly electron-neutrinos (from quasi-elastic scattering, $\nu_e + {}^{40}Ar \rightarrow e^- + {}^{40}K$). The detector systematic errors on oscillation measurements are also different.

The usage of liquid argon seems to be optimal, since: (1) it is dense ($\sim$1.4 g/cm^3), (2) has large neutrino cross sections, (3) inert and ionization electrons can drift through it (it does not to much attach electrons), (4) it is easy to obtain (can be liquefied from air) and relatively cheap compared to other gases e.g. freon which has many similar

properties (Tab. 1.3 - the heavy-liquid freon CF_3Br was used in the Gargamelle[2] bubble chamber [28,29]). However, the LAr must be kept extremely pure, allowing the ionization electrons to drift across the TPC without significant attenuation, as was recently shown by ICARUS collaboration [30]. In addition, LAr-TPC provides a very good discrimination between electron and photon interactions, a fact which is of great importance for neutrino experiments.

Some physical parameters of gaseous argon are shown in Tab. 1.1, whereas liquid argon physical characteristics are presented in Tab. 1.2.

Table 1.3: Comparison of some parameters of LAr and heavy-liquid freon CF_3Br, used in Gargamelle chamber [7].

Parameter	LAr	CF_3Br
Nuclear collision length	53.2 cm	49.5 cm
Absorption length	80.9 cm	73.5 cm
dE/dx minimum	2.11 MeV/cm	2.3 MeV/c
Radiation length	14 cm	11 cm
Density	$\sim$1.4 g/cm^3	$\sim$1.5 g/cm^3

1.3 Principle of operation

In LAr-TPC detectors liquid argon, which is an interaction medium, serves also as a neutrino target. Neutrinos passing through LAr interact with argon atoms. It results in production, among others, ionization particles and light. Charged particles propagate in an electric field through liquid argon and leave a path of ionization electrons. The quasi-free ionization electrons easily drift in liquid argon with the drift velocity (V_d) of 1.5–2 mm/μs in an electric field of 0.5–1 kV/cm (Fig. 1.1). The positively charged ions are not used for particle detection. The ionization electrons induce current in the anode wire planes and finally their charge is collected. The measurements of: (1) the wire signals and (2) ionization electron drift time and velocity (e.g. $V_d = 1.55$ mm/μs at 0.5 kV/cm and $T = 89$ K; Tab. 1.2 and Fig. 1.1) provide all the information needed for the 3D reconstruction of an ionizing event. The determination of the absolute time of the ionizing event is accomplished by the detection of the prompt scintillation light produced in LAr by charged particles (about 5000 γ/mm of path at 0.5 kV/cm; see Tab. 1.2). The simulated ionizing electron drift path and corresponding evolution of a signal in two induction planes of anode wires is shown in Fig. 1.2.

1.4 Various LAr-TPC concepts

Among the LAr-TPC detectors operating, or being planned to be built or still being in R&D, phase two classes can be distinguished. One is based on size (large dimension

[2]Gargamelle was a heavy liquid bubble chamber detector in operation at CERN between 1970 and 1979. It was designed to detect neutrinos and antineutrinos. In 1973, Gargamelle Collaboration confirmed the electroweak theory of the Standard Model by detecting neutral currents.

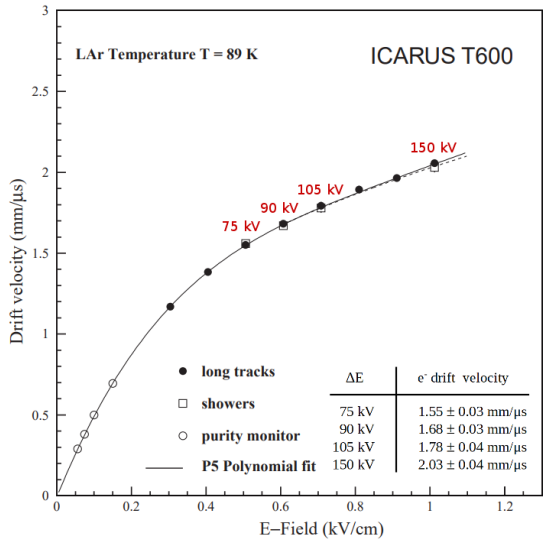

Figure 1.1: Electron drift velocity $\langle V_d \rangle$ in LAr (at 89 K) as a function of the electric field value E_d measured in the ICARUS T600. Data measurements from: (open circles) purity monitor, (full circles) crossing single muon tracks and (squares) shower data. The result of the P5-polynomial fit through all points (solid line) together with the analytical prediction [31] (dashed line). Adapted from [32].

and modular detector) and the other on the structure (phase) of the detector (single and double[3] phase) (Fig. 1.3). Both are described in the following sections.

1.4.1 Large scale and modular LAr-TPCs

The simplest design of LAr-TPC is the single LAr container of a huge size (may be ∼100 kton). But in such a case the whole volume of ultra-pure LAr will be totally contaminated even by a tiny accidental leak. Besides the construction of a container vessel for ∼100 kton is rather unrealistic. Fortunately the size increase of a single container does not introduce significant physics arguments in its favor. A reasonable single volume unit can be e.g. of about $8 \times 8\,\mathrm{m}^2$, with a drift gap of 4 m and a length of about 50–60 m, which corresponds to about $3800\,\mathrm{m}^3$ of LAr or 5400 tons of LAr (compare MODULAr detector in section 1.5.5). Thus instead of building a large scale detector, the construction of the so called modular detector consisting of several separated vessels is being considered. Such a modular detector should be (1) safer in use than a single large one, taking into account potential LAr leaks and (2) much easier to maintain considering the purification of LAr and/or hypothetical construction distortion (e.g. non-planarity of the cathode).

[3] Double or dual - both names are used in literature.

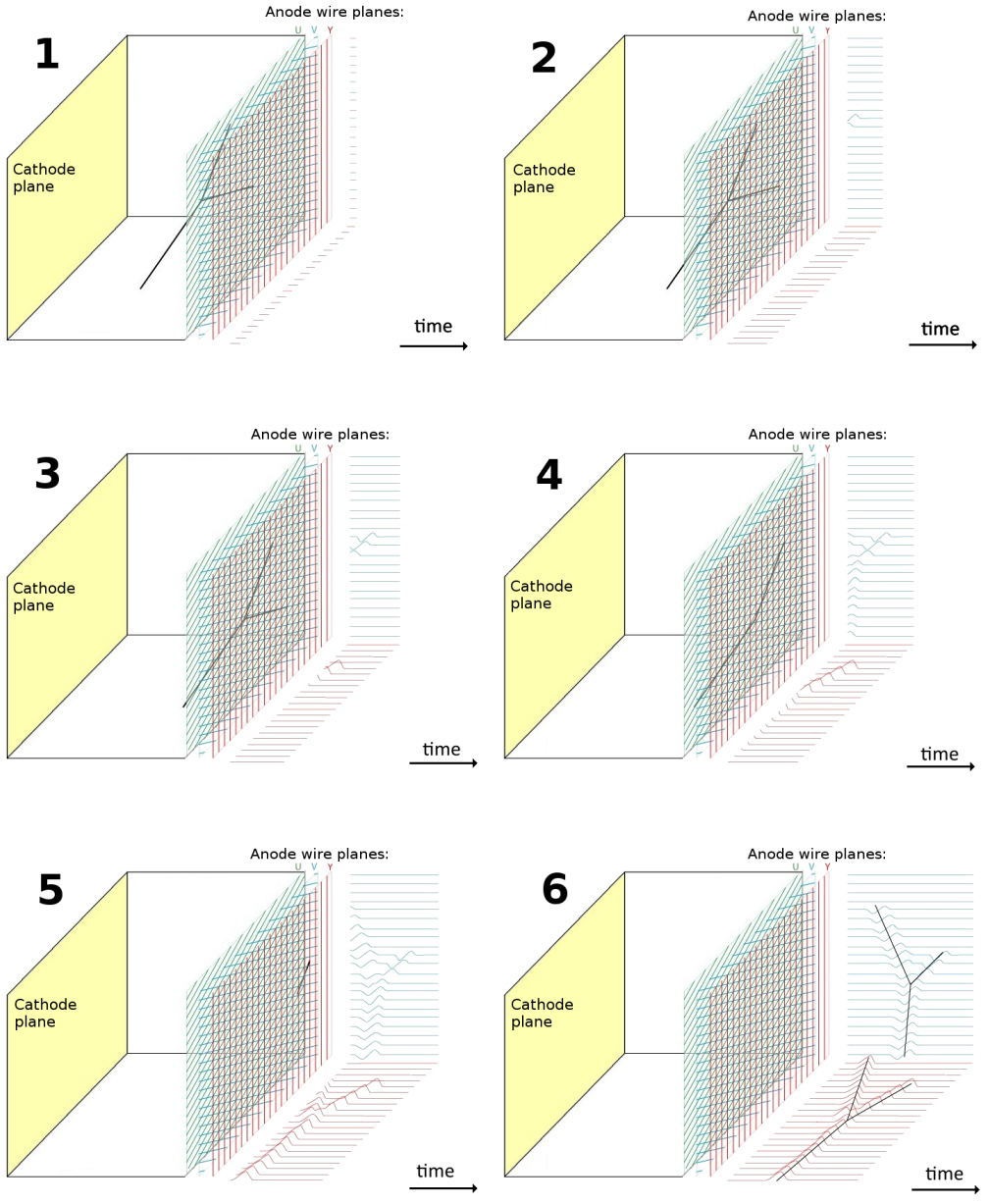

Figure 1.2: Evolution of signal in LAr-TPC. Adapted from [33] (individual images were created by extraction of frames from animated pictures).

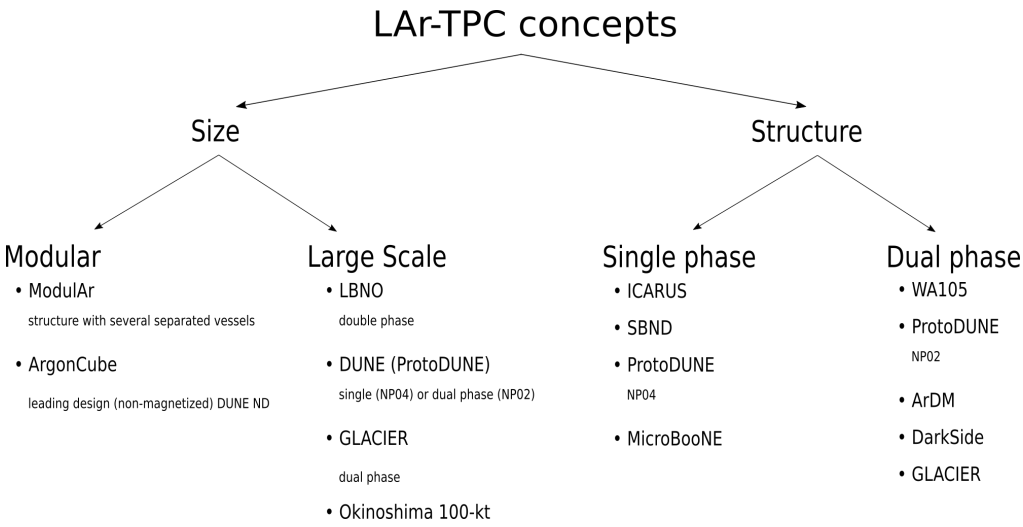

Figure 1.3: LAr-TPCs concepts taking into account scale and structure of the LAr detector. In plot a few example of the LAr-TPC detectors fulfilling concepts criteria are included.

1.4.2 Single and dual phase LAr-TPCs

The second approach to the construction of a detector based on liquid argon is the use of the single or dual phase concept. Of course the single or dual phase detector can be either a large sized or a modular one. The single phase corresponds to a detector where information about the particle track and energy comes only from ionization occurring in liquid argon. Whereas in the dual phase, after ionization, electrons are extracted from the liquid to the gaseous phase, where the charge is amplified in a high electric field before its collection on anode (e.g. by using Micro-pattern detectors like the Large Electron Multipliers (LEM), located just above the liquid level as shown in Figs. 1.4 and 1.14). Multiplication in the gaseous phase opens up the possibility of using very large drift distances, up to tens of meters, with less stringent constraints on the liquid argon purity, thus reducing the number of readout channels for large detectors. The first proposition of such a solution came from A. Rubbia [34] as an alternative to building giant LAr-TPC, viewed by many as a technically impossible and unsafe task. Key features of the dual phase is the amplification of the signal by a charge avalanche in the gas phase, thus (1) a larger signal/noise ratio and (2) overall better image quality. The fantastic example of this novel technology is the large scale demonstrator WA105[4] (section 1.5.6.1) or ProtoDUNE experiment (NP02; section 1.5.6.1), both localized at CERN. This effort should pave the way to the DUNE Dual Phase detector of dimension $60 \times 12 \times 12\,\mathrm{m}^3$ and 10 kt of liquid argon (see section 1.5.6). The comparison of the single and dual phase LAr-TPC concept is shown in Fig. 1.4.

[4] In 2017 WA105 becomes part of the DUNE prototyping effort known as ProtoDUNE-DP.

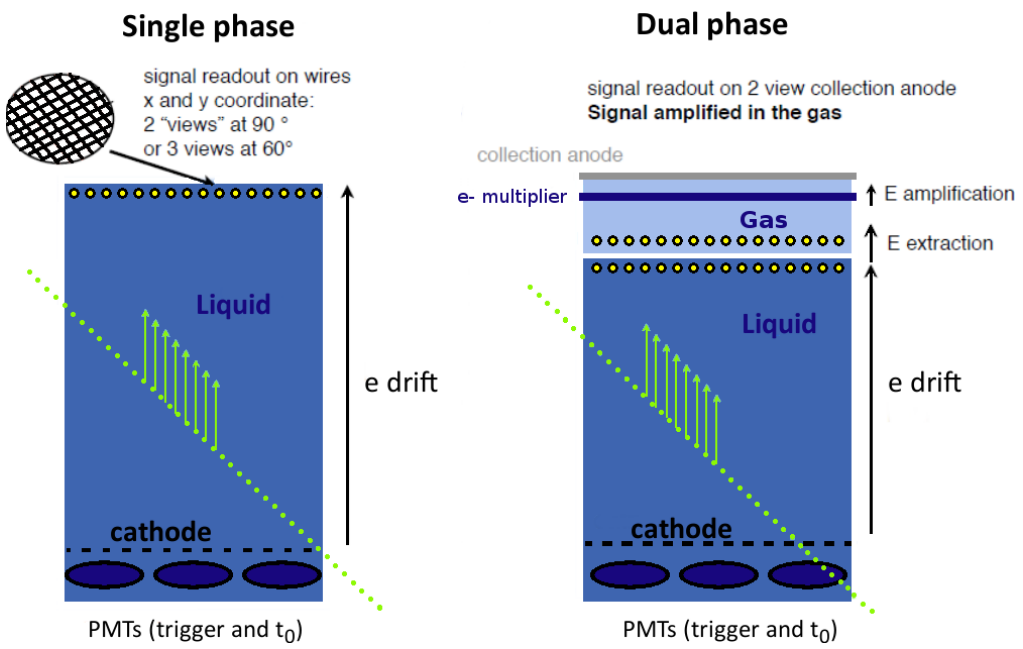

Figure 1.4: The scheme view of the single and dual phase LAr-TPC. Adapted from [35].

1.5 Selected past, present and future LAr-TPC experiments

The LAr-TPC is a successful marriage between the "gaseous" TPC chamber and "the liquid argon calorimeter" to obtain a combined dense and very fine-grained three-dimensional tracking device with local dE/dx information and a homogeneous full sampling calorimeter. Therefore it can cover a broad physics program, including the observation of atmospheric neutrinos, solar neutrinos, supernova neutrinos and the search for proton decays, in addition to the accelerator neutrino physics.

In Tab. 1.4 and Fig. 1.5 a selected past, present and planned experiments exploiting LAr-TPC detection technique are listed, together with used/planned neutrino beam location and energy. The details of some of them are presented in the following sections whereas the ICARUS T600 detector is described in details in chapter 2.

It should also be noted that LAr detectors, not only LAr-TPC, but also *pure* LAr, may also be included in larger experiments, where they are used as auxiliary ones among others. For example in the ATLAS experiment at the LHC at CERN the LAr detector, which serves as a sampling calorimeter [37], is made of liquid argon as the active material and lead, copper or tungsten as the passive absorber, depending on the position. Among the LAr detectors were also those that never went beyond the stage of plans, for example: (1) LANNDD (**L**iquid **A**rgon **N**eutrino and **N**ucleon **D**ecay **D**etector) [38], which was planed to be a 70 kt magnetized tracking detector designed for the Carlsbad Underground National Laboratory (CUNL), or (2) Mini-LANNDD T40 use of the NuMI beam.

Table 1.4: The summary of the past, present and the future LAr-TPC neutrino experiments and demonstrators. R&D stands for Research & Development, LoI - Letter of Intent, FNAL (Fermilab) - Fermi National Accelerator Laboratory (USA), BNB - Booster Neutrino Beam, NuMI - Neutrinos at the Main Injector - neutrino beamline, LANL - Los Alamos National Laboratory (USA), SURF - Sanford Underground Research Facility (USA), J-PARC - Japan Proton Accelerator Research Complex, LSC - Laboratorio Subterráneo de Canfranc (Spain), LNGS - Gran Sasso National Laboratory (Italy), CUNL - Carlsbad Underground National Laboratory (USA), LNL - Legnaro National Laboratory (Italy). Updated table from [36].

Experiment	**LAr mass [l, t]**	**Physics goals**	**Baseline [km]**	**$E_{\nu,\mathrm{WIMP}}$ [GeV]**	**Detector location**	**Current status**
ArgoNeuT	175 l	R&D, cross sections, accelerator ν	1	∼0.1–10	FNAL (NuMI beam)	Completed data under analysis
LArIAT	550 l	Study of charged particle interaction in LAr	-	0.2–1.2	FNAL (dedicated tertiary char. beam line)	Running since 2015
CAPTAIN	2 t - prototype 10 t	ν interaction		< 0.05, 1.5–5	LANL FNAL (NuMI)	LoI 2014
SBND (LAr1-ND)	220 t 112 t active	sterile ν short-baseline	0.110	∼0.800	FNAL (BNB)	Design phase
MicroBooNE	170 t 89 t active	R&D sterile ν short-baseline	0.470	∼0.1–3	FNAL (BNB)	Start 2015
ICARUS	760 t 476 t active	R&D, sterile ν atm. ν long-baseline short-baseline	732 0.6	∼5–25	LNGS (CNGS), FNAL (BNB)	2010–2013 Start ∼2018
MODULAr	5000 t	long-baseline	730	∼5–25	LNGS	Proposed
GLADE	5000 t	long-baseline	810	∼0.5–2	FNAL (NuMI beam)	LoI
DUNE (LBNE)	68000 t (4x17000 t)	long-baseline	1300	∼0.5–5	FNAL, SURF	Planned ∼2021
LAGUNA\ LBNO (e.g. GLACIER)	40000 t 100000 t 20000t	long-baseline long-baseline	2300 2300	∼few sub-GeV - - multi-GeV	Europe Pyhäsalmi	R&D future
ArgonCube	2.8 t DUNE ND: 39 t				CERN FNAL	R&D R&D
Okinoshima	up to 100 kt	long-baseline underground	665	∼0.5–2	Okinoshima (new J-PARC beam)	R&D proposal at J-PARC
DarkSide-20k	20 t	WIMP	-	1–10 TeV/c^2	LNGS	R&D
ArDM-1t	ton scale	WIMP	-	1–10 TeV/c^2	LSC	∼2017-2018
ARIADNE	1 t				Liverpool, CERN	R&D
LANNDD	70 kt	long-baseline	1691–8097	sub-GeV - - multo-GeV -	CUNL CUNL	∼2003
WARP	2.3 l, 100 l	WIMP	-	1–10 TeV/c^2	LNL,LNGS	∼2001
Demonstrators						
WA105	300 t				CERN	R&D
ProtoDUNE (NP02, NP04)	0.77 kt				CERN CERN	Under construction

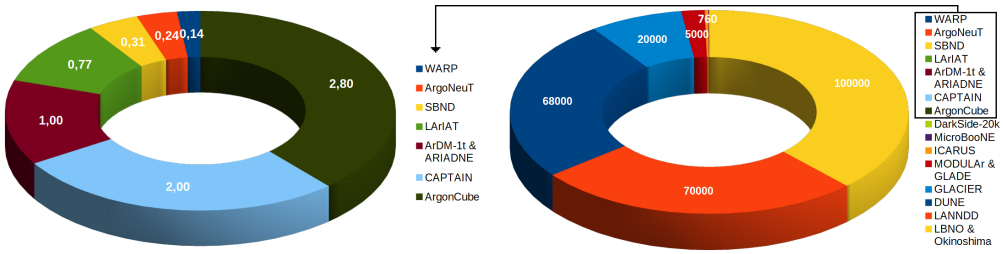

Figure 1.5: Pie chart of LAr detector with the division into the mass of liquid argon (in tons). In cases where the mass was expressed in liters, it was converted into tons with an average argon density of $\rho \simeq 1.4\,\mathrm{g/cm^3}$. Left: Detectors with LAr mass up to 3 tons. Right: All detectors.

1.5.1 ArgoNeuT - forerunner of low energy neutrinos

ArgoNeuT was a project conducted at Fermilab to expose a mini-scale (175 l) detector to the Fermilab's NuMI (Neutrinos at the Main Injector) neutrino beam. Data-taking was concluded in March 2010 whereas the analysis is still ongoing. Detector collected thousands of neutrino and anti-neutrino events in the 0.1 to 10 GeV energy range. It is worth mentioning that it provided the first ever data for low energy neutrino interactions in LAr-TPC. The experiment measured also the cross section of the neutrino and anti-neutrino Charged Current Quasi-Elastic (CCQE) interaction on Ar target and analyzed the vertex activity associated with such events [39].

1.5.2 LArIAT

The acronym stands for **L**iquid **Ar**gon **I**n **A** **T**estbeam. The goal of the experiment was not to measure neutrino interactions, but rather precise measurements of particles that come out of neutrino interactions and the characterization of the LAr-TPC performance in the range of energies relevant to the upcoming short- and long-baseline neutrino experiments. The physics program covered the following: (1) charged pion interaction cross section measurements, (2) experimental measurement of e/γ separation capability, (3) optimization of pion and kaon signature, (4) development criteria for muon charge sign determination with and without magnetic field and (5) study of energy resolution and particle identification improvement by combining information from scintillation light and ionization charge signals. To achieve this the LArIAT uses the dedicated tertiary charged beam line at Fermilab [40]. The beam line produces low momenta (0.2–2.0 GeV/c) particles extracted from a high energy pion beam. The first physics run was carried out from April 30^{th} to July 8^{th} 2015. Results from this run will be helpful to design and construct future multi kilotons LAr detectors. In addition in 2017 the LArIAT experiment began a proof-of-concept test to check some technical aspects for the planned Deep Underground Neutrino Experiment (DUNE [26]). It will test whether the DUNE detector will have acceptable resolution in track reconstruction with wires spaced 5 mm apart, which is significantly larger than the 3 mm spacing used in the ICARUS T600, SBND [11] or MicroBooNE [12] detectors.

1.5.3 CAPTAIN

Cryogenic **A**pparatus for **P**recision **T**ests of **A**rgon **I**nteractions with **N**eutrino employs two detectors: (1) a primary detector with approximately 10 tons of LAr which is designed for physics measurements and, (2) a prototype detector with 2 tons of LAr for a configuration test. The physics program includes: (1) neutrino interaction measurements in low (< 0.05 GeV) energy range, at stopped pion sources[5] for supernova neutrino studies, (2) neutrino interaction measurements in medium energy range (1.5–5 GeV) at Fermilab NuMI beam and, (3) measurements of a neutron interactions at Los Alamos Neutron Science Center [41].

1.5.4 SBND, MicroBooNE and ICARUS

Another two LAr-TPC detectors (with exclusion of ICARUS T600 which is characterized in chapter 2) are presented in this section, as they are part of the Short-Baseline Neutrino Program (SBN) [6]. The detectors are located along the BNB at Fermilab. Currently the SBN is the nearest program which will come into force in neutrino physics exploiting the LAr technique. It mainly aims to give a definite answer to the "sterile neutrino puzzle", i.e. resolve a class of experimental anomalies in neutrino physics and to perform the most sensitive search for sterile neutrinos through both appearance and disappearance oscillation channels. The experimental setup will consist of three detectors:

- **S**hort-**B**aseline **N**ear **D**etector (SBND [11]) which contains 220 tons of LAr in total and 112 tons of LAr active mass. It is still in the design phase.
- **Micro Boo**ster **NE**utrino detector (MicroBooNE [12]) which contains 170 tons of LAr total and 89 tons active mass. It is currently collecting data.
- ICARUS T600 - 760 tons total and 476 tons of active mass, being currently installed at Fermilab.

These three detectors will be installed at 110, 470 and 600 meters from the target, respectively. In absence of anomalies, signals from all three detectors should be a copy of each other giving conclusive answer to the "sterile neutrino puzzle" [6].

1.5.4.1 SBND

SBND detector, formerly known as LAr1-ND, will be the nearest to the target detector (110 m), with TPC dimensions of $4 \times 4 \times 4\,\mathrm{m}^3$ and 2 m maximum drift distance (Fig. 1.6). SBND uses three wire planes with 3 mm wire pitch. It also includes the UV laser based calibration system, light collection system for detection of scintillation light and external cosmic ray tagging system. SBND will provide a detailed characterization of the neutrino beam before oscillations can occur i.e. precise measurement of the un-oscillated neutrino flux (Fig. 1.7) and therefore will significantly reduce systematical errors on the expected neutrino flux in the far sites i.e. at MicroBooNE and ICARUS locations.

[5] Pions stopped in the target, horn and surrounding structures of the Booster Neutrino Beam (BNB) at FNAL.

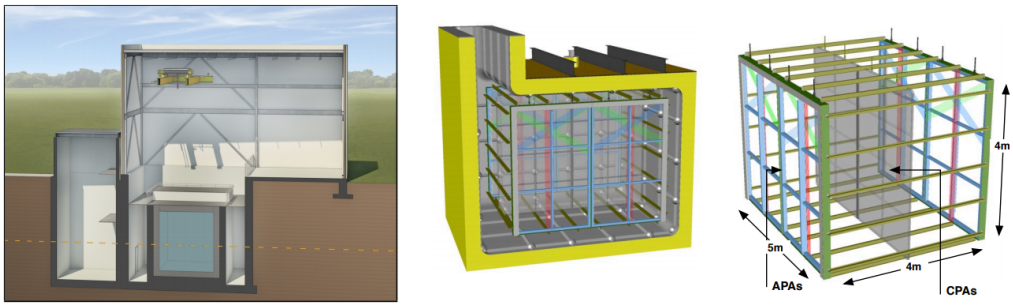

Figure 1.6: Left: The SBND detector building concept. The neutrino beam center is indicated by the orange dashed line and enters from the left. Right: The SBND conceptual design [6].

1.5.4.2 MicroBooNE

It is planned that MicroBooNE experiment will collect the total data for $13.2 \cdot 10^{20}$ protons on target (pot) in the neutrino running mode. In July 2015 the detector was filled with liquid argon for the first time and a month later first UV laser tracks were registered in TPC. The first neutrino beam was delivered on October 15^{th} and two weeks later, on November 2^{nd} the first neutrino event candidate was recorded (Fig.1.8).

The detector dimensions are $2.5 \times 2.3 \times 10.2\,\text{m}^3$, with 2.5 m maximum drift distance. MicroBooNE holds the same as SBND and ICARUS T600, 3 planes of wires with 3 mm wire spacing, with 8256 wires total and 30 PMT's which provide the absolute event time and triggering information [12].

Fig. 1.9 shows screenshot from the VENu mobile application (Android and iOS) with run 5189, event 665. Application allows to see data from the MicroBooNE experiment. VENu uses real data collected by the MicroBooNE neutrino detector, modeled in a 3D environment to create an interactive neutrino-hunting experience [44].

1.5.5 MODULAr

MODULAr is a concept of a single phase modular LAr-TPC. It consists of two identical units, following the design of the ICARUS T600 detector (Fig. 1.10). Both units are independent. Size of each unit is $8 \times 8\,\text{m}^2$ (maximum electron drift length of 4 m) and length of about 60 m with 6 mm wire pitch. Each unit hosts 5370 tons of LAr, with total number of anode wires of ∼50 k channels [45].

1.5.6 DUNE

Dune stands for **D**eep **U**nderground **N**eutrino **E**xperiment. The idea of Long-Base Neutrino Experiments (LBNE) has not been abandoned. The work on a high capable Long-Base Neutrino Facility (LBNF) and Deep Underground Neutrino Experiment (DUNE[6]) is continued in USA. The DUNE will be a dual-site experiment focused around two central components: (1) a high intensity neutrino beam and (2) two neutrino detectors, far and near, spaced apart by ∼1300 km. The near detector will be located at

[6]Formerly, before January 2015, known as Long Base Neutrino Experiment (LBNE).

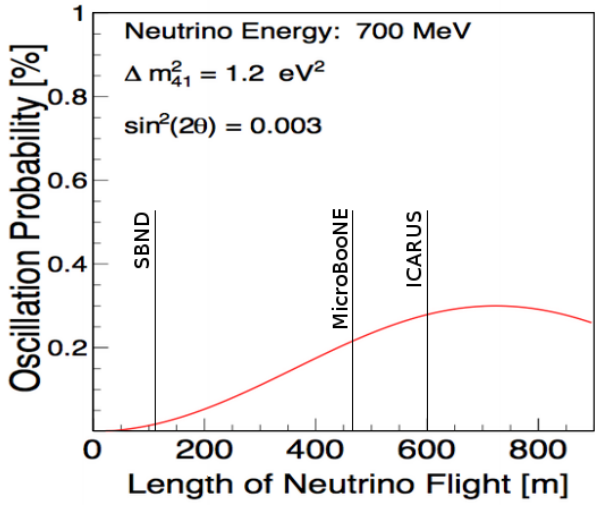

Figure 1.7: Neutrino oscillation probability for "3+1" model (LSND Best Fit - see Fig. 4.8, "3+1" model - see Fig. 4.5) versus distance from Fermilab booster neutrino source [42].

Fermilab, just downstream to the ν beam and its principal role will be to characterize the neutrino beam, before it travels to the far side. The far detector will be a massive LAr-TPC detector located deep underground at the Sanford Underground Research Facility (SURF; site of the former Homestake Mine in Lead, South Dakota, USA). Neutrino beam energy (Fig. 1.11 - left) will provide the optimal sensitivity to the neutrino charge-parity symmetry violation searches and neutrino mass ordering measurements [26]. A wide band neutrino beam is needed to cover the first and second $\nu_\mu \rightarrow \nu_e$ oscillation maxima, which are expected to be approximately at 2.4 and 0.8 GeV [46] for a 1300 km baseline (Fig. 1.11 - right).

1.5.6.1 DUNE far detector

The DUNE far detector will be installed 1475 meters underground, therefore the large amount of rock above will stop the vast majority of cosmic rays. The four cryostats of the far detector will hold a total of 68 ktons of liquid argon as the target material. The detector will consist of four cryogenic modules, each with 10 kt of fiducial mass. The schematic layout of four cryostats and supporting infrastructure is shown in Fig. 1.13. DUNE plans to construct the first module using the single-phase technology and the second one using the dual phase [13]. The choices for the third and fourth modules technology have not been decided on yet.

1.5.6.1.1 WA105

The WA105 collaboration (LBNO-DEMO) foresees the construction of a large scale prototype of dual phase LAr-TPC within CENF, to validate technical solutions and perform physics studies with charged particle beams in 2018. The final fiducial volume

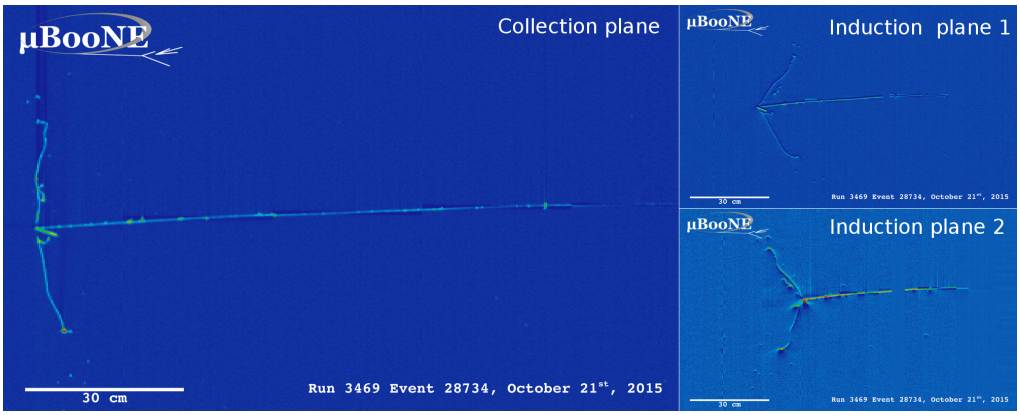

Figure 1.8: One of the first (November 2nd, 2015) neutrino interaction candidates recorded by the MicroBooNE detector after being exposed to the Fermilab BNB [43].

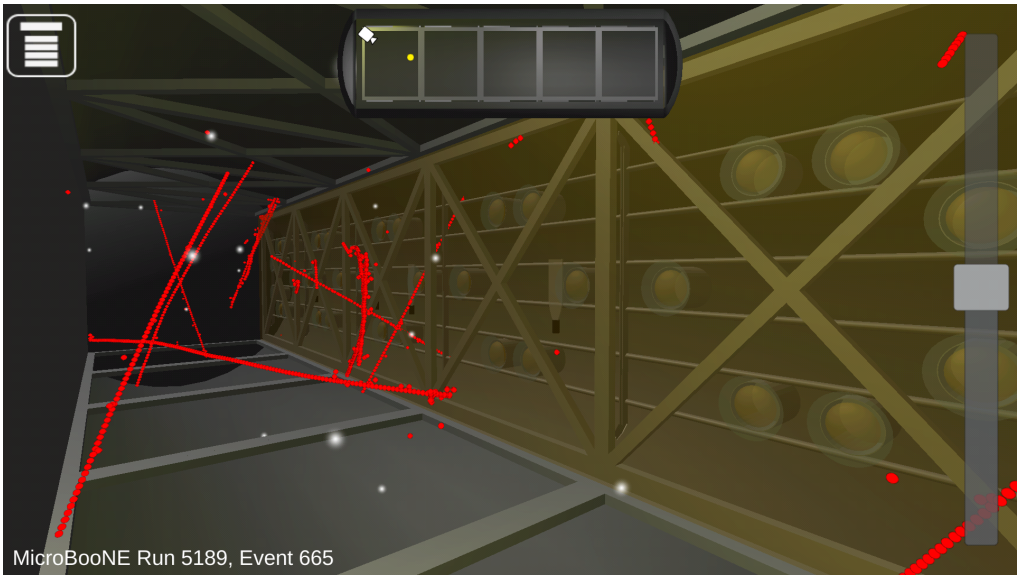

Figure 1.9: Screenshot from the VENu, mobile application. The development of VENu started in 2014, as the MicroBooNE team prepared to bring the detector online [44].

is $6 \times 6 \times 6\,\mathrm{m}^3$ (about 300 t of LAr). The smaller detector of volume $3 \times 1 \times 1\,\mathrm{m}^3$ (20 t of LAr) was constructed first. In 2017 WA105 became part of the DUNE prototyping effort known as protoDUNE-DP (DP stands for Dual Phase).

1.5.6.1.2 ProtoDUNE - NP02, NP04

There are two LAr-TPCs considered in ProtoDUNE project: a single (NP04) and dual (NP02) phase detector.

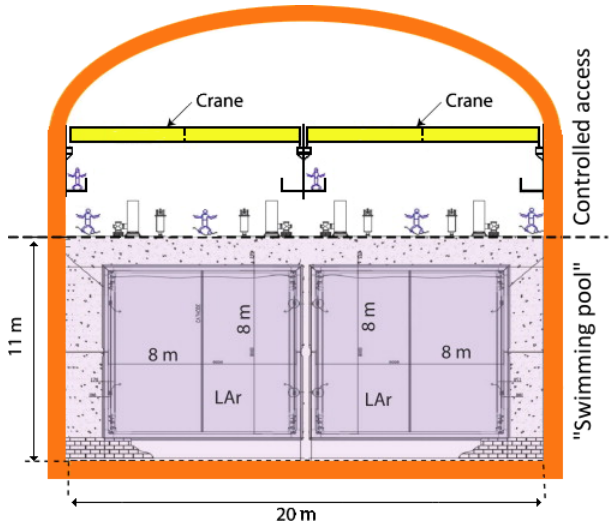

Figure 1.10: The concept of the MODULAr detector. Adapted from [45].

ProtoDUNE-SP (Single phase ProtoDUNE [49]): DUNE Far Detector prototype that is under construction and will operate within the CERN Neutrino Platform in 2018. Total liquid argon mass will be equal to 0.77 kt. The ProtoDUNE-SP TPC contains two adjacent drift volumes, sharing the central cathode plane that is flanked by two anode planes consisting of three parallel planes of sense and shielding wires oriented at different angles. Entire active volume is surrounded by a field cage held at -180 kV providing the 0.5 kV/cm drift field in the 3.6 m deep drift regions. The active volume is $6 \times 7 \times 7.2\,\mathrm{m}^3$. It is housed in an extension to the EHN1[7] hall in the CERN North Area.

ProtoDUNE-DP (Dual phase ProtoDUNE): The active volume ($6 \times 6 \times 6\,\mathrm{m}^3$) of the detector uses the same $3 \times 3\,\mathrm{m}^2$ Charge Readout Plane (CRD) units foreseen for the 10 kton Dual Phase DUNE Far Detector (Fig. 1.15). Maximum drift length is 6 m. The LEM (1 mm thick) electric field is of 25–35 kV/cm.

1.5.6.2 DUNE Near Detector

The leading design for DUNE Near Detector (DUNE ND) is the non-magnetized ArgonCube [51,52] (see section 1.5.7) version[8]. As a near DUNE detector it is to comprise 15 modules with overall cryostat dimensions $5 \times 7 \times 4\,\mathrm{m}^3$, with total LAr mass of ∼2.8 t per module. In addition, there will be a multi-purpose tracking (MPT) detector. The most likely option for the tracking technology is the magnetized straw-tube tracker (STT) or the magnetized high-pressure (argon gas) TPC.

It will be located at Fermilab, a few hundred meters downstream of the muon-neutrino

[7] CERN, building 887 CENF.

[8] The decision on near detector concept is to be made in the first half of 2018, the Conceptual Design Report in early 2019, wheres Technical Design Report in early 2019. When I started writing this chapter in September 2017, the DUNE ND detector concept was completely the opposite. The magnetized ArgonCube was the leading detector while STT was only an alternative.

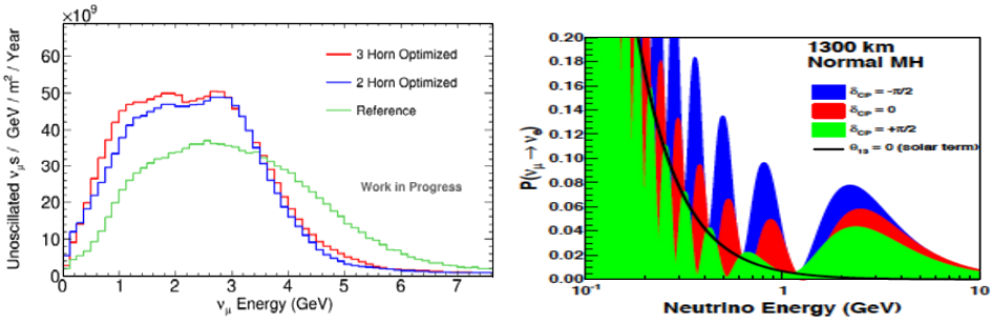

Figure 1.11: Left: Neutrino mode fluxes of muon-neutrinos from LBNF beam as a function of neutrino energy for the reference design and a 2-horn and 3-horn optimized design. Right: the $\nu_\mu \rightarrow \nu_e$ oscillation probability (maxima) as a function of neutrino energy for different values of the δ phase at the distance of 1300 km for normal mass hierarchy (MH) [47].

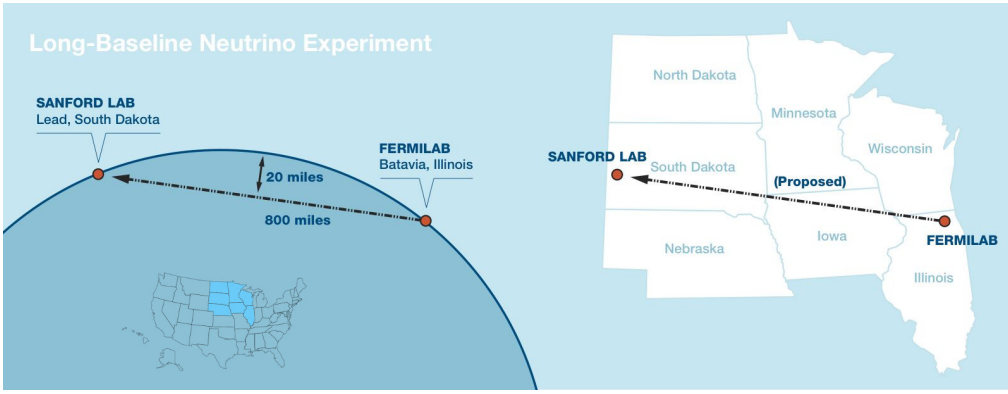

Figure 1.12: A diagram showing the 1300 km (∼800 mile) baseline of the DUNE experiment from the Fermi National Accelerator Laboratory near Chicago to the SURF in Lead, South Dakota. Adapted from [13].

beam. Its main role will be to characterize the neutrino beam at the production point.

1.5.7 ArgonCube

It is a novel LAr-TPC approach based on a fully-modular design, based on modules with dimensions of $2 \times 2 \times 3\,\mathrm{m}^3$, encased into a rectangular box with electrically transparent ∼1 cm thick walls made of fiberglass. Thickness of the walls can be small because individual modules do not have to hold a liquid hydrostatic pressure higher than a few tens of millibar during the detector operation. This allows to keep the amount of inactive material at a level of few percent of the total detector-target mass. The ArgonCube module featured a double-drift volume configuration with an aluminum cathode at the center of the chamber biased to -100 kV and two mirrored drift volumes on either side. The maximum drift length is 1–2 meters. The drift field cage is made of a number of

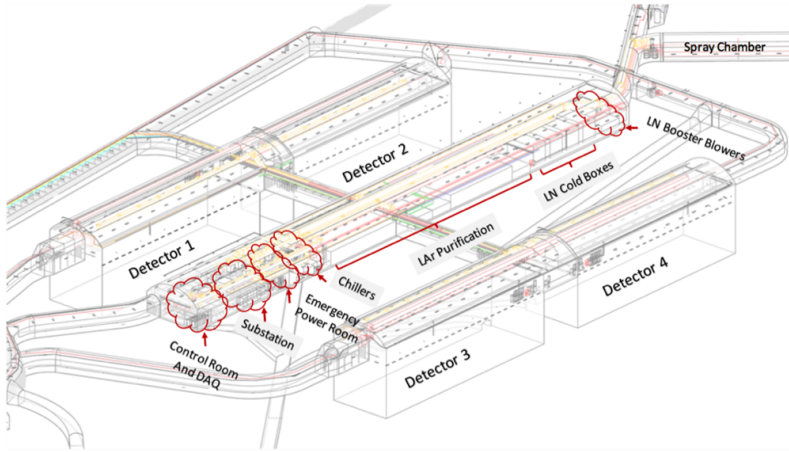

Figure 1.13: The scheme of location of the four cryostats and the supporting infrastructure of the DUNE far detector [48].

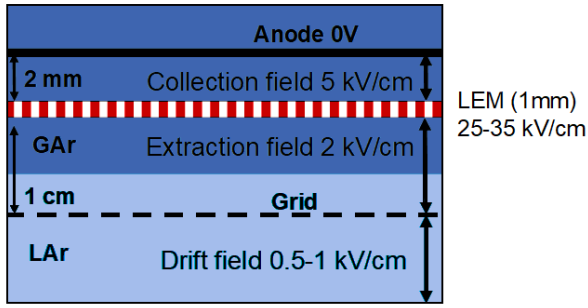

Figure 1.14: The principle of the dual phase LAr detector. The values shown refer to the ProtoDUNE-DP detector. Adapted from [35].

field-shaping loops electrically biased via a resistive divider. The schematic view of the basic module of ArgonCube is shown in Fig. 1.16. More details of the ArgonCube design can be found in [51, 52].

1.5.8 LAGUNA-LBNO, GLACIER

LAGUNA-LBNO is a design of a Pan-European infrastructure for **L**arge **A**pparatus studying **G**rand **U**nification and **N**eutrino **A**strophysics for **L**ong **B**aseline **N**eutrino **O**scillation. The project addresses the feasibility of a new European research infrastructure hosting a deep underground neutrino detector designed for fundamental research in astrophysics and particle physics. The scientific goals of the project are related to the frontiers of particle physics and astrophysics with extended scientific capabilities, such as: (1) determination of the neutrino mass hierarchy, (2) understanding the origin of matter dominance in the Universe, (3) discovery of the CP-violation in the leptonic sector,

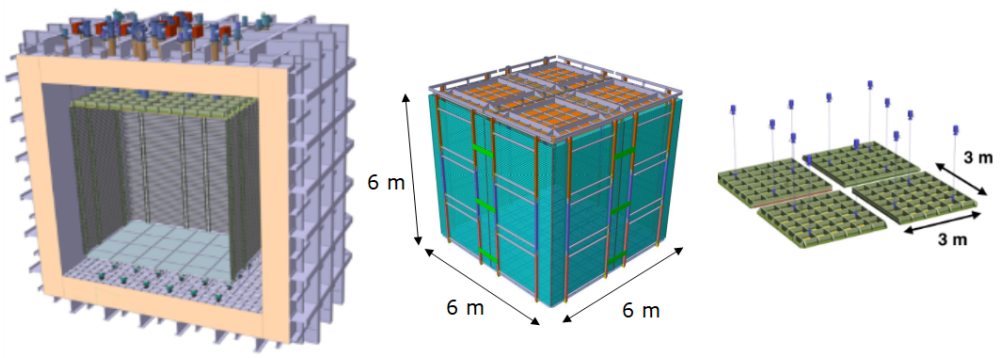

Figure 1.15: The scheme of the ProtoDUNE-DP detector. Left: Detector-cryostat integration. Middle: detector unit. Right: 4 CRDs. Adapted from [50].

(4) execution of a broad neutrino astrophysics program with a large scale detector and finally (4) searches for new physics beyond the Standard Model. The project assumed exploiting the neutrino beam from CERN. Three sites were recommended to host detector, with increasing priority: Umbria in Italy at distance about 670 km from CERN, Fréjus in France at 130 km and Pyhäsalmi in Finland at 2300 km. Simultaneously with detector underground location three various detector technologies were studied: (1) Water Cherenkov, (2) Liquid Scintillator and (3) LAr-TPC. The location for the LAr-TPC was proposed at Pyhäsalami [53]. The LAr-TPC detector concept for LAGUNA-LBNO consists of a single non-evacuable cryo-tank module based on industrial liquefied natural gas technology, with masses up to 100 kton. The initial phase of LBNO considers one, 20 kton detector called GLACIER, hosting a magnetized iron calorimeter (MIND [54]).

1.5.8.1 GLACIER

GLACIER stands for **G**iant **L**iquid **A**rgon **C**harge **I**maging **E**xpe**R**iment. It is a proposed giant, multi-purpose, next-generation dual phase liquid argon detector (LAr LEM-TPC) scalable up to masses of 100 kton [34,55,56] in the shape of the flattened tube with height of about 20 m and diameter of about 70 m (Fig. 1.17), with a strong vertically-oriented electric field. The main features of the detector are the following: (1) total argon volume: 73118 m^3 (102365 tons), (2) hydrostatic pressure at bottom: ∼2 atm, (3) maximum electron drift length: 20 m, (4) electric field: $HV = 2$ MV for $E_d = 1$ kV/cm ($V_d \approx 2$ mm/μs, maximum drift time $t_d \approx 10$ ms) (5) scintillation light readout: 1000 immersed WLS[9]-coated 8 PMTs, (6) visible light readout (option) 27000 immersed 8 PMTs, (7) charge readout views: LEM-TPC with 2 independent perpendicular views, 3 mm pitch.

[9] Wavelength shifter.

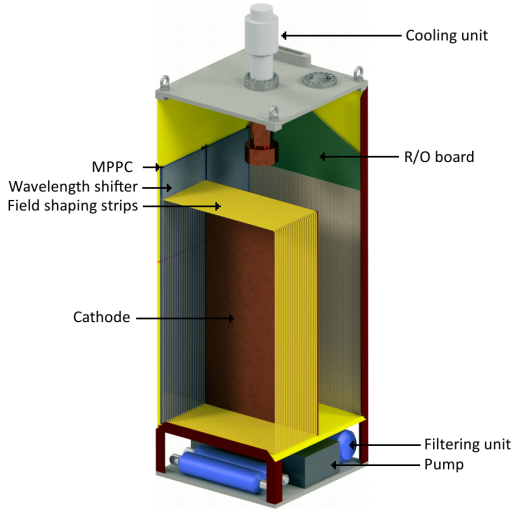

Figure 1.16: Schematic design of the ArgonCube basic module. Filters and a recirculation pump are housed in the base. The instrumented volume is divided into two TPCs by a cathode running across the center of the module. The multi-pixel photon counters (MPPC) mounted on opposing walls of the module (only one shown). Adapted from [51, 52].

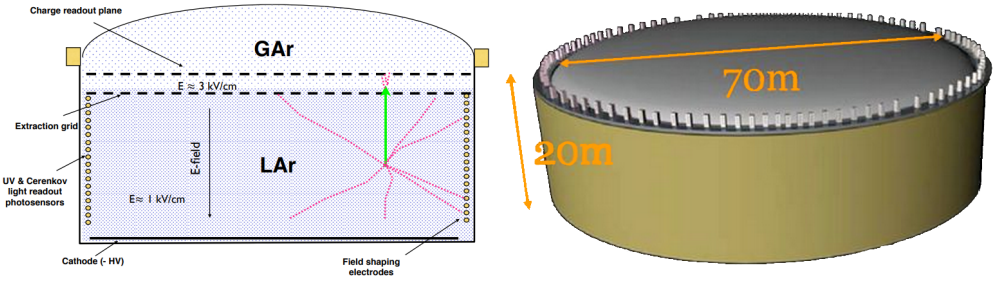

Figure 1.17: Sketch of the double phase GLACIER detector. Adapted from [34, 57].

1.5.9 Okinoshima 100-kt

It is a proposition of the next generation, single, far LAr-TPC detector with volume of LAr about of 100 kton e.g. of a kind based on the GLACIER concept. The proposed localization at shallow depth, coupled to the J-PARC neutrino beam facility with 30–50 GeV the Main Ring Synchrotron (MR). The detector could be located in three places: (1) the region of Okinoshima island with baseline about 658 km, (2) Kamioka (baseline ∼295 km), or (3) eastern Korean coast (baseline ∼1025 km). It will aim to measure the θ_{13} and δ_{CP} parameters and exploration of the proton decay existence. The detector will see the J-PARC neutrino beam at an off-axis angle of: ∼0.8° at Okinoshima, ∼2.5° at Kamioka and ∼1.0° on the eastern Korean shore. The detector should allow to study

both 1st and 2nd oscillation maximum peaks with good statistics [58].

1.5.10 ArDM

The Argon Dark Matter (ArDM-1t) experiment is a ton-scale LAr double-phase time projection chamber designed for direct dark matter (WIMP[10]) searches via elastic scattering from argon nuclei. A 1-ton detector was initially installed on the surface at CERN (2006–2012) to fully test all its functionalities. Currently, the detector is located at the experimental hall of the Laboratorio Subterráneo de Canfranc (LSC) excavated in the rock, 850 m deep under the Mount Tobazo on the Spanish side of the Aragon Pyrenees [59]. It has a diameter of 80 cm and a maximum drift length of 120 cm. In December 2017 ArDM reached a successful dual phase operation phase [60].

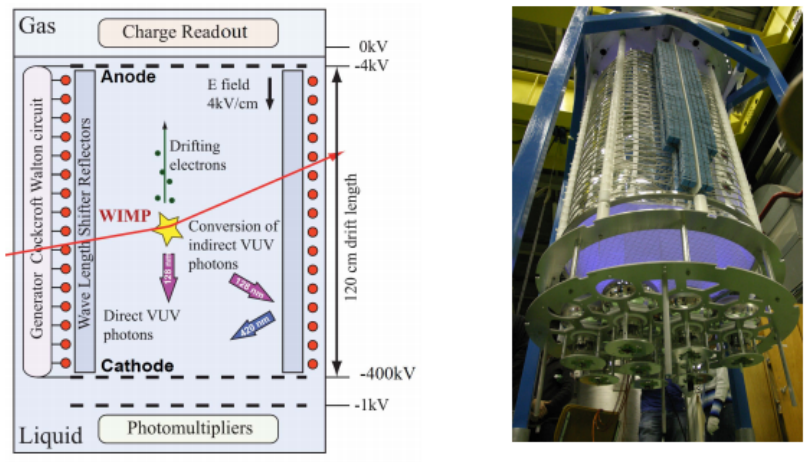

Figure 1.18: Left: Conceptual layout of ArDM. Right: View of the ArDM detector from bottom. Adapted from [60].

1.5.11 DarkSide detectors

DarkSide detectors are a series of dual phase argon TPCs designed for searching a rare nuclear recoils, possibly induced by the WIMP. They are built (will be built) using low-background techniques and materials, filled with low-radioactivity underground argon (UAr). DarkSide-10 was the first built detector in the series [61], with an active volume of 10 kg of liquid argon and localized at Gran Sasso, Italy.

The second one, DarkSide-50 [62] (Fig. 1.19) with a 46.4 ± 0.7 kg active mass, operates inside a 30 t organic liquid scintillator neutron veto, which is in turn installed at the center of a 1 kt water Cherenkov veto for the residual flux of cosmic rays. Based on the successful experience in operating the DarkSide-10 and currently working DarkSide-50, the DarkSide Collaboration is going to construct a giant dual phase LAr-TPC detector

[10] Weakly Interacting Massive Particles.

called DarkSide-20k. It will be an another direct WIMP search detector with an active mass of 23 t. The detector will be deployed within a spherical Liquid Scintillator Veto (LSV), inside a cylindrical Water Cherenkov Veto (WCV). It will be localized at LNGS, Gran Sasso. The argon used in the detector will be extracted from a deep underground source, which guarantees low ^{39}Ar contamination, being the dominant source of background[11]. Additionally argon will be purified in an ARIA plant [63], a 350 m tall purification column. The purification will be done using a standard distillation process. The ARIA tower will be installed in a disused shaft of a coal mine on Sardinia, Italy. More about DarkSide-20k and ARIA can be found in [63, 64].

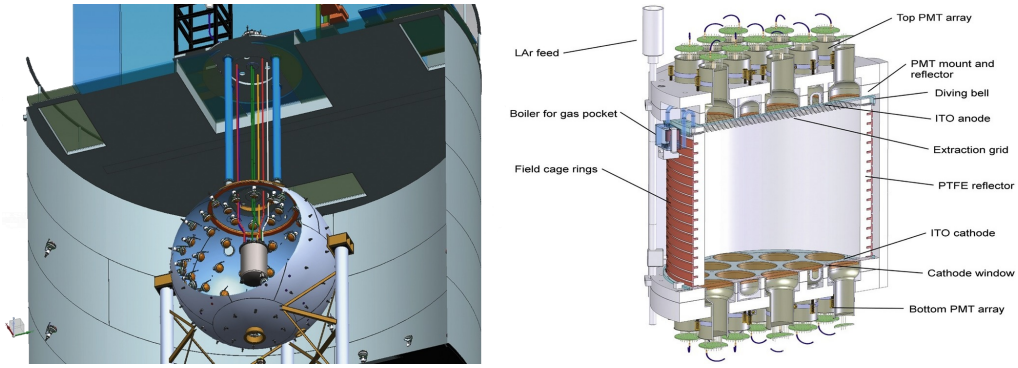

Figure 1.19: DarkSide-50 detector systems. Left: The nested system containing: (1) the outermost grey cylinder is the WCV, (2) the sphere is the LSV and (3) the grey cylinder at the center of the sphere is the LAr-TPC cryostat. Right: LAr-TPC cryostat. Adapted from [62].

1.5.12 WARP, WArP

The WARP means **W**imp **AR**gon **P**rogramme. The WARP is a double phase liquid argon detector, aimed at the unambiguous identification of the WIMPS by means of the detection of nuclear recoils in liquid argon. These particles may produce, via weak interactions, nuclear recoils in the energy range 10–100 keV. The proposed technique combined the experience and the tools developed for the ICARUS experiment for: (1) handling ultra-purified liquid argon and (2) detecting the argon scintillation light. At the beginning of the century, the first 2.3 liters prototype was built. The 100 l detector is the last iteration of the project: it consists of an inner double phase chamber, which is surrounded by a larger volume of LAr. Such configuration serves as anticoincidence to reject all those events producing a signal in both volumes. It is a unique feature, for the first time introduced by the WARP program, to effectively eliminate spurious nuclear-recoil signals, produced by neutron elastic scatterings. The detector has been installed underground in Hall B of the Gran Sasso laboratory [65–67].

[11] The UAr has been shielded from cosmic radiation for many half-lives of ^{39}Ar (269 years, beta decay) and therefore is expected to be very low in the isotope.

1.5.13 ARIADNE

ARIADNE[12] (**AR**gon **I**m**A**ging **D**etectio**N** chamb**E**r) is the next detector that benefits from the ability to detect the particles that liquid argon provides. It is a Photographic LAr-TPC within the CENF. The detector uses a novel approach to the detection of particles using Electron Multiplying CCD (EMCCD) technology. Essentially, the EMCCD, sometimes known as *on-chip multiplication*, is an image sensor that is capable of detecting single photon events without an image intensifier, achievable by way of a unique electron multiplying structure built into the chip. It is an alternative readout method to the currently accepted segmented LEMs (Large Electron Multiplier) or THGEMs (THick Gaseous Electron Multiplier) which require many thousands of charge readout channels for kton-scale dual phase LAr-TPCs.

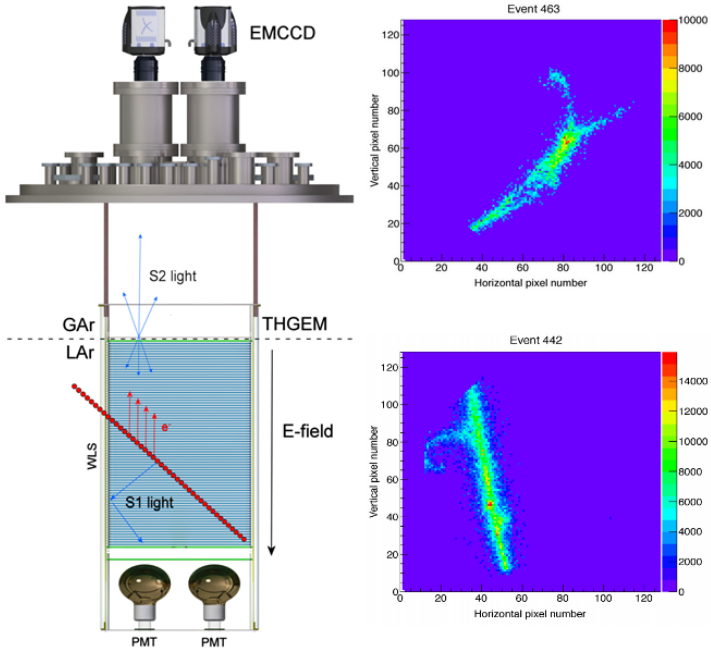

Figure 1.20: Left: A section through the ARIADNE LAr-TPC. Right: Typical 2D images captured on an EMCCD of the secondary emission derived from the passage of a cosmic muon through the detector. Adapted from [68].

ARIADNE will be a 1-ton dual phase LAr-TPC utilizing THGEM and EMCCD camera readouts. The operation principles of dual phase LAr-TPC (THGEM) with EMCCD differ a little from the previously presented approach for dual phase LAr-TPCs. The charged secondary particles traveling through LAr cause the liquid argon to scintillate, producing light (in the UV range), detected by the PMTs. By default, in LAr-TPCs, this signal (S1 in Fig. 1.20, called *prompt* scintillation) is used as a timing reference to mark the start of an event. The ionized electrons, generated during an interaction

[12] The name of the Greek mythological goddess who helps to find a way out.

of primary or secondary charged particles with argon nuclei, are drifted through the liquid phase to the gas phase, where they produce secondary delayed electroluminescence light. When the multiplication process takes place inside THGEM, the avalanche of electrons is produced and the secondary scintillation emission occurs as a result of electroluminescence. In the traditional approach, the amplified electrons are collected by a segmented anode at the top/side of the gas chamber. In the novel ARIADNE approach the high sensitivity EMCCD cameras detect emitted light (S2 in Fig. 1.20), resulting in the creation of the 2D images of the emission. The pulses from the PMTs, the electronic signals from the segmented THGEM and the EMCCD images allow for the 3D track reconstruction and also for the extraction of calorimetric information on the energy of the particles [68]. This technology has already been demonstrated at the Liverpool LAr facility with the photographic capturing of cosmic muon tracks and single gammas using a 40-liter ARIADNE prototype.

1.5.14 LANNDD

The next two described detectors had never gone beyond the stage of plans, however, they are particularly interesting due to the attempt at using a magnetic field in a liquid argon detector. The proposal to construct these detectors dates back to the beginning of the twentieth century, before the successful operation of the first huge LAr-TPC - ICARUS T600 detector.

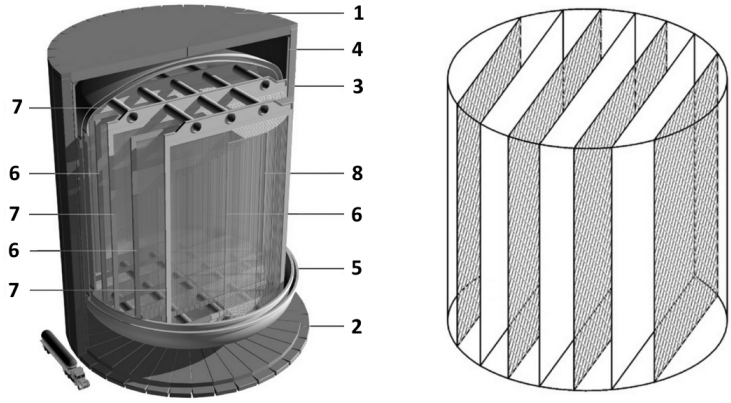

Figure 1.21: Left: Sketch of LANNDD: (1) top end cap iron yoke, (2) bottom end cap iron yoke, (3) barrel iron return yoke, (4) coil, (5) cryostat, (6) cathodes, (7) wire chamber frames and (8) field shaping electrodes. Right: Schematic layout of chamber (hatched regions) and cathodes planes (white regions). Adapted from [38].

The LANNDD (**L**iquid **A**rgon **N**eutrino and **N**ucleon **D**ecay **D**etector) was supposed to be a 70 kt magnetized LAr-TPC. Much of the scientific studies concerning LANNDD affected the final success of ICARUS detector program.

It was planned that LANNDD could observe neutrinos from any of the possible neutrino sites: (1) BNL[13] (2839 km baseline), (2) FNAL (1691 km), (3) CERN (8097 km)

[13] Brookhaven National Laboratory, USA.

and (4) KEK[14] (9073 km). Three configurations of the detector were considered: (1) single module, with active (fiducial) volume of LAr 50 m^3 (∼41.3 m^3), (2) 8 modules (active: as previous, fiducial: ∼33.6 m^3) and (3) 64 modules (active: as previous, fiducial: ∼21 m^3). The configuration and internal structure of the detector was relied to the maximum usable electron drift distance. For 8 modules and at 0.5 kV, electron lifetime of 5–10 ms and a maximum drift of 5 m between cathode plane and wire chamber (compare to ICARUS T600 achievements - section 2.4). The wire chamber consisted of 2 readout planes, oriented 0° and 90° (alternatively ±45°) w.r.t. the horizontal plane, with 3 mm wire pitch. The detector was foreseen to be located 655 m underground.

1.5.14.1 Mini-LANNDD T40

Mini-LANNDD T40 was supposed to be a 40 ton small version of the LANNDD detector (38.5 t active mass) LAr-TPC with a magnetic field, to be used in the NuMI beam, in the vicinity of the LANNDD project.

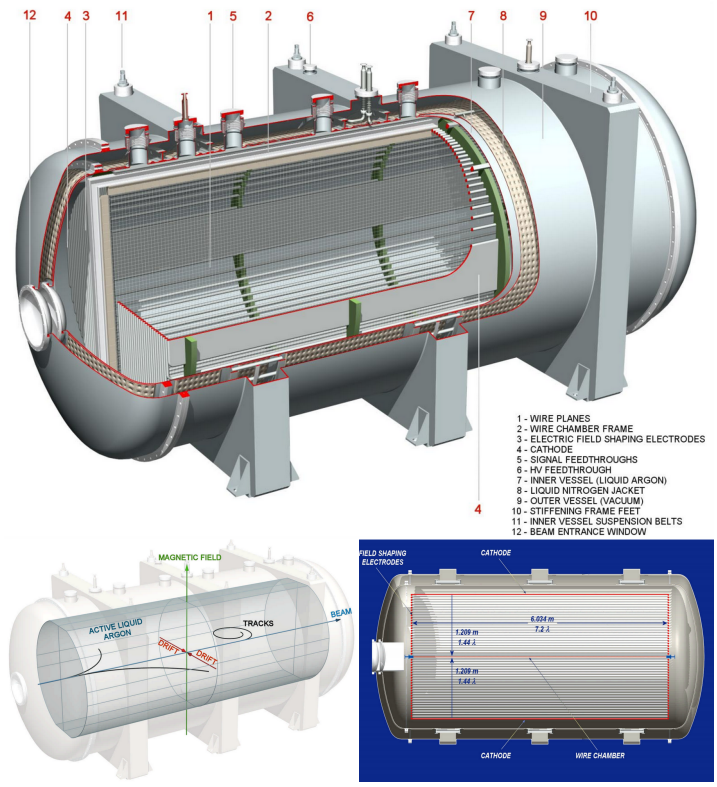

Figure 1.22: Left: Cutaway view of the vacuum insulated and liquid nitrogen (LN_2) cooled Mini-LANNDD T40 cryostat. Right: Mutual orientation of electric field (drift directions), magnetic field and beam axis for an optimum reconstruction of bent tracks. Adapted from [69].

[14] Kō Enerugī Kasokuki Kenkyū Kikō - High Energy Accelerator Research Organization, Japan.

It was planned to be a near or vertex detector in neutrino beam, configured with: (1) cylindrical LAr volume (total: 42.2 m^3, GAr: 0.9 m^3), with horizontal axis, (2) 2 drift regions, (3) 2 × 1.2 m drift length, (4) 2 cathode planes, (5) 0° and 90° orientation of readout wires, (6) active liquid argon size: 2.4 (width) × 2.3 (height) × 6.0 (length) m^3 and (7) number of readout wires of 5632. The tracks bent in a magnetic field (Fig. 1.23). In case of operation on a particle beam, the magnetic field had to be orthogonal to the beam axis [69].

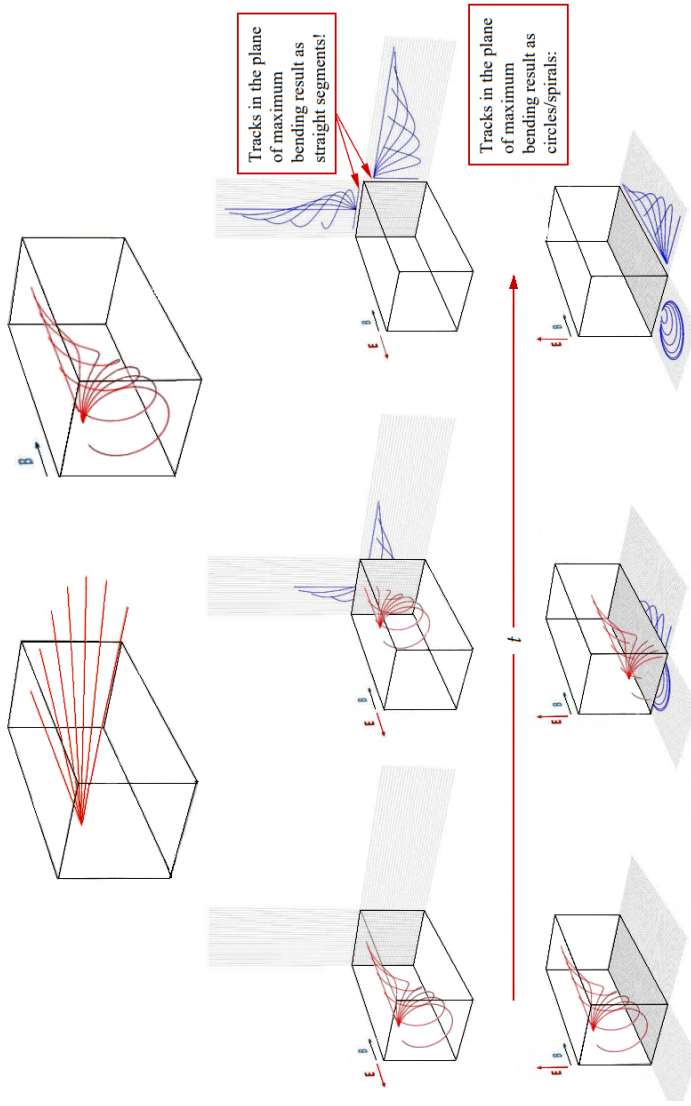

Figure 1.23: Simulated view of the tracks from magnetized Mini-LANNDD T40, with their projection on the planes of wires. Adapted from [69].

Chapter 2

ICARUS T600 - a single phase Liquid Argon TPC

The ICARUS Collaboration has developed the LAr-TPC technology from prototypical dimensions to the mass of 760 tons of liquid argon with the so-called T600 detector [8] (see Fig. 2.1), installed in the underground INFN-LNGS[1] Gran Sasso Laboratory. In the following chapters the main features, working principles, the most important parameters and performance tests of the ICARUS T600 detector are described.

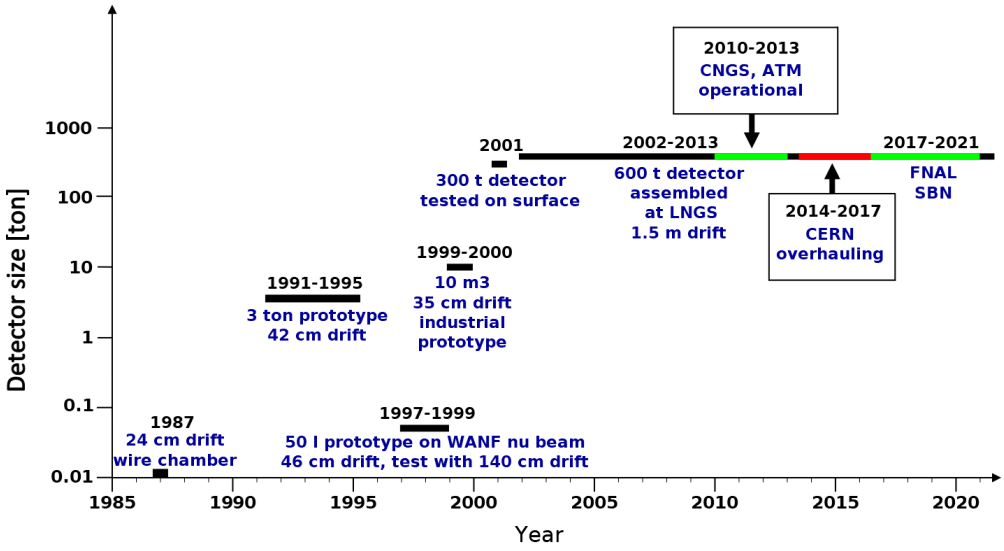

Figure 2.1: The ICARUS R&D steps towards kton size LAr detector.

[1] **I**nstituto **N**azionale di **F**isica **N**ucleare - **L**aboratori **N**azionali del **G**ran **S**asso.

2.1 Detector overview

The ICARUS T600 (Fig. 2.2) module comprises a large cryostat splitted into two identical, adjacent half-modules. Their internal dimensions are $3.6 \times 3.9 \times 19.6\,\mathrm{m}^3$. Each is filled with about 380 tons of ultra-pure liquid argon. Each half-module (called East and West) houses: (1) two Time Projection Chambers (TPC) which share a common cathode in the middle, (2) a field shaping system, (3) two arrays of photomultiplier tubes (PMT) and (4) monitors and probes. Each TPC is made of three parallel planes of wires, 3 mm pitch and plane spacing, facing the drift region, with wires oriented vertically at 0° and ±60°. Globally, 53248 wires with length of up to 9 m are installed in the detector. By appropriate voltage biasing, the first two planes (called 'Induction 1' and 'Induction 2') provide signals in a non-destructive way. The third 'Collection' wire plane finally collects the charge. The distance between the cathode and the wire planes (the maximum electron drift path) is 1.5 m. The nominal electric field is equal to $E_d = 0.5\,\mathrm{kV/cm}$. The signals from each wire are independently digitized every 400 ns.

Position of a track along the drift coordinate is determined by combining the knowledge of the electron drift velocity $V_d \sim 1.6\,\mathrm{mm}/\mu\mathrm{s}$ at $E_d = 0.5\,\mathrm{kV/cm}$ and the measurement of the absolute time of an ionizing event. The last one is determined via the prompt scintillation light produced by charged particles in LAr. For this purposes a total of 20 and 54 PMT's (ETL 9357FLA photomultiplier tubes [70], Fig. 2.3 and section 2.5.1) are immersed in the LAr in the West and East cryostats, respectively, deployed along three horizontal rows behind the TPCs wire planes. To detect the prompt photon emission in the vacuum-ultraviolet (VUV) spectrum with $\lambda = 128\,\mathrm{nm}$ produced by charged particles interacting in the LAr volume, the PMT windows are coated with wavelength shifters (here tetra-phenyl-butadiene (TPB[2])).

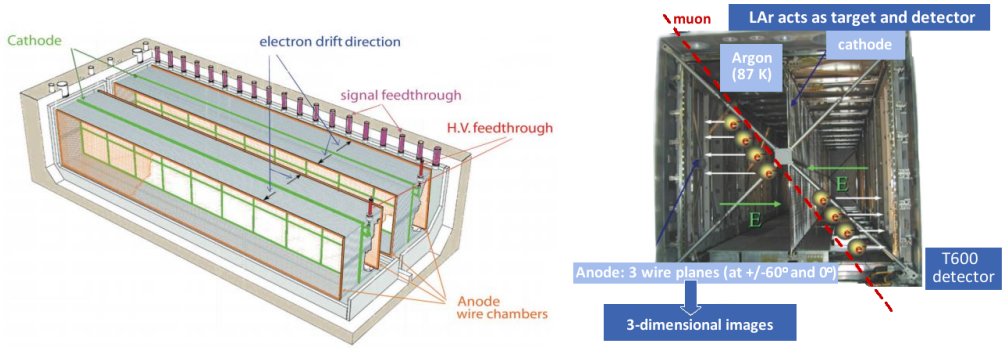

Figure 2.2: Scheme of the detector (left) and a picture of the LAr-TPC with an artistic view of the working principle (right). Adapted from [25].

The electronics was designed to allow continuous readout, digitization and independent waveform recording of signals from each wire of the TPC. The overall gain is about 1000 electrons per ADC count, setting the signal of minimum ionizing particles (m.i.p.)

[2]IUPAC (International Union of Pure and Applied Chemistry) name: 1,1,4,4-tetraphenyl-1,3-butadiene. It glows blue with an emission spectrum peak wavelength at 430 nm.

Figure 2.3: The ETL 9357FLA photomultiplier: 12-stage LF-dynode PMT with an hemispherical glass window of 200 mm diameter. Length and diameter: 293 mm; 203 mm. Maximum gain: $5{\cdot}10^7$ at HV=1.5 kV. Cathode type: K_2CsSb on Pt layer. Spectral response: 300–500 nm. Adapted from [70].

to ∼15 ADC counts with a dynamic range of about 100 m.i.p. The average electronic noise was measured to be well within expectations on practically all channels: 1500 electrons r.m.s. to be compared with ∼15000 free electrons produced by m.i.p. in 3 mm (S/N ∼ 10). The obtained spatial resolution is ∼1 mm^3. Identification of protons, kaons, pions and muons is obtained through energy deposited per track length unit (dE/dx) versus particle range and by studying the decay/interaction topology. Electrons are identified by their characteristic electromagnetic showering (Fig. 2.4). They can be, at the level of per-mil, distinguished from gammas by dE/dx comparison on the first few wires (Fig. 2.5).

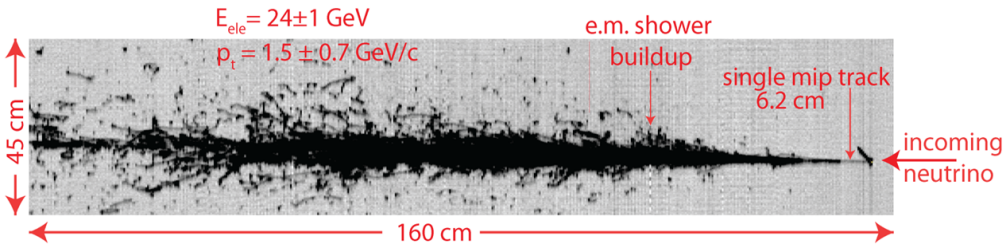

Figure 2.4: An example event with clear electron signature. The evolution of the actual dE/dx from single track to electromagnetic shower is clearly visible (see Fig. 2.5). First segment of the developing cascade comes from a single m.i.p. ($dE/dx < 3.1$ MeV). See also: Fig. 4.22 and section 4.4.2.

The main features of the TPCs inner detector can be found in Tab. 2.1, whereas Fig. 2.6 shows wire planes in TPC.

2.2 The dimensions of the ICARUS T600 detector

The size of the inner and active (instrumented) volume of T600 cryostat is given in Tab. 2.2. The active volumes are defined as the parallelepipeds with the side surfaces equal to the wire chamber surface and with width equal to twice the distance between

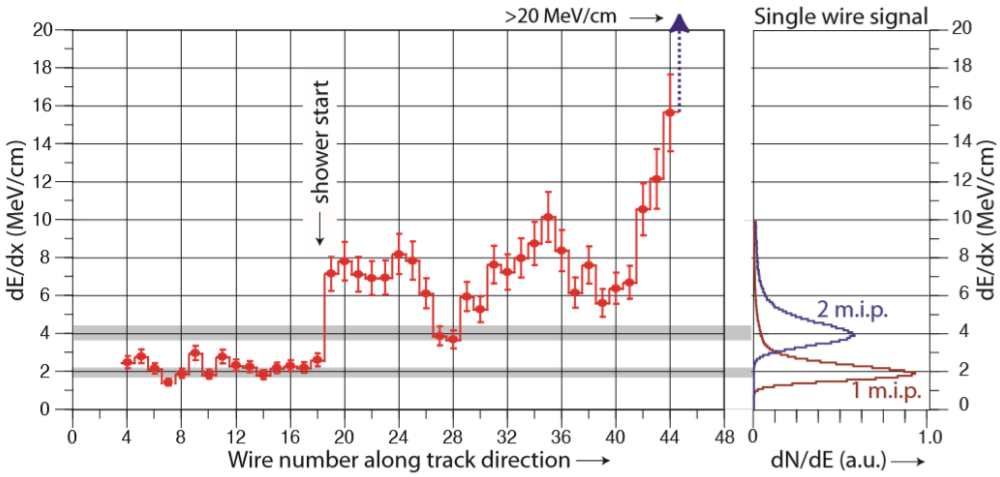

Figure 2.5: The evolution of the dE/dx from a single track to an electromagnetic shower for an electron along individual wires is shown (see also Figs. 2.4 and 4.22).

the first wire plane (0°) and the cathode. The Cartesian reference frame is shown in Fig. 2.7.

The fiducial volume (FV) is defined by subtracting from the instrumented volume (IFV = length × width × height = 17.95 × 3.165 × 1.482 m^3 = 84.195 m^3) of each TPC chamber 20 cm in the longitudinal beam direction (5 cm upstream and 15 cm downstream), 3 cm in the horizontal direction (1.5 cm per side) and 4 cm in the vertical direction (1.5 cm per side and 0.5 cm from cathode). As a result, the scanning fiducial volume is SFV = 4 × (17.75 × 3.125 × 1.452 m^3) = 322.162 m^3. It corresponds to fiducial mass exposed to CNGS beam: SFM = SVF $\times \rho_{LAr}$(90 K) = 322.162 × 1.383 t/m^3 ≃ 445.5 t. It assumes no failure of detector components resulting in the reduction of active volume of the detector (see section 4.4).

2.3 Cryogenic plant

The ICARUS T600 cryostat was composed of two identical adjacent aluminum containers for LAr (East and West module). Both modules have independent argon content and are purified separately in two purification plant, however they have a common cooling shield and insulation vessel. Both T600 half-modules are surrounded by thermal insulation in the shape of evacuated honeycomb panels in order to ensure a tight contained vessel [8]. Between the insulation and the aluminum containers a thermal shield is placed. Boiling nitrogen circulates inside the shield to intercept the heat and maintain uniform (within 1 K) and stable (at 89 K) temperature in the cryostat volume. Liquid nitrogen used to cool the modules is stored in two tanks placed at the top of the detector ($2 \times 30\ m^3$ of LN_2). The temperature inside the tanks was set by maintaining the pressure of ∼2.1 bar (corresponding to the temperature of about 84 K). At the beginning of T600 detector operation the two half-modules were cooled down to 90 K in about 8 days while

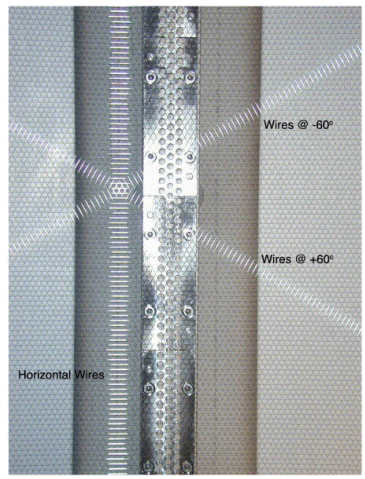

Figure 2.6: The three wire planes of the ICARUS T600 detector.

injecting ultra-pure argon gas to ensure uniform temperature throughout the detector volume. As the next step both cryostats were filled with commercial LAr, at the rate of $\sim$1 m^3/hour/cryostat. Liquid argon was delivered with 47 trucks in about 2 weeks for a total amount of 610511 liters. It was purified in-situ before entering the detector. During the whole period the four gaseous re-circulation systems were operating at maximum speed to intercept the impurities which could have come from degassing components of the detector. One month after filling, the forced liquid argon recirculation and purification started on both cryostats at the rate of 1 m^3/hour/cryostat. The ICARUS T600 cryostat was designed in partnership with the Air Liquide Italia Company. In Fig. 2.8 an artistic view of the T600 detector with the cryogenic plant is shown.

2.4 Purification of LAr and ionizing electrons lifetime

The key requirement of a LAr-TPC operation is extremely high liquid argon purity which is needed to transport ionization electrons over macroscopic distances with small attenuation. The presence of impurities (most of all O_2, but also H_2O and CO_2) cause electrons trapping and lead to the exponential electron signal attenuation along the drift coordinate. Therefore the level of electronegative impurities in LAr must be kept exceptionally low to ensure $\sim$m long drift path of ionization electrons. The residual compounds with high electron affinity have to be kept as low as 0.1 parts per billion (ppb) all over the argon volume during the data taking, allowing the ionization electrons to be transported practically undistorted to a multi-wire anode plane placed at the end of their drift path. It requires continuous recirculation, filtering and purification of liquid argon. The solutions invented by the ICARUS Collaboration for the argon recirculation and purification systems, permitted to reach an extremely low level of electronegative impurities. The measured content of O_2-equivalent contamination was less than 40 parts per trillion (ppt) measured with cosmic muons (12% maximum charge attenuation on

Table 2.1: The main features of the T600 TPCs inner detector [8].

Numbers of read-out chambers (TPC) in T600	4
Number of wire planes per chamber	3
Distance between wire planes	3 mm
Wire orientation with respect to horizontal	0°, ±60°
Wire diameter	150 μm
Wire length	
Horizontal wires	9.42 mm
Wires at ±60°	3.77 m
Wires at the corners (±60°)	3.81–0.49 m
Wire pitch (normal to the wire direction)	3 mm
Wire capacitance Ind.-1, Ind.-2, Coll.	20, 21, 20 pF/m
Wire nominal tension	12 N (5 N for horizontal wires)
Number of wires/wire module	32
Number of wire modules/chamber	
Horizontal wires	66
Wires at ±60°	2×145
wires at the corners (±60°)	2×30
Number of wires/chamber	
Horizontal	2112
at ±60°	2×4640
at the corners (±60°)	2×960
Total	13312
Total number of wires in T600	53248
Wire plane voltage biasing (typical)	-220 V, 0 V, +280 V
Cathode HV (nominal)	75 kV
Cathode to Collection plane distance	1.5 m
Sensitive volume/chamber	85 m^3
Length	17.95 m
Width	1.5 m
Height	3.16 m
Maximum drift length in LAr	1482 mm
Maximum drift time in LAr (at nominal field)	950 μs

Table 2.2: Dimension of the inner and active volumes for each T300 half modules.

Inner	length	$L_I = 19600$ mm	$V_I = 275.2\,m^3$
	width	$W_I = 3600$ mm	
	height	$H_I = 3900$ mm	
Active	length	$L_A = 17958$ mm	$V_A = 168.5\,m^3$
	width	$W_A = 2964$ mm	
	height	$H_A = 3165$ mm	

1.5 m). This corresponds to a free electron lifetime $\tau_e > 7$ ms (see Fig. 2.9). In order to reach such a level of purity the commercial argon filters, Hydrosorb^{TM} and Oxysorb^{TM}, operating directly in the liquid phase were used for water and oxygen removal.

After upgrade of the detector infrastructure (installation of a new non-immersed pump in the East cryostat) in April 2013 the measured content of O_2-equivalent contamination dropped down to less than 20 ppts and corresponded to $\tau_e > 15$ ms (Fig. 2.9). This indicates the importance of the purity of liquid argon and demonstrates that even several meters long ionizing electron drift paths in LAr are achievable. It also shows the effectiveness of the single phase LAr-TPC detection technique paving the way to huge detectors with longer drift distance as required for e.g. the LBNF/DUNE project

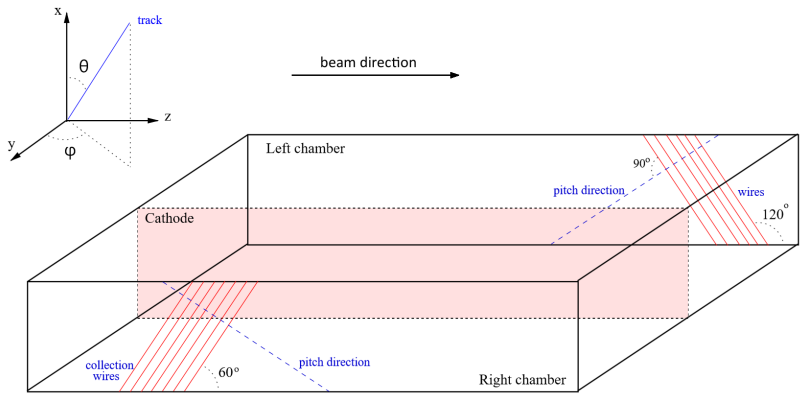

Figure 2.7: Sketch of the half module (IL, West, T300) of the ICARUS T600 detector, including Collection wire directions and the Cartesian reference frame: z - longitudinal (along beam direction), x - vertical and y - along drift direction [71].

(see section 1.5.6). The details of the electron lifetime and signal attenuation measurement can be found in [30], while cryogenic and purification systems are widely described in [73].

2.5 Trigger system of the ICARUS T600 detector

The ICARUS T600 trigger consists of three main components: (1) Photomultiplier Tube (PMT) system, (2) S-Daedalus system and (3) synchronization with CERN SPS proton extraction. The last component has been set up including the prediction of the CERN SPS proton beam extraction time provided by an "early warning" message sent from CERN to LNGS before each CNGS proton extraction, with order of nanosecond resolution. The jitter between the predicted and the actual proton extraction time was limited to 20 μs. The message was sent via an UDP[3] packet. The synchronization with the CNGS neutrino beam was achieved by means of a common GPS[4] time base, shared at the CERN and LNGS sites and by "early warning" message, which allows generating on-line a CNGS-gate signal in coincidence with the arrival of neutrinos. The details of the trigger components can be found in [76].

2.5.1 Photomultiplier Tube system

The ICARUS T600 trigger exploits scintillation light emission in LAr, produced in the radiative decay of excited molecules of Ar_2^* produced by ionizing particles. The released monochromatic VUV photons ($\lambda \sim 128$ nm) come from transitions from the

[3]User Datagram Protocol. With UDP, computer applications can send messages to other hosts on an Internet Protocol (IP) network. Prior communication is not required in order to set up communication channels or data paths [74].

[4]Global Positioning System. GPS is a satellite navigation system used to determine the ground position of an object [75].

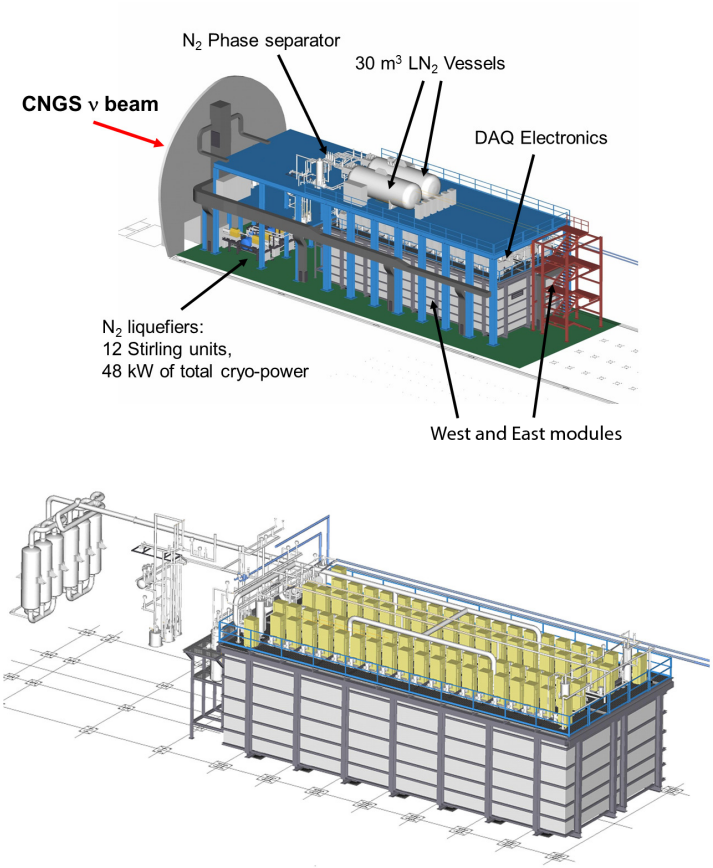

Figure 2.8: Top: Schematic view of the ICARUS T600 plant in the Hall B at LNGS. Bottom: Schematic view of the T600 cryostat with representation of the electronic racks and gaseous argon re-circulation systems on the top, the liquid nitrogen circulation pumps and liquid argon re-circulation systems in the rear side. The major safety equipment is visible: the vent line with the electrical heater connected to all the possible exhausts and the collecting pipes from the T600 modules [72].

lowest excited molecular state to the dissociative ground state. VUV photons are converted to visible light by means of an appropriate wavelength shifter. The isotropic light signal propagates with negligible attenuation throughout each TPC volume (LAr is fully transparent to its own scintillation light, with measured attenuation length in excess of several tens of meters and Rayleigh-scattering length of the order of 1 m). The light is detected by set of PMTs immersed in the LAr, for giving absolute event incident time for trigger purpose.

The PMTs were located 5 mm behind the Collection wires. In each chamber of the East module (left and right) 27 PMTs (in 3 rows of 9 PMTs each, spaced by 2 m) were mounted. In the West module only two central rows of PMTs were installed. Additional two PMTs were placed in the top and bottom positions in the right chamber at the

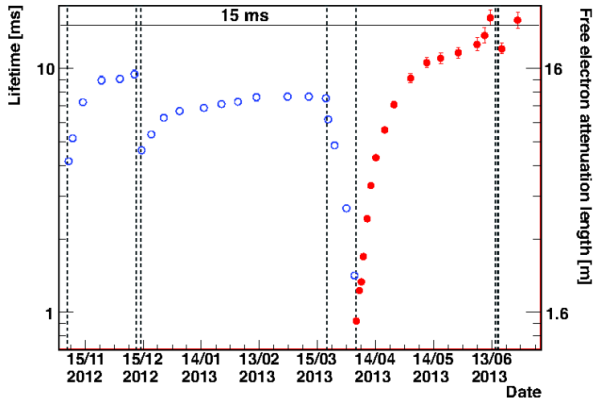

Figure 2.9: Electron lifetime measurements for the East half-module as a function of time, during the last period of data taking. The red points depict the measurements after the installation of a new pump in April 2013. The dashed vertical lines represent the stops and restart of the LAr recirculation (during this period the GAr recirculation system continued to operate) [30].

center of the longitudinal direction. It gives an overall amount of 20 PMTs in the West module (see Fig. 2.10). The trigger rate based on scintillation was mostly dominated by cosmic rays muons and is equal to 40 mHz.

2.5.2 S-Daedalus system

The second component of the trigger was implemented at the end of 2011. It was based on an algorithm (based on Double Rebinning Sliding Windows (DR-slw) [77]) that detects the ionizing tracks through a digital filter of each TPC wire signal. This allowed triggering on charge deposition. Its purpose was to increase the efficiency of the T600 detector for low energy events down to few MeV and to provide a reference for measuring the PMT trigger performance.

2.6 ICARUS T600 overhauling at CERN (WA104/NP01)

The ICARUS T600 detector after acquiring data in the underground LNGS laboratory was moved in 2014 to CERN for overhauling and refurbishing. The overhauling performed in the framework of the CENF for LAr-TPC development for short/long-baseline neutrino experiments, as WA104 project [15].

The following activities were undertaken during overhauling:

- new cold vessels with purely passive thermal insulation were mounted,
- the cathode planarity was improved by mechanical/thermal stress to the cathode panels,
- the cryogenics and LAr purification system were upgraded,
- the light collection system with new PMTs were upgraded: 90 PMTs per chamber - in order to (1) increase the detection coverage to be sensitive to low energy

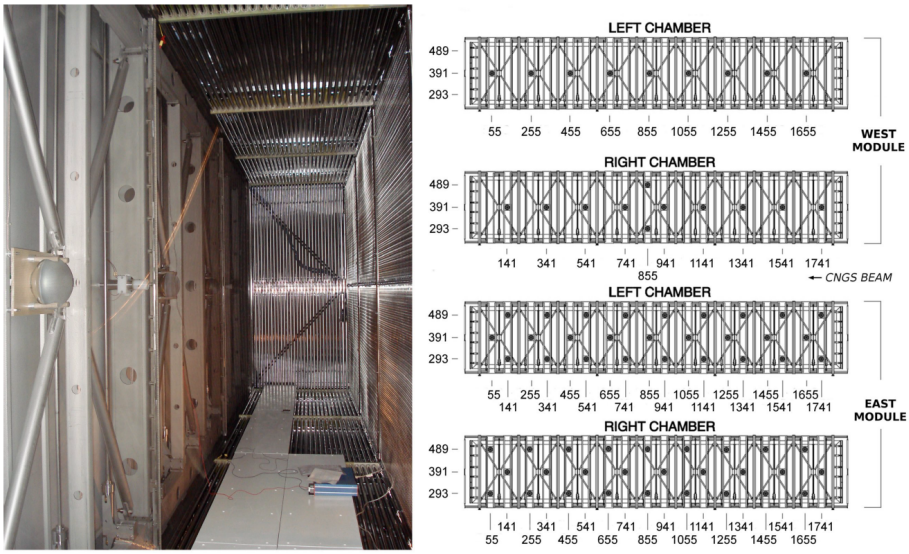

Figure 2.10: Left: Inside picture of one TPC chamber, with a few PMTs visible together with their sustaining structure. Right: Location of PMT in each module. The numbers are location coordinates referring to a reference frame in Hall B (Fig. 3.7) [76].

deposition (100 MeV), (2) have a higher granularity and allow matching light and charge deposition and, (3) improve readout time resolution (1 ns) to take advantage of the bunched beam structure,

- replacement of the existing "warm" electronics by a new faster, higher performance read-out.

On parallel several R&D activities, in view of the detector future within the LBNF program at FNAL, were carried out:

- study of LAr-TPC magnetization and as a consequence,
- replacement of the PMTs with photodetectors insensitive to the external magnetic field (e.g. Silicon Photomultiplier (SiPM [78])),
- design of a external cosmic tagging system (CRT) for operations at shallow depth recognizing incoming cosmic particles, which will be made of scintillating bars surrounding T600. Bars will be equipped with optical fibers driving light to SiPMs for readout. The total surface of the CRT is $\sim$1250 m^2.

The last point is crucial for ICARUS T600 operation at FNAL. It is estimated that several uncorrelated cosmic rays can occur in the T600 per triggering event within the 1 ms readout window. In average $\sim$12 muon tracks per drift in each T300 were measured in Pavia during the test run on surface performed in 2001.

All the overhauling operations on the T600 detector have been completed by the end of March 2017 making detector modules ready for the transporting to FNAL, what took place in April 2017 (see chapter 5).

Chapter 3

CNGS muon-neutrino beam

3.1 CNGS beam at CERN

The CERN to Gran Sasso muon-neutrino beam (CNGS [10]) was commissioned in early August 2006 and first neutrinos were sent at low intensity to the underground laboratory at Gran Sasso (GS) on August 17, 2006. The CERN CNGS complex is presented in Fig. 3.1

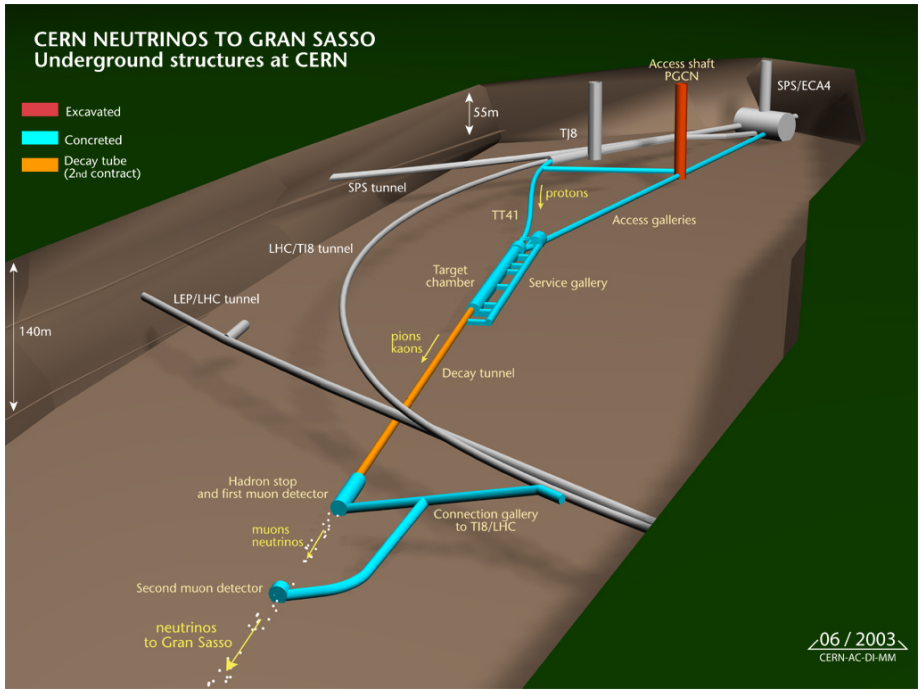

Figure 3.1: The SPS/CNGS underground structure at CERN [10].

The most common method used for ν_μ beam production can be described in several points:

- production of high energy protons,
- collision of protons with a target resulting in production of secondary particles, among others, kaons and pions,
- kaons and pions delivery through a system of magnetic horns towards the experiment,
- pions and kaons decay in flight in, among others, muons and muon-neutrinos, in an evacuated decay pipe (Eqs. 3.1 and 3.3),
- stop of non interesting, non decaying hadrons in a hadron stopper and measure muons in a muon detector which can be used to estimate the beam intensity,
- produced neutrinos (mostly muon-neutrinos with small contamination of the other flavors) will continue their way towards neutrino detector.

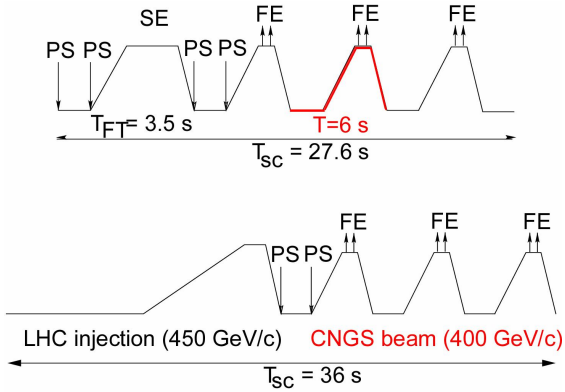

Figure 3.2: The structure of proton beam extracted from SPS with a fast kicker system in two batches (FE - fast extraction, SE - slow extraction) of 10.5 μs each, with 50 ms time between the two extractions. The microstructure of the beam reflects the 200 MHz radiofrequency system of the SPS - each batch consists of a train of bunches interspaced by 5 ns. The length of a single bunch was about 2–3 ns [10].

In CERN the muon-neutrino production starts from protons which were accelerated through the existing chain of accelerators: Linac, Booster, Proton Synchrotron (PS) and Super Proton Synchrotron (SPS) (Fig. 3.6). A proton beam from SPS was extracted and transported to the CNGS target twice per SPS cycle i.e. every 6 s (Fig. 3.2). In each extraction $2.4 \cdot 10^{13}$ 400 GeV/c protons were sent down to the graphite target. It was estimated that $\sim 4.5 \cdot 10^{19}$ protons per year were delivered to the CNGS target, assuming an overall efficiency $\sim$55% and a running time of 200 days per year in a co-user mode (filling also the Large Hadron Collider, LHC) (Fig. 3.4). The same set of switch magnets was used to sent a beam either to CNGS or to LHC. The extracted protons hit the graphite target producing various particles. From the CNGS muon-neutrino beam point of view the most interesting were the secondary pions and kaons. Those, positively

charged, after energy selection, were focused into a parallel beam by two magnetic lenses (called horn and reflector) in the direction of GS. A long 992 m decay pipe allowed the pions and kaons to decay into ν_μ and μ (see Eqs. 3.1 and 3.3). The remaining hadrons were absorbed in a beam dump consisting of 3.2 m of graphite and 15 m of water cooled iron which at the hottest point was heated up to 170° C after 200 days of running. The muons from the decay were monitored by two sets of detectors downstream of the dump allowing to determine the intensity and ν_μ beam profile. Knowledge of the ν_μ flux is crucial for the determination of the expected number of ν_μ interactions in the Gran Sasso (see section 4.4.7). The CNGS beam was optimized to observe the most tau-neutrinos at two detectors at Gran Sasso, namely OPERA and ICARUS T600. The simulated energy distribution of the beam at Gran Sasso is shown in Fig. 3.5 together with the convolution of the probability for $\nu_\mu \to \nu_\tau$ oscillation over 732 km (see Fig. 3.3 and section. 4.1.3) and the interaction cross section for ν_τ in matter.

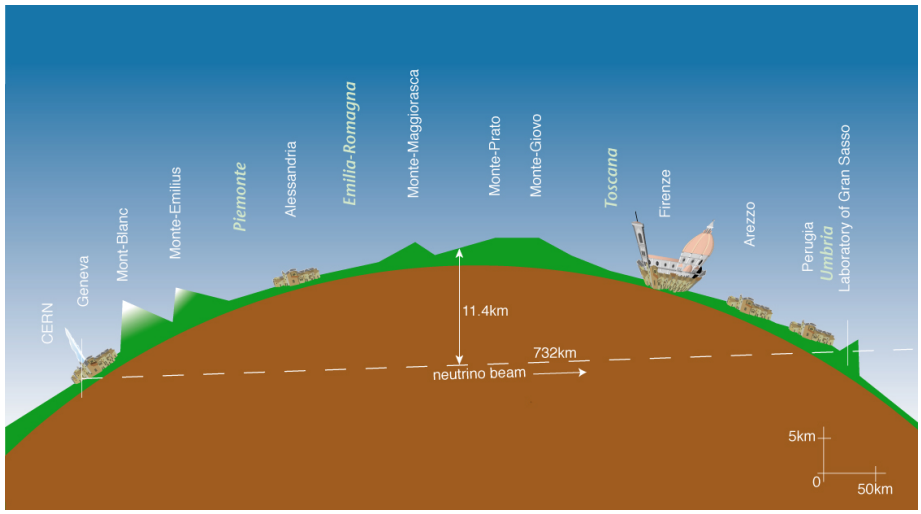

Figure 3.3: Route taken by neutrinos through the Earth's crust from CERN to the Gran Sasso laboratory [10].

The selected CNGS beam parameters are as follows:

- average muon-neutrino energy: 17.5 GeV/c,
- ν_e ($\overline{\nu}_e$) contamination in the beam: $< 1\%$,
- contamination of $\overline{\nu}_\mu$: $\sim 2\%$,
- contamination of ν_τ: negligible,
- μ beam size at the second muon detector: $\sigma \sim 1$ m and
- ν_μ beam size at GS: $\sigma \sim 1$ km [80, 81].

The primary and secondary most common decay mode of charged pions, with branching fractions are shown in Eqs. 3.1 and 3.2 [82]. The mean lifetime of pion is equal to $2.6 \cdot 10^{-8}$ s. Considering the energy of the produced pions, this is sufficient time to decay in a $\sim$1000 m decay pipe of CNGS plant.

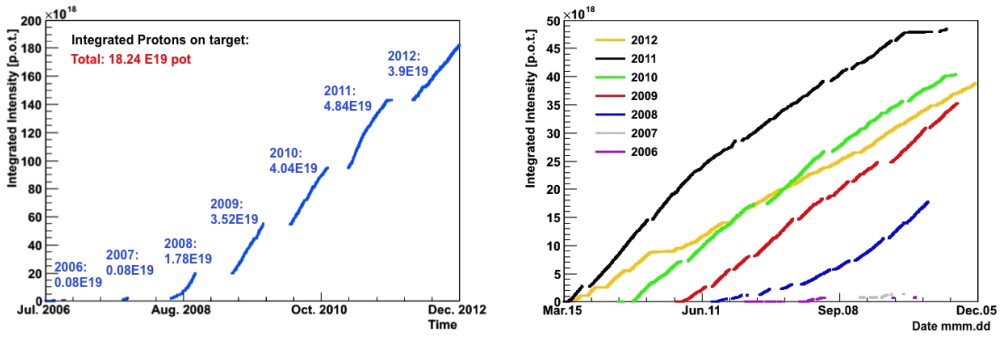

Figure 3.4: Left: Integrated intensity of protons on target in CNGS beam during 2006-2012. Right: Comparison year after year of proton on target intensity [10].

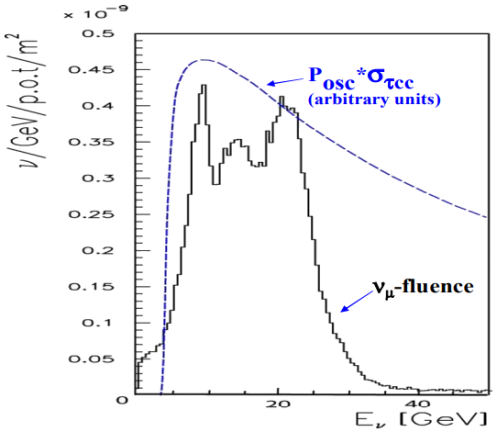

Figure 3.5: Black curve: Monte Carlo simulation of the muon-neutrino energy spectrum at Gran Sasso. Blue curve: the convolution of the probability for $\nu_\mu \to \nu_\tau$ oscillation over 732 km and the interaction cross-section for ν_τ in matter [79].

$$\begin{aligned} &\pi^+ \to \mu^+ + \nu_\mu \quad \text{(branching ratio : 0.999877)}, \\ &\pi^- \to \mu^- + \overline{\nu}_\mu, \end{aligned} \tag{3.1}$$

$$\begin{aligned} &\pi^+ \to e^+ + \nu_e \quad \text{(branching ratio : 0.000123)}, \\ &\pi^- \to e^- + \overline{\nu}_e. \end{aligned} \tag{3.2}$$

The highest branching ratio of kaon decay is into muon-neutrino and muon (Eq. 3.3) and is equal to 0.6355±0.0011 [82]. Other branching ratios of kaon decay are not relevant for the ν_μ beam production. The mean lifetime of kaon is $1.2384 \pm 0.0024 \cdot 10^{-8}$ s.

$$K^+ \to \mu^+ + \nu_\mu \quad (0.6355 \pm 0.0011). \tag{3.3}$$

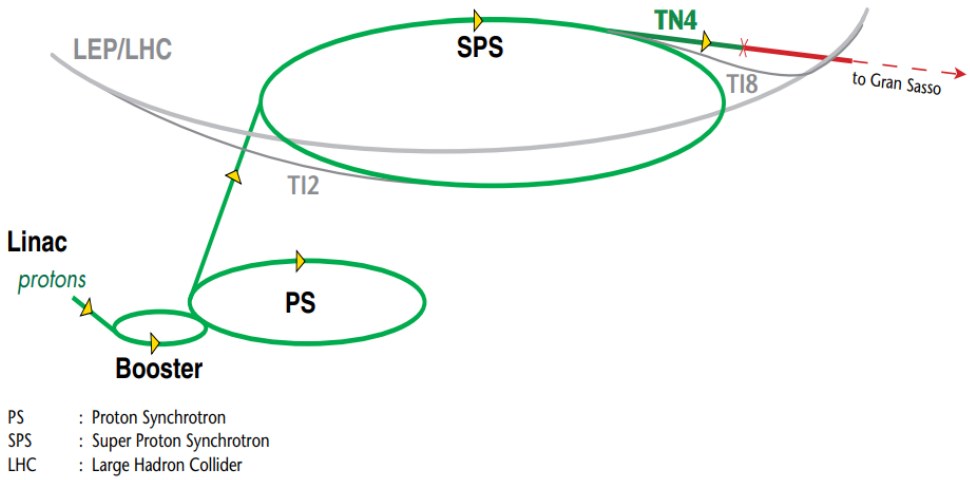

Figure 3.6: The CERN proton accelerators used for the CNGS beam [2].

On the basis of the CNGS beam calculations [83,84] one can find that muon-neutrinos originate from:

- 75% from π's decay,
- 6% from K's decay,
- 19% from tertiary decays,

whereas the electron-neutrinos originate from pions by:

- 37% through subsequent μ's decay,
- 43% from K decay,
- 20% due to tertiary decays.

A detailed description of the CNGS operation can be found in [10].

3.2 The underground Gran Sasso laboratory

The Gran Sasso National Laboratory is one of four INFN laboratories in Italy. It is the largest underground laboratory in the world and hosts particle physics, particle astrophysics and nuclear astrophysics experiments. It is located between the towns of L'Aquila and Teramo, about 120 km from Rome. Access to experimental halls is horizontal because the underground facilities are located on the side of the ten kilometer long freeway tunnel crossing the Gran Sasso Mountain.

The ICARUS T600 detector was localized in Hall B, one of the three main experimental halls of the laboratory. The location of other experiments at LNGS during ICARUS T600 operation is shown in Fig. 3.7.

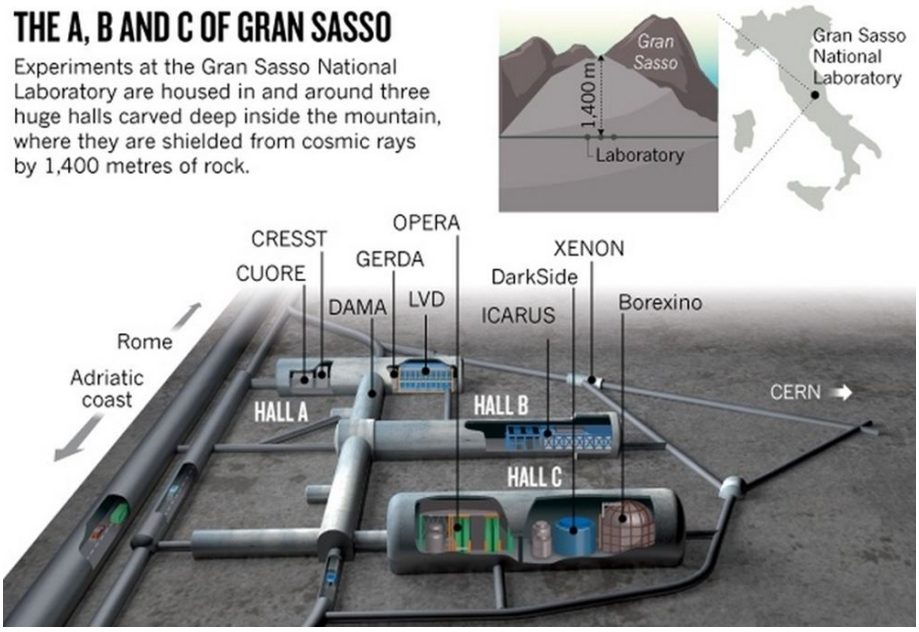

Figure 3.7: Layout of LNGS in Gran Sasso with depicted location of individual experiments [85].

Chapter 4

Physics results of the ICARUS T600 experiment

4.1 Neutrino time of flight measurements

In 2012 the OPERA experiment reported results [4] indicating a superluminal[1] propagation of CNGS neutrinos from CERN to LNGS. Cohen and Glashow [86] argued that such neutrinos should lose energy producing photons and electron-positron pairs ($\nu \rightarrow \nu + e^- + e^+$), through Z_0 mediated processes. Since neutrinos are electrically neutral the conventional Cherenkov radiation of superluminal neutrinos does not arise or is otherwise weakened, however they carry electroweak charge and therefore may emit Cherenkov like radiation via weak interactions when traveling at superluminal speed.

Taking into account the data collected by the T600 detector, the ICARUS Collaboration found that the rates and deposited energy distributions of neutrino events agree with the expectations for an unperturbed spectrum of the CERN neutrino beam. This led to refuting the superluminal interpretation of the OPERA result according to the Cohen and Glashow prediction for a weak current analog to Cherenkov radiation. In particular no superluminal Cherenkov like $e^- e^+$ pair or gamma emission event has been directly observed inside the fiducial volume of the T600 detector [87]. No candidate event was found, setting a tight negative limit on $\delta < 2.5 \cdot 10^{-8}$ (Eq. 4.1, relative difference of the neutrino speed v_ν with respect to that of light c in the vacuum is measured) at the 90% confidence level comparable to the observations of neutrinos from Supernova SN1987a at energies ∼10 MeV, where $\delta < 2 \cdot 10^{-9}$ [88]. The observations of high energy neutrino events by Super-Kamiokande [89–91] and IceCube [92] experiments also point to a much stricter limit on δ.

$$\delta \equiv (v_\nu - c)/c, \tag{4.1}$$

where:

v_ν - velocity of neutrinos,

[1] Superluminal - travel at a speed faster than light, so called propagating superluminally.

c - speed of light in vacuum.

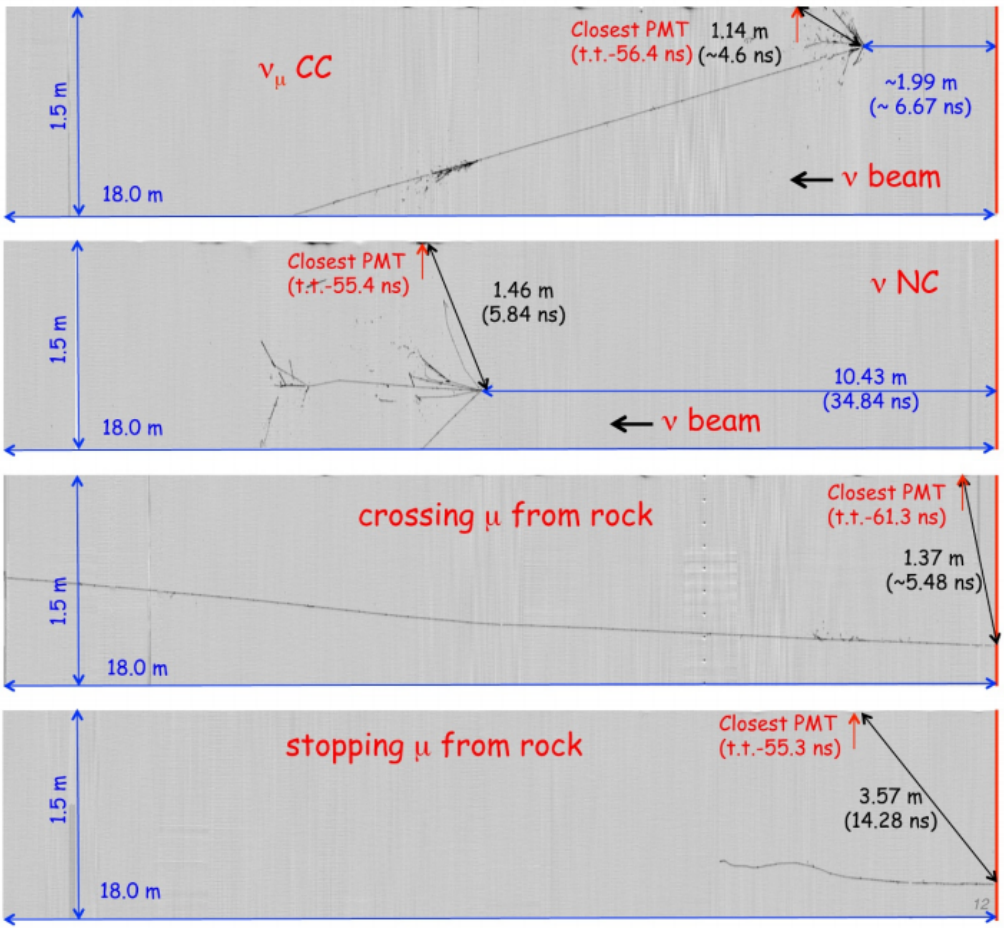

Figure 4.1: Examples of different event topologies in the ICARUS LAr-TPC from the 2012 CNGS bunched beam run. A 2D view of the Collection wire plane is shown. For each event the distance from the 'ICARUS reference entry point' (red line on the right side of the image) is reported as well as the photon path to the nearest PMT and the associated transit time in the PMT itself. Among all collected events only one stopping muon from CNGS beam was recorded.

The OPERA result triggered neutrino time of flight measurements (TOF). At the end of the 2011 run, the CNGS neutrino beam was briefly operated in a lower intensity mode with a bunched proton beam (∼3 ns wide, separated by 524 ns) allowing for the first neutrino TOF measurement on an event-by-event basis. ICARUS detector collected 7 beam-associated events (corresponding to $2.2 \cdot 10^{16}$ pot) measuring a difference $\delta t = \text{tof}_c - \text{tof}_v = \pm 0.3 \pm 0.9_{stat} \pm 9.0_{sys}$ ns (Fig. 4.2) [93], compatible with the arrival of

all events with the speed equal to that of light. This was in striking difference to the reported result of OPERA claiming that high energy neutrinos from CERN arrive at LNGS ∼60 ns earlier than expected from luminal speed. The CERN and the LNGS experiments (Borexino, ICARUS, LVD, OPERA) agreed to perform an additional new dedicated campaign (from May 10^{th} to May 24^{th} 2012) with the aim to improve the accuracy of the neutrino time of flight measurement. For this purpose a new dedicated CERN SPS bunched beam was prepared with 10^{12} pot per spill (see section 4.1.1). In total $\sim 1.8 \cdot 10^{17}$ pot was delivered over a period of two weeks. In comparison to the previous measurement, performed in 2011, the accuracy of the experiment was improved by combining the event-by-event analysis and the timing measurements performed at various stages of the measurement path.

During the 2012 campaign 25 collected events consisted of 8 neutrino interactions (6 CC and 2 NC) with the interaction vertex inside the fiducial volume and 17 muons generated by CNGS neutrino interactions in the upstream rock. The various neutrino event topologies are shown in Fig. 4.1.

The neutrino time of flight was measured combining detection time of neutrino event at LNGS and transit time of a proton bunch at the Beam Current Transformer (BCT) monitor at CERN (see section 4.1.2). The neutrino velocity was calculated knowing the accurate CERN-LNGS distance (see section 4.1.3) and the time of flight. The ICARUS results have been confirmed by the Borexino [94] and the LVD [95] experiments participating in bunched beam time of flight measurements.

The difference δt between ν time of flight (tof_ν) and the expected time of flight based on the speed of light ($\text{tof}_c = 2439096.1$ ns) is shown in Fig. 4.2. The $\delta t = \text{tof}_c - \text{tof}_\nu = 0.10 \pm 0.67_{stat} \pm 2.39_{sys}$ ns was measured between the BCT and the 'ICARUS reference entry point' (the T600 entry wall, see e.g. Fig. 4.1).

4.1.1 The CNGS bunched beam for the ν_μ time of flight measurements

During May 2012, the CERN-CNGS neutrino beam was operated for two weeks with a characteristic to maximize accuracy of ν_μ time of flight measurements. The single extraction contained 4 batches (Fig. 4.3 - left) separated by 300 ns and 16 proton bunches per batch separated by 100 ns. Each bunch had a narrow width of about 4 ns FWHM (1.8 ns rms[2]). Such a very tightly bunched beam structure allowed for a very accurate neutrino time of flight measurement on an event-by-event basis. For comparison, in Fig. 3.2, the structure of proton beam used for CNGS data collection in 2012 is shown.

4.1.2 Time synchronization between CERN and LNGS

For precise time synchronization between CNGS beam extraction and its LNGS arrival dedicated infrastructure was designed. The proton beam structure shown in Fig. 4.3 was recorded in 743.391 ± 0.002 m upstream of the CNGS neutrino target (position marked in Fig. 4.4 as BFCTI40.00344). The beam time structure at BCT detector was recorded by a 1 GS/s Wave Form Digitiser (WFD) Acqiris DP110 triggered by the SPS kicker magnet signal. At every extraction, the BCTFI.400344 waveform was stored in the CNGS database. Every acquisition was time-tagged with respect to the SPS timing

[2]Root mean square.

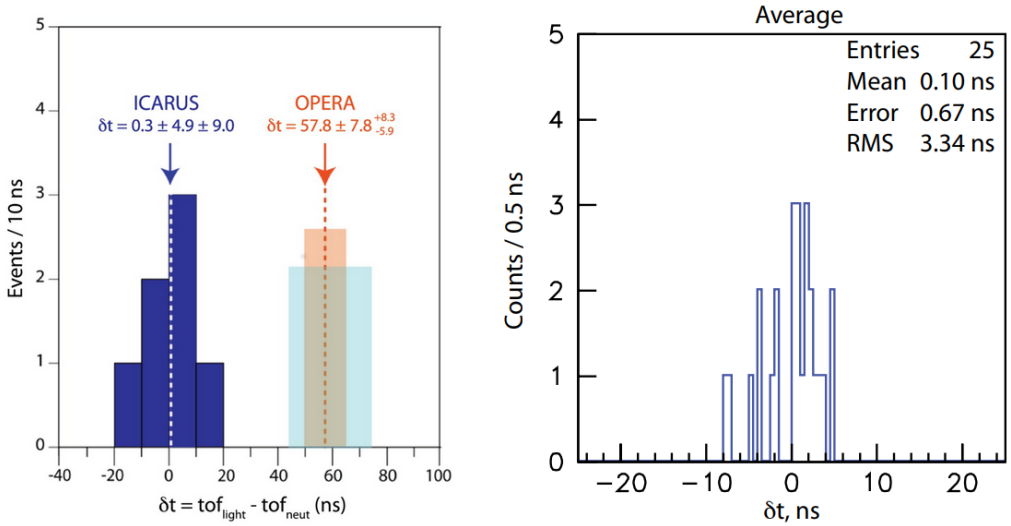

Figure 4.2: Left: 2011 bunched beam campaign: event distribution in ICARUS for $\delta t = \text{tof}_c - \text{tof}_v$ [93]. The first OPERA claim is also shown. Right: 2012 bunched beam campaign: event distribution in ICARUS for $\delta t = \text{tof}_c - \text{tof}_v$ [96], according to the averaging procedure of all various time synchronization paths. The details about time synchronization paths can be found in [4, 97].

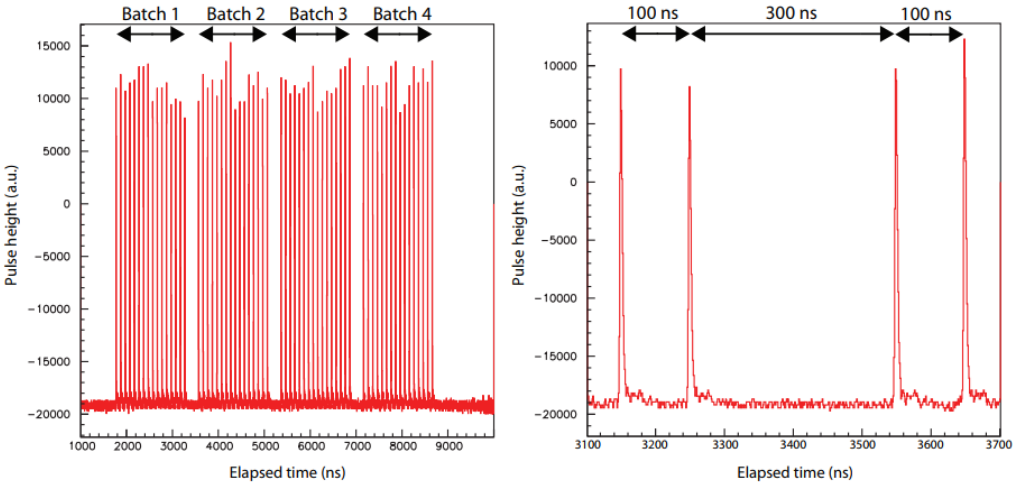

Figure 4.3: CNGS proton beam structure for neutrino time of flight measurement. Left: single extraction with 4 batches. Right: 300 ns separation between batches and 100 ns between bunches in a single extraction [96].

system, associating each neutrino event at LNGS to a precise proton bunch. The absolute UTC[3] timing signal at LNGS was provided every second by the GPS system ESAT 2000 [98] disciplining a Rubidium oscillator which operated on the LNGS laboratory surface. Then every milisecond the time signal was sent underground and was used to provide the absolute time-stamp for the recorded events [4, 96].

Additionally to time synchronization, for triggering purpose, "early warning" message was sent from CERN to LNGS 150 ms before each SPS proton extraction. This message contained the predicted extraction time. The precision of this prediction was about 20 μs, higher than the jitter of the local clock (GPS based), enough for triggering purpose.

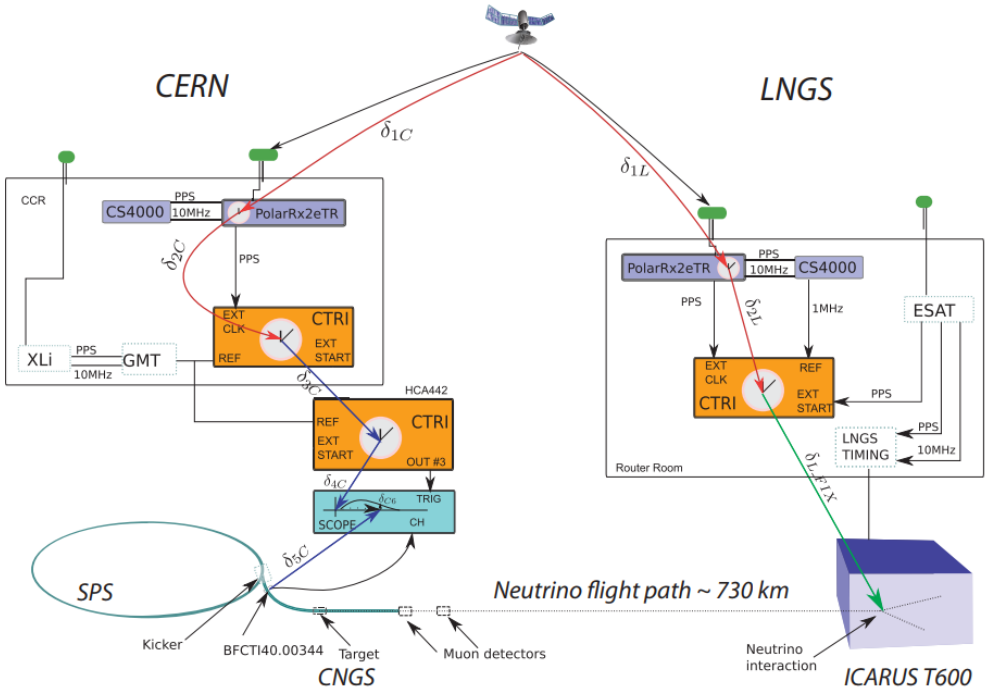

Figure 4.4: Schematic view of CERN-LNGS time synchronization. The origin of the neutrino time of flight measurement is at BFCTT40.0034. For the ICARUS experiment, the arrival reference point is the T600 entry wall (see Fig. 4.1) [96].

4.1.3 Distance between CERN and LNGS

Usually the CERN-LNGS distance is referred to 732 km. The additional precise geodetic measurement was performed by Politecnico di Milano just before the 2012 bunched beam run. The distance used for neutrino velocity measurements was 731221.95 ± 0.09 m. It resulted (for v equal to c) in the expected time of flight equal to 2439096.08 ± 0.3 ns.

[3] Coordinated Universal Time.

The result includes 2.2 ns contribution due to the Sagnac effect (Earth rotation) [99]. The position of CERN and LNGS was estimated with accuracy of 3.7 cm in the common geodetic reference frame [100].

4.2 ICARUS search for an LSND-like effect with CNGS beam

The LSND-like effect is related to possible presence of neutrino oscillations into a sterile[4] states (Fig. 4.5). Such oscillation was proposed by B. Pontecorvo [101, 102]. An experimental search for an anomalous oscillation at short distances has been reported by the LSND experiment (Liquid Scintillator Neutrino Detector) [3] at the Los Alamos 800 MeV proton accelerator. The LSND collaboration found excess of electron-neutrinos in $\langle E_\nu \simeq 30 \rangle$ MeV muon-neutrino beam. The propagating distance was $L \simeq 30$ m. The LSND signal with $\overline{\nu}_\mu$ to $\overline{\nu}_e$ oscillation probability $P_{\overline{\nu}_\mu \to \overline{\nu}_e}$ equal to $2.64 \pm 0.67 \pm 0.45 \cdot 10^{-3}$ corresponds to an excess of $87.9 \pm 22.4 \pm 6.0$ events, namely a 3.8σ effect at L/E_ν of about 0.5–1.0 m/MeV.

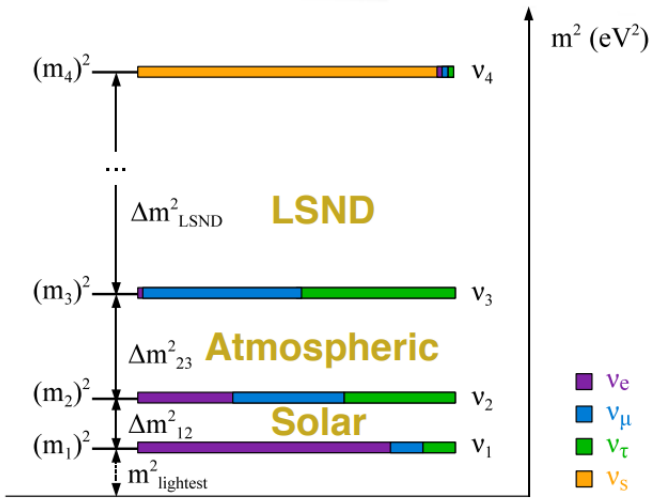

Figure 4.5: Minimal modification of the standard three neutrino scheme taking into account a sterile neutrino (ν_s, "3+1" neutrino mixing). The new sterile neutrino would be mainly composed by a heavy neutrino ν_4 such that the new $\Delta m^2 = \Delta m^2_{41} \simeq [0.1 - 10]\,\mathrm{eV}^2$ and m_1, m_2, $m_3 \ll m_4$ [103].

Later the anomaly was studied by MiniBooNE [104] experiment using both, ν and $\overline{\nu}$ beams with energy about 8 GeV (BNB beam) and confirmed a ν oscillation signal (in ν and $\overline{\nu}$ channels) in the similar L/E_ν range at 3.4σ and 2.8σ for ν_e and $\overline{\nu}_e$, respectively (Fig. 4.6). Additionally, ν_e or $\overline{\nu}_e$ disappearance anomalies have been detected

[4] The term *sterile* neutrino concerns a particle which does not interact via any fundamental interactions of the Standard Model except gravity. The term was proposed by Bruno Pontecorvo.

from nuclear reactors [105] and from Mega-Curie k-capture calibration sources [106,107], originally developed for the gallium experiments to detect solar ν_e.

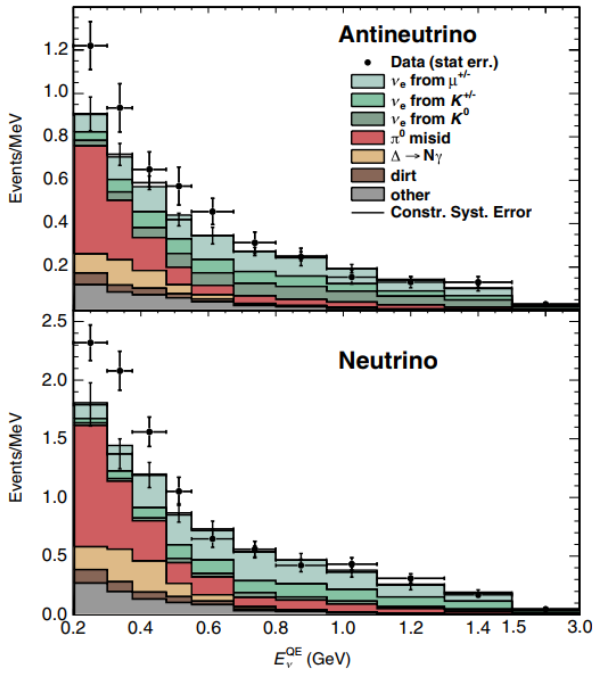

Figure 4.6: The antineutrino (top) and neutrino mode (bottom) reconstructed neutrino energy (E_ν^{QE}) distributions for ν_e charged-current quasielastic data (points with statistical errors) and background (histogram with systematic errors) in MiniBooNE experiment. A clear excess in ν_e ($\nu_\mu \rightarrow \nu_e$, 3.4σ) and $\overline{\nu}_e$ ($\overline{\nu}_\mu \rightarrow \overline{\nu}_e$, 2.8σ) appearance is observed in low energy range [104].

The obtained results correspond to the new neutrino oscillation signal (implying the presence of an additional mass-squared difference) somewhere within a wide interval $\Delta m^2_{new} \simeq 0.01 - 1.0\,\mathrm{eV}^2$ and associated value of $\sin^2(2\theta_{new})$ related by two flavor oscillation probability:

$$\langle P_{\nu_\mu \rightarrow \nu_e} \rangle = \sin^2(2\theta_{new}) \sin^2(1.27\Delta m^2_{new} \frac{L}{E_\nu}). \tag{4.2}$$

In comparison to experiments where LSND anomaly was observed, the ICARUS experiment had a much bigger value of $L/E_\nu \simeq 36.5\,\mathrm{m/MeV}$, with distance $L \simeq 732\,\mathrm{km}$ and energy $\langle E_\nu \rangle$ of about 17.5 GeV. It means that a hypothetical $\nu_\mu \rightarrow \nu_e$ LSND anomaly, in first approximation, will produce fast oscillations as a function of neutrino energy E_ν averaging to the value of 1/2 (Fig. 4.7)

$$\sin^2(1.27\Delta m^2_{new} \frac{L}{E_\nu}) \simeq \frac{1}{2}, \tag{4.3}$$

and therefore the oscillation probability averages to

$$\langle P_{\nu_\mu \to \nu_e} \rangle \simeq \frac{1}{2} \sin^2(2\theta_{new}). \tag{4.4}$$

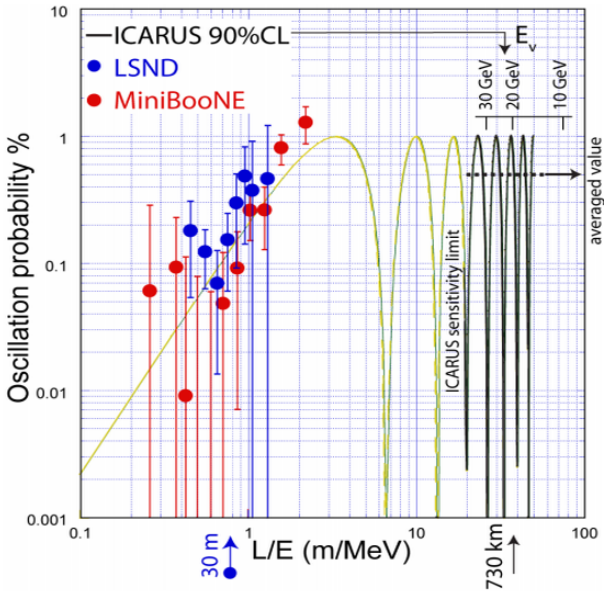

Figure 4.7: Muon-neutrino oscillation probability versus L/E_ν.

One of the great achievements of the ICARUS collaboration is excellent e/γ separation capability (see Figs. 2.4 and 2.5). It was essential during the search of ν_e excess in the ν_μ CNGS beam. The ICARUS experiment was to search for the ν_e signal by performing visual scanning of CNGS events (2650 neutrino interactions corresponding to $7.93 \cdot 10^{19}$ pot, see section 4.4). For each, the following was determined [108, 109]:

- neutrino interaction vertex,
- the entire visible energy obtained from cumulative charge collected by the TPC wires corrected for: (1) electronic response, (2) electron lifetime and (3) recombination,
- two dimensional projections of both: particle tracks and electromagnetic showers,

under the following conditions:

- the interaction vertex at a distance > 5 cm from each side of the active volume of the TPC and > 50 cm from downstream walls,
- reconstructed (visible) energy $E < 30$ GeV, what resulted in 50% reduction of the beam ν_e background events but only a 15% reduction of the expected signal.

Additionally, it was requested that the electron-neutrino signature fulfills the following [108]:

- a primary charged track starts from the vertex with $dE/dx < 3.1\,\mathrm{MeV/cm}$ (i.e. consistent with a minimum ionizing particle) and subsequently building up into a shower. The dE/dx was calculated as an average over at least 8 wires after removing visible delta rays,
- separation, within 150 mrad near the primary vertex, of the electron candidate track from the other ionizing tracks (except for short proton as recoils produced in the interactions).

Taking into account these conditions, seven ν_e events were found (see section 4.4.2).

Additionally to the signal (ν_e excess in the ν_μ CNGS beam), background from conventional sources has to be considered, namely: (1) $\sim 4.9 \pm 0.7$ events due to the estimated ν_e beam contamination, (2) $\sim 2.2 \pm 0.4$ events due to the presence of $\nu_\mu \to \nu_e$ oscillations with $sin^2(\Theta_{13}) = 0.0234 \pm 0.002$ (an updated value of the $sin^2(\Theta_{13})$ equal to 0.0242 ± 0.0026 has been used for analysis), reported in [110] and (3) $\sim 1.3 \pm 0.1$ events due to $\nu_\mu \to \nu_\tau$ oscillations with the electron production. It gives a total of 8.4 ± 1.1 expected events (see Tab. 4.1) [111]. The errors represent the uncertainty on the NC and CC contributions. The selection efficiency, validated on MC sample of ν_e events is equal to (1) $\eta = 0.74 \pm 0.05$ for the expected signal in the $E_\nu < 30\,\mathrm{GeV}$ energy region (in a good approximation, η is independent from the shape of the energy spectrum) and (2) $\eta = 0.65 \pm 0.06$ for the intrinsic ν_e contamination. The expected signal is of 6.2 events after applying the $\eta = 0.74 \pm 0.05$ reduction. It is in agreement with observed the number of seven ν_e events. Additionally, on the basis of the expected number of electron like neutrino events one can conclude that a tau-neutrino interaction with τ decaying in an electron could be present in the analyzed sample.

Table 4.1: Limits on the number of events (LoF) due to LSND anomaly and corresponding new limits on the oscillation probability (LoP) reported by the ICARUS Collaboration. In the number of expected events only systematic errors are included.

	Confidence level 90%	Confidence level 99%	pot ($\cdot 10^{19}$)	No. of ν event interactions	No. of expected ν_e	No. of found ν_e	Ref.
LoF	3.4	7.3	3.28	1091	3.7 ± 0.6	2	[108]
LoP	$5.4 \cdot 10^{-3}$	$1.1 \cdot 10^{-2}$					
LoF	3.7	8.3	6.00	1995	6.4 ± 0.9	4	[109]
LoP	$3.4 \cdot 10^{-3}$	$7.6 \cdot 10^{-3}$					
LoF	5.2	10.3	7.23	2450	7.9 ± 1.0	6	[112]
LoP	$3.85 \cdot 10^{-3}$	$7.6 \cdot 10^{-3}$					
LoF	5.7	11.4	7.93	2650	8.4 ± 1.1	7	[111]
LoP	$3.92 \cdot 10^{-3}$	$7.83 \cdot 10^{-3}$					

This resulted in setting new limits on the oscillation probability [111]:

$$\begin{aligned} P_{\nu_\mu \to \nu_e} &\leqslant 3.92 \cdot 10^{-3} \text{ at } 90\% \text{ CL}, \\ P_{\nu_\mu \to \nu_e} &\leqslant 7.83 \cdot 10^{-3} \text{ at } 99\% \text{ CL}. \end{aligned} \tag{4.5}$$

The exclusion plot with ICARUS T600 result is shown in Fig. 4.8.

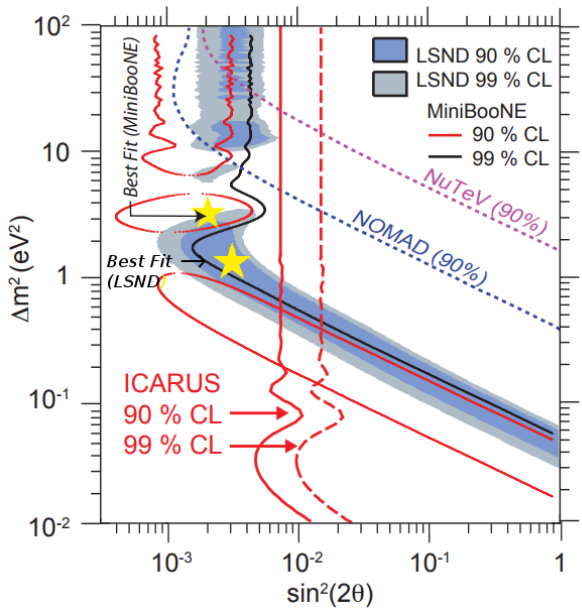

Figure 4.8: Δm^2 versus $\sin^2(2\theta)$ for the main experiments sensitive to the $\overline{\nu}_\mu \to \overline{\nu}_e$ and $\nu_\mu \to \nu_e$ anomalies: LSND [3], MiniBooNE [113], KARMEN [114], NOMAD [115] and NuTeV [116]) and for ICARUS T600 (continuous red lines). The "Best Fit" for MiniBooNE and LSND experiments is shown [103, 112].

The ICARUS T600 result is in agreement with the search performed by the OPERA experiment, using the same CNGS beam [117] and constrains the allowed neutrino to sterile neutrino oscillation parameters to a narrow region around:

$$\begin{aligned} \Delta m^2_{new} &\sim 0.5 \text{ eV}^2, \\ sin^2(2\theta_{new}) &\sim 0.005, \end{aligned} \tag{4.6}$$

where all reported results can be coherently accommodated at 90% CL.

However, the hypothesis of the existence of sterile neutrinos is not ruled out completely and therefore there is a need to perform an "ultimate" experiment. This can be achieved within the SBN program [6] for the sterile neutrino search with three LAr-TPCs (see chapter 5).

4.3 Search for the atmospheric $\nu_{\mu,e}$ interactions in the ICARUS T600 detector

Apart from the CNGS beam events, the ICARUS T600 detector collected also cosmic rays in two periods: (1) during CNGS ν_μ beam data taking and (2) after CNGS beam stop (December 3$^{\text{rd}}$ 2012) until June 26$^{\text{th}}$ 2013 (when the ICARUS T600 detector decommissioning procedure started), with total exposure of 0.73 kt/year. As the data

from the second period are of better quality the analysis started from this sample. In the second period the exposure was equal to 0.48 kt/year. According to FLUKA Monte Carlo (FLUKA MC) simulations of atmospheric neutrino interaction in ICARUS T600 TPC [118, 119], 129 atmospheric neutrinos are expected for 0.48 kt/year exposure (see Tab. 4.2) [120, 121], among them 29 ± 3 atmospheric neutrino events with at least two charged particles (multiprong topology) and 45 ± 3 with one charged particle (oneprong topology).

Table 4.2: The FLUKA MC expectations for 0.48 kt/year exposure [120, 121].

	ν_μCC	ν_eCC	NC	Total
Total	47 ± 3	36 ± 3	46 ± 3	129 ± 5
Empty ($E < 20$ MeV)	6 ± 1	5 ± 1	30 ± 3	41 ± 3
Cluster candidate $E > 400$ MeV	5 ± 1	8 ± 1	1 ± 1	14 ± 2
Oneprong candidates	22 ± 2	13 ± 2	10 ± 1	45 ± 3
Multiprong candidates	14 ± 2	10 ± 1	5 ± 1	29 ± 3

The selection of atmospheric neutrino interactions started with two automatic classification procedures (sections 4.3.1 and 4.3.2), complemented by visual scanning to reject misidentified events, mainly muons which originated from interactions outside the fiducial volume of the detector. The algorithms have been prepared for multiprong events of ν_μ and ν_e.

So far 7 ν_μCC and 7 ν_eCC events have been identified. Taking into account the percentage of the events scanned up to now (∼58%), these values do not differ from expectation.

The examples of atmospheric ν_μ and ν_e interaction are shown in Figs. 4.9, 4.10 and 4.11. In Fig. 4.12 the dE/dx evolution for ν_e event candidate shown in Fig. 4.11 is presented.

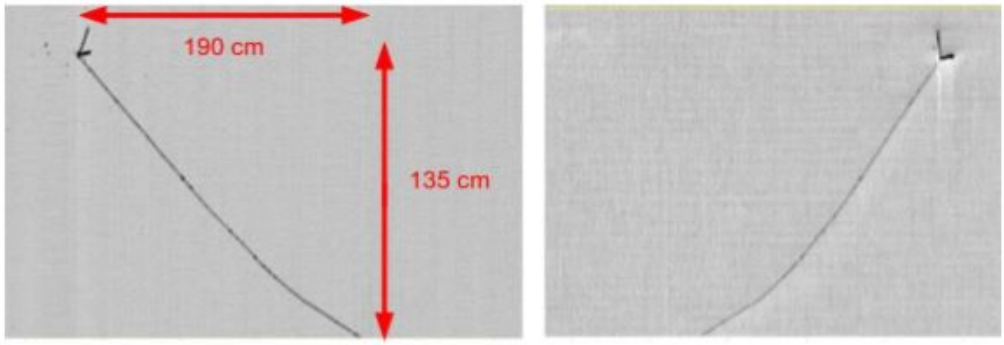

Figure 4.9: The multiprong ν_μ event candidate with deposited energy E_{dep} equal to 630 MeV. Left: Collection view. Right: Induction 2 view. The muon exiting the detector and the hadronic part (two small tracks) are clearly visible.

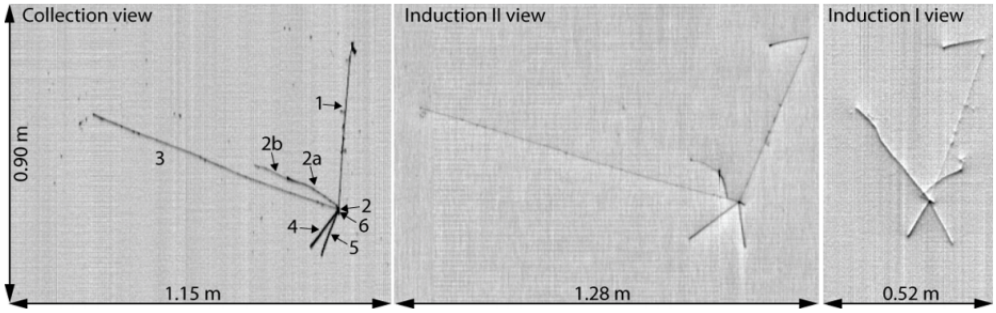

Figure 4.10: The example of 6-prong atmospheric low energy neutrino interaction confined in less than 1 m^3. Numbers: (1) π, (2) decays into 2a, (2a) μ decays at rest into 2b, (2b) e, (3) μ, (4) p merged with 5, (5) p, (6) - merged with others [122].

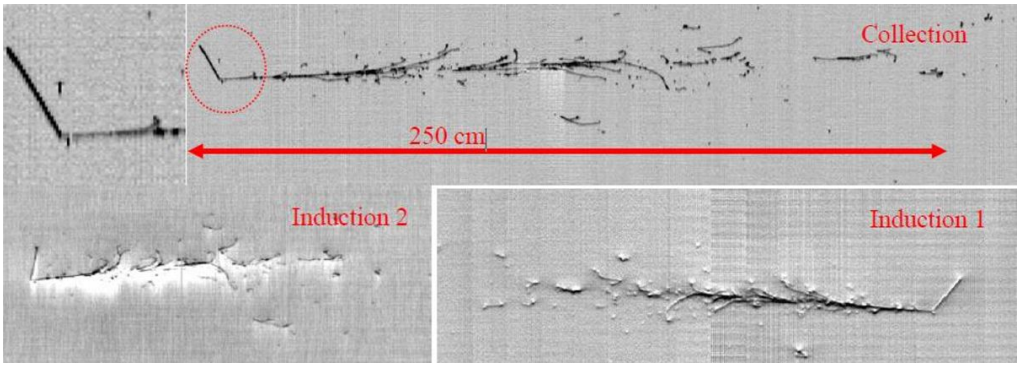

Figure 4.11: An atmospheric ν_e event candidate with deposited energy $E_{dep} = 2.1$ GeV. Collection, Induction 1 and Induction 2 views are shown. The electron track, electromagnetic cascade and the hadronic (short track) are clearly visible.

4.3.1 The atmospheric ν_μ and ν_e classification algorithm

In search of both electron-like and muon-like multiprong candidate events the presence of at least two prongs originating from an interaction vertex inside the fiducial volume is required. When a single particle originates from the vertex initiates an electromagnetic cascade, the event is identified as electron-like, whereas the reconstructed track leaving the multiprong (without electromagnetic cascade) interaction vertex allows to classify the event as a muon-like.

The automatic classification procedure reduced the data sample selected for visual scanning for multiprong and oneprong candidates to ∼0.5% and ∼2% of the total amount of collected events, respectively. The algorithm was tested on the basis of 250 MC (dedicated FLUKA simulation) events obtaining identification efficiency of the multiprong

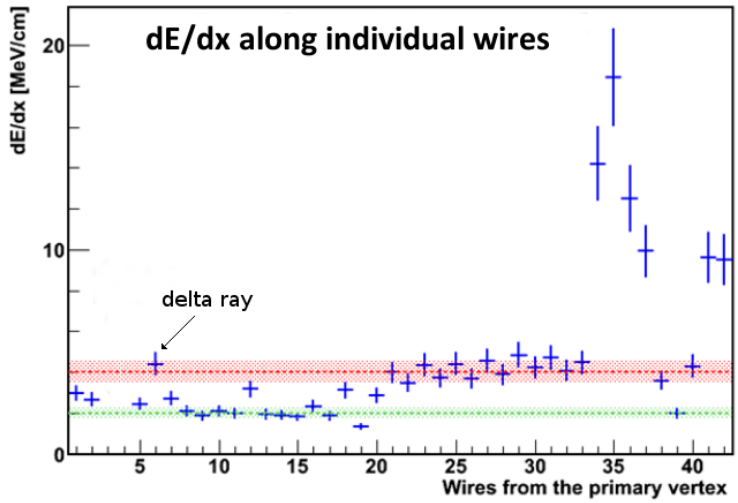

Figure 4.12: Evolution of the dE/dx from a single track to an electromagnetic shower for electron-neutrino event is shown in Fig. 4.11. The green and red lines refer to expected dE/dx for single m.i.p. and double m.i.p. signals, respectively.

neutrino interactions of about $\sim 29.2 \pm 2.8\%$ and $\sim 28.5 \pm 1.0\%$ for ν_μCC and ν_eCC, respectively,

Until mid-February 2018 about 51% of the 2012–2013 runs have been analyzed. Taking into account (1) the filtering and scanning efficiency ($> 80\%$), (2) the fiducial volume ($\sim$96% of total LAr volume), (3) the noise (crates removal) ($\sim$96%) (4) the trigger efficiency ($\sim$85%) and (5) studied statistics, 4.3 ± 0.6 ν_μ and 3.4 ± 0.5 ν_e multiprong atmospheric neutrino events are expected. In the analyzed data sample 6 ν_μCC and 3 ν_eCC event candidates was found.

4.3.2 The atmospheric ν_e classification algorithm

The selection criteria of this algorithm has been tuned to increase the efficiency of the electron-neutrino events classification while maintaining a reduced number of cosmic events to be visually studied. The procedure has been tested and tuned on a sample of 10^4 MC neutrino interactions (dedicated FLUKA simulation). A 70% and 18% efficiency has been reached for the electron-neutrino and muon-neutrino, respectively. Algorithm reduced the data sample selected for visual scanning to about $\sim$1%. About $\sim$65% of the events, corresponding to a 0.31 kt year exposure, have been studied. In total 7 electron-neutrino events have been identified, including 2 events previously found by the multiprong procedure. In addition 3 ν_μCC interactions have been noted.

4.4 CNGS neutrino study

The results presented in this section come from the study of the neutrino events corresponding to the $7.93 \cdot 10^{19}$ pot collected[5] by the ICARUS T600 detector during the 2010–2012 runs. Total number of 2650 neutrino interactions (Tab. 4.3) was identified in the defined fiducial volume [111].

Table 4.3: The summary of the scanning CNGS events collected in 2010–2012, divided into individual categories of events: (1) μ candidates - neutrino interaction where the muon was recognized ($L_\mu > 2.5\,\mathrm{m}$), (2) NC[6]candidates - events with neutral current interaction; if neither electromagnetic shower close to the vertex nor muon tracks are clearly visible, (3) e.m. candidates - ν_e candidates, at least one electromagnetic shower near the primary vertex and no visible muon, (4) XC - either no muon track or track length $< 2.5\,\mathrm{m}$ are visible; also there exists a doubt as to the identity between ν_μ and NC interaction, (5) rock μ - muons created in rocks surrounding detector; only muons inside fiducial volume, (6) external - residual from external interactions; no neutrino vertex visible, (7) empty - no physical activity inside the detector [111, 121, 123].

ν interaction	2010	2011	2012	Total
pot	$0.58 \cdot 10^{19}$	$4.11 \cdot 10^{19}$	$3.24 \cdot 10^{19}$	$7.93 \cdot 10^{19}$
μ candidates	114	829	574	1517
NC candidates	46	207	160	413
e.m. candidates	1	155	251	407
XC	7	149	157	313
Total ν events	168	1340	1142	2650
rock μ	596	4641	4007	9244
external	208	2027	1334	3569
empty	1110	1651	894	3655

Because the data from 2011–2012 are of better quality, only they have been subjected to further analysis. The number of neutrino interactions collected with the ICARUS T600 detector during 2011–2012 run has been compared with FLUKA Monte Carlo simulations (Tab. 4.4), taking into account the following [111]:

- the DAQ[7] dead-time, evaluated as percentage of CNGS trigger requests that have not been fulfilled because they were issued while the detector was in the busy state: $\langle 0.2\% \rangle$ throughout 2011 (except a short time interval when it increased to 0.6%) and $< 0.1\%$ in 2012,
- the data processing efficiency,
- the fiducial mass of LAr. On average 433 tons of LAr for 2011 and the dynamic evolution of the LAr mass during 2012 followed by calculating the corrections on a run-by-run basis (areas were taken into account where the readout electronics

[5] 92% of the total $8.6 \cdot 10^{19}$ pot delivered by CERN.

[6] In hadronic neutrino interaction (ones involving a nucleon) one can tell the two classes apart by noting if the neutrino continues on it's way (neutral current, NC) or if a charged lepton (e, μ or τ) appears in it's place (charged current, CC).

[7] Data Acquisition System.

were out of order, resulting in active volume reduction). This affected the average fiducial mass of 442 t of LAr in 2011–2012 period.

The predicted MC ν_μ events for $7.35 \cdot 10^{19}$ pot were about 1973. After applying to the MC data $L_\mu > 2.5$ m requirement, the number of ν_μ events decreased from 1973 to 1401 (∼71%). In addition, a sample of 5000 simulated NC interactions have been studied to verify whether a pion track can be misidentified as a muon candidate (i.e. whether (1) pion track can be longer than 2.5 m and (2) no clear nuclear interaction within). This resulted in 81 events out of 4809 (out of 5000 in the fiducial volume) neutrino interactions giving the suppression by a factor of 60 the NC background. Therefore the MC expected contamination from the NC interaction satisfying the muon identification request was ∼11 events out of 641 (NC events in the SFV expected in the CNGS data). Thus the expected number of neutrino interactions satisfying the moun identification is 1412 ± 38 (1401+11; stat. error only). This is in agreement with 1403 events from the visual scanning of CNGS data.

Table 4.4: The comparison between collected neutrino interactions and FLUKA MC expectations for 2011–2012 runs. In the MC calculation fiducial mass, different beam conditions, DAQ dead-time and possible inefficiencies of data processing are taken into account. Event categories are explained in Tab. 4.3. Coll. - stands for Collected [111].

	2011		**2012**		**Total**		
ν interactions	$4.11 \cdot 10^{19}$		$3.24 \cdot 10^{19}$		$7.35 \cdot 10^{19}$		
	Coll.	MC	Coll.	MC	Coll.	MC	
						all L_μ	$L_\mu > 2.5$ m
μ candidates	829	1078	574	895	1403	1973	1401
NC candidates	207	351	160	290	367	641	11
e.m. candidates	155	12	251	9	406	21	
XC	149		157		306		
Total	1340	1441	1142	1194	2482	2635	

The stability of the detector performance with time has been checked by analyzing the trends of ν and the rock μ interactions, inside the fiducial volume, per 10^{17} pot during 2011 and 2012 (Figs. 4.13 and 4.14). The stability is clearly visible. On average, about 3.5 neutrino interactions and 12.4 beam related muons per 10^{17} pot were recorded.

4.4.1 Measurement of muon momentum via Multiple Coulomb Scattering

Due to the lack of magnetic field surrounding the ICARUS T600 detector the Multiple Coulomb Scattering (MSC) was used for the determination of momenta of charged particles [71]. A dedicated MSC algorithm was initially applied to a sample of 1000 simulated (FLUKA) horizontal stopping muon events with a flat energy spectrum of the 1–5 GeV range. Then it was validated on a sample of 500 muons produced in CNGS ν_μCC interactions in upstream rocks and stopping/decaying inside the T600 LAr fiducial volume. For MCS muon momentum estimation the tracks with length > 5 m were selected, but for muon momentum calculation only the first 4 m of muon track, without visible nuclear interactions along the track, was used. The limit of up to 4 meters was

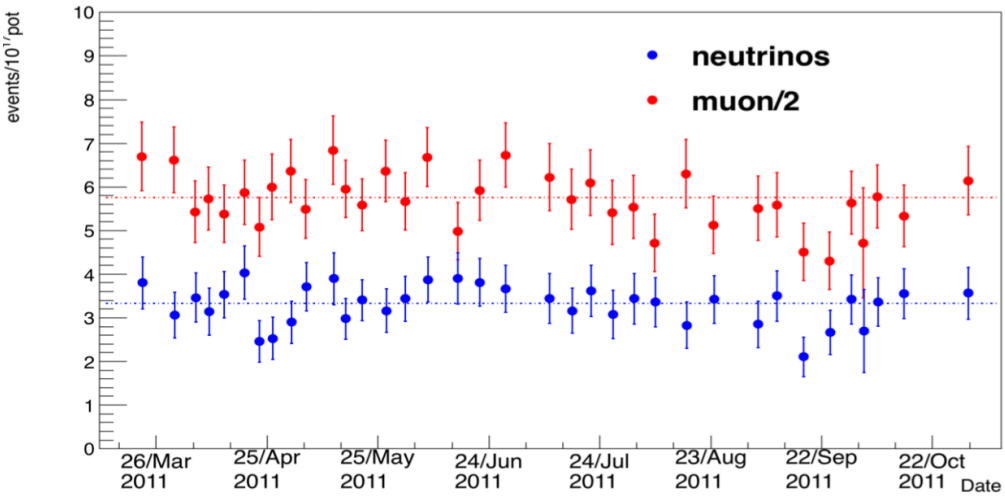

Figure 4.13: The number of collected ν interactions per 10^{17} pot as a function of date during 2011 runs. The neutrino interactions occurred inside the fiducial volume (blue) and rock muons (red, divided by 2), normalized by pot statistics and trigger/DAQ/re-alignment efficiency as a function of run time (only statistical errors are quoted) [111].

to avoid biasing the measurement with the knowledge of the higher ionization density in the final region of the muon track, close to range-out, where dE/dx increases significantly. Such a sample provided a good reference for the event by event comparison of the muon momentum obtained from the MCS (p_{MSC}) with the corresponding calorimetric measurement (p_{CAL}). The measurement algorithm was based on statistical analysis of direction deflections along muon tracks, projected on the two dimensional wire position and drift time plane corresponding to the Collection view. The deflections were measured between consecutive segments of the muon track and computed by taking into account the position of segments' center of gravity and the direction of segments obtained from the polygonal and linear fit (Fig. 4.15). The rms of the averaged deflection angle over the finite segment length, between two consecutive segments due to multiple scattering can be expressed as:

$$\theta_{MSC} = \frac{13.6 MeV/c}{\beta p_i} \sqrt{\frac{L_{seg}}{X_0 \cos\delta}} \frac{w_0}{\cos\delta}, \tag{4.7}$$

where:

- β - is equal to v/c,
- p_i - momentum of i-th segment of muon track,
- L_{seg} - length of segment ~19.2 cm,
- w_0 - quantitative factor, estimated to be $w_{0,poly} \sim 0.74$ and $w_{0,lin} \sim 0.86$ within 1% for the polygonal and the linear-fit respectively with a numerical model simulating individual Coulomb scatterings on a large number of $\sim 10^6$ tracks,

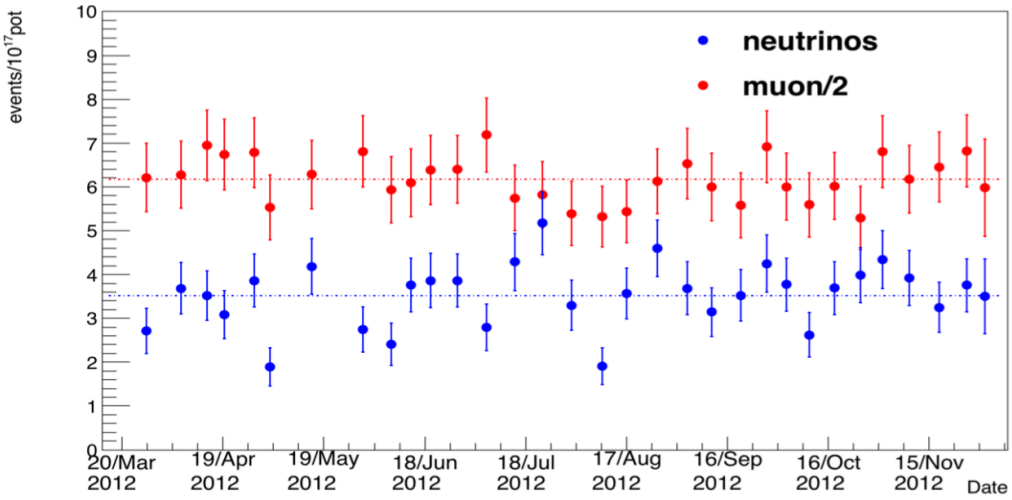

Figure 4.14: The number of collected ν interactions per 10^{17} pot as a function of date during 2012 runs. The neutrino interactions occurred inside the fiducial volume (blue) and rock muons (red, divided by 2), normalized by pot statistics and trigger/DAQ/re-alignment efficiency, as a function of run time (only statistical errors are quoted) [111].

X_0 - radiation length in liquid argon,

$\cos\delta$, $\sqrt{\cos\delta}$ - factors ($\cos\delta = L_{2D}/L_{3D}$) account for the projections on the Collection plane of the 3D MCS angle and the 3D muon length, respectively.

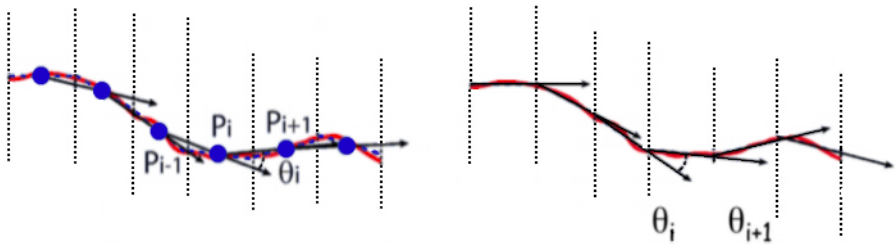

Figure 4.15: Scheme of the polygonal (left) and linear fit (right) deflection angle [71].

The p_{CAL} of each muon has been calculated from its kinetic energy measured by integration of all ionizing charge along the muon track, including delta rays and bremsstrahlung photons [124]. The electron-ion recombination and signal attenuation due to electronegative impurities were taken into account. The accuracy of p_{CAL} in data was estimated to be better than ∼1%. As an alternative, purely geometrical estimation was also computed giving the resolution of ∼4%.

Finally the MSC algorithm has been applied to the selected CNGS stopping muons. The results have been compared event by event to the corresponding p_{CAL} (see Fig. 4.16).

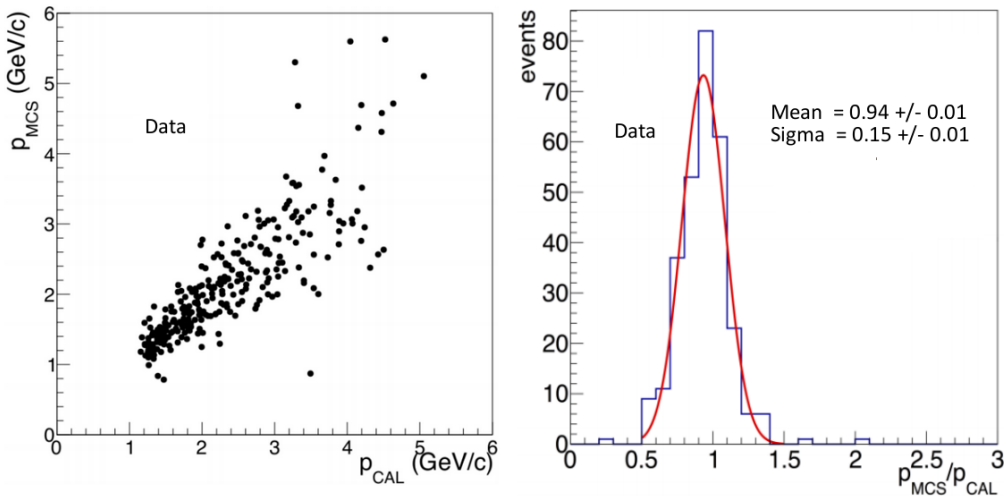

Figure 4.16: Left: The scatter-plot of p_{MCS} versus p_{CAL}. Right: The distribution of the p_{MCS}/p_{CAL} ratio. Both Figures refer to the full stopping CNGS muon sample. The FWHM width of the p_{MCS}/p_{CAL} distribution is ∼0.33 [71].

A momentum resolution of $\Delta p/p \sim 16\%$ was achieved in the 0.4–4 GeV/c range, which is of interest for future short/long-baseline experiments (see chapter 5). The detail description of the ICARUS T600 MSC algorithm can be found in [71].

4.4.2 The seven identified ν_e events from CNGS beam

The importance of the search for electron like neutrino interactions was shown in chapter 4.2 where the search for ν_e excess in ν_μ beam was described. The scanning of 2650 neutrino events, corresponding to $7.93 \cdot 10^{19}$ pot, resulted in the identification of 7 electron like neutrino events. The brief description of these events is presented below. The identified ν_e events and the results on their reconstruction are shown in Tab. 4.5 whereas pictures of them in Collection, Induction 1 and/or Induction 2 views are shown in Figs. 4.17 to 4.23 [111].

Table 4.5: The seven identified electron-neutrino events from CNGS beam. E_{dep} - total energy deposited inside fiducial volume and collected by the TPC wires, E_e - electron reconstructed energy, p_T - electron transversal momentum [111].

No.	Run	Event	E_{dep} [GeV]	E_e [GeV]	p_T [GeV/c]	Figure
1	10529	25901	5.2	2.0 ± 0.1	0.9 ± 0.3	4.17
2	10684	296	17	7.5 ± 0.3	1.3 ± 0.2	4.18
3	10871	9185	11.5	10.0 ± 1.8	1.8 ± 0.4	4.20
4	11319	2862	14	6.4 ± 0.3	1.2 ± 0.2	4.21
5	11580	7943	24	24.0 ± 1.0	1.5 ± 0.7	4.22
6	11731	4278	27	6.3 ± 1.5	3.5 ± 1.9	4.23
7	11845	12764	19.5	17.6 ± 0.8	1.1 ± 0.4	4.19

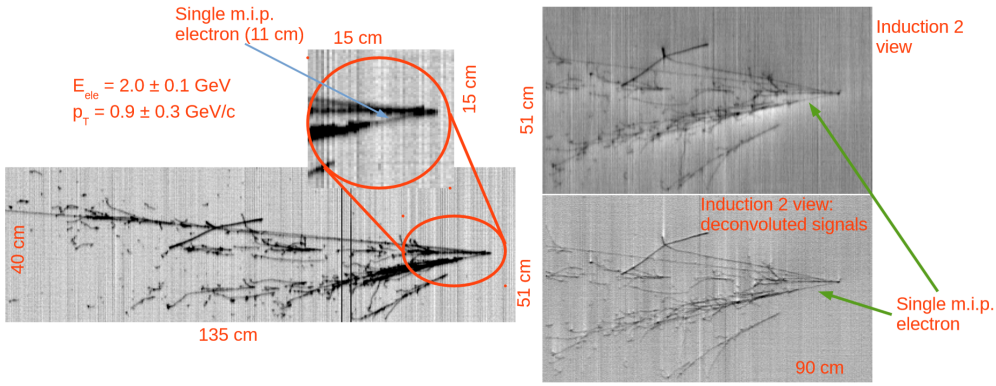

Figure 4.17: A CNGS ν_e event: Run 10529, event 25901. Collection (left) and Induction 2 (right) are shown.

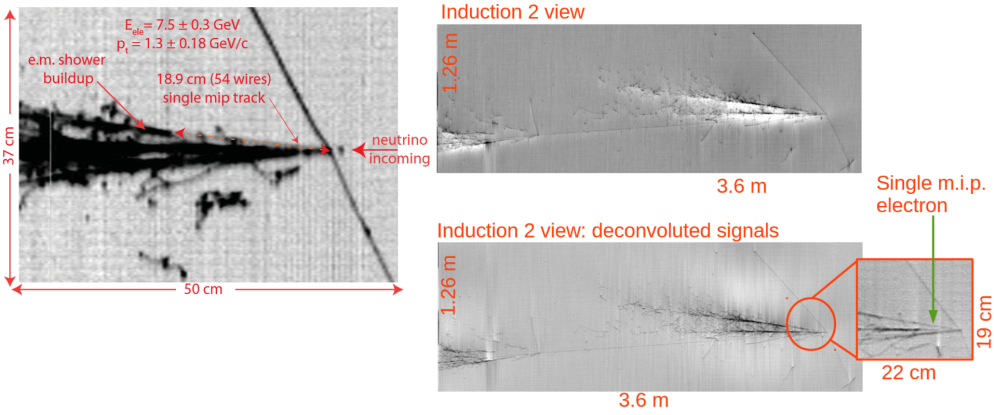

Figure 4.18: A CNGS ν_e event: Run 10684, event 296 [108]. Collection (left) and Induction 2 (right) views are shown.

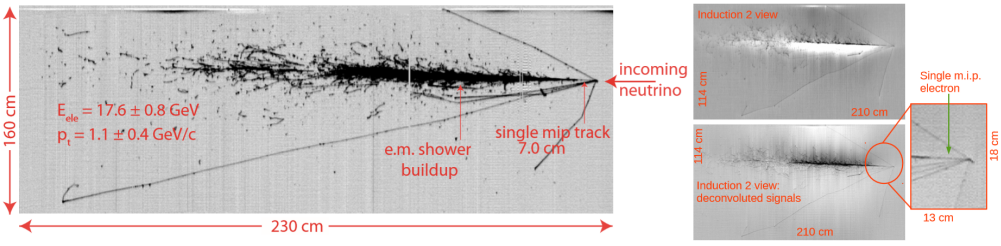

Figure 4.19: A CNGS ν_e event: Run 11845, event 12764. Collection (left) and Induction 2 (right) views are shown.

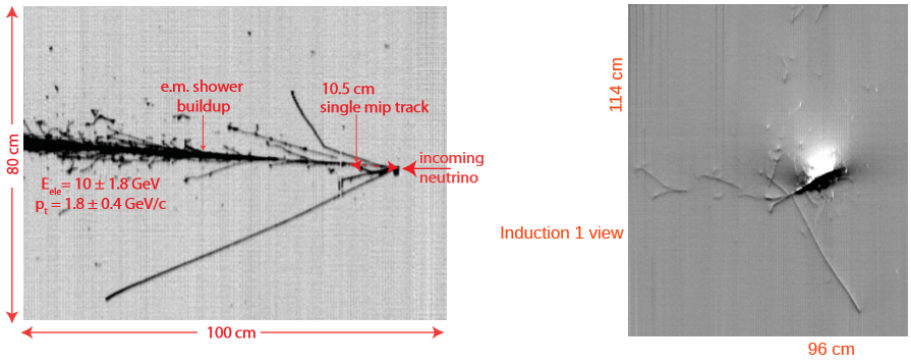

Figure 4.20: A CNGS ν_e event: Run 10871, event 9185 [108]. Collection (left) and Induction 1 (right) views are shown. The Induction 2 view was not available due to readout problems.

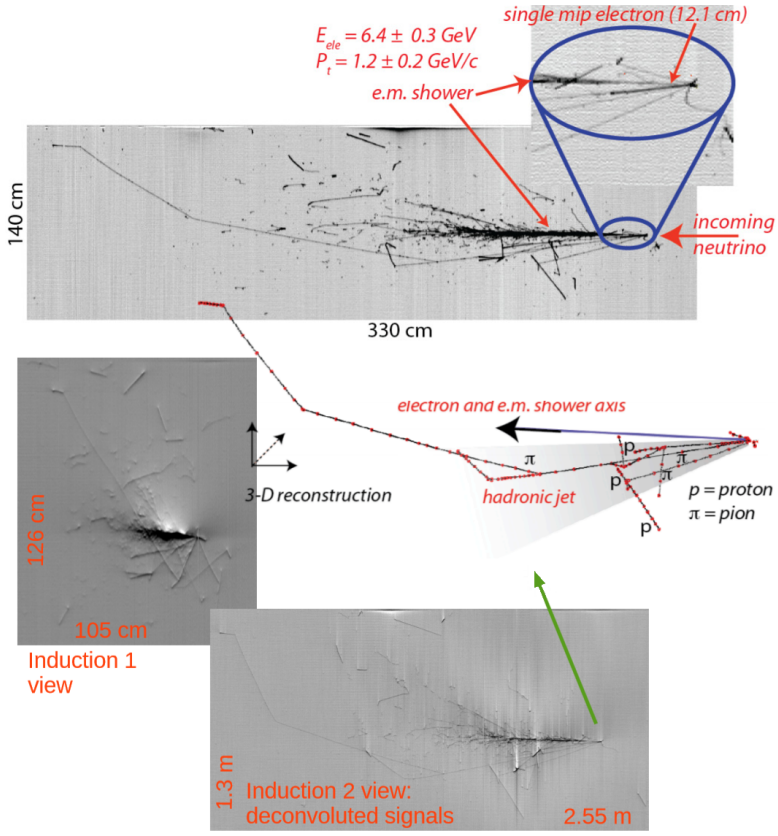

Figure 4.21: A CNGS ν_e event: Run 11319, event 2862 [109]. Collection (top), Induction 1 and 2 (bottom) views are shown.

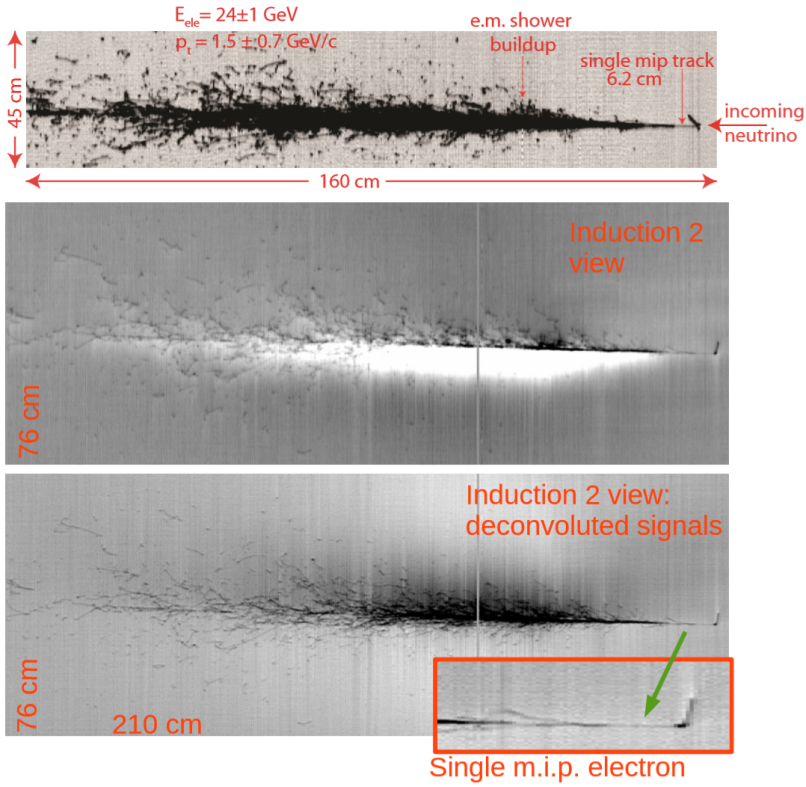

Figure 4.22: A CNGS ν_e event: Run 11580, event 7943. Collection (top) and Induction 2 (middle-bottom) views are shown.

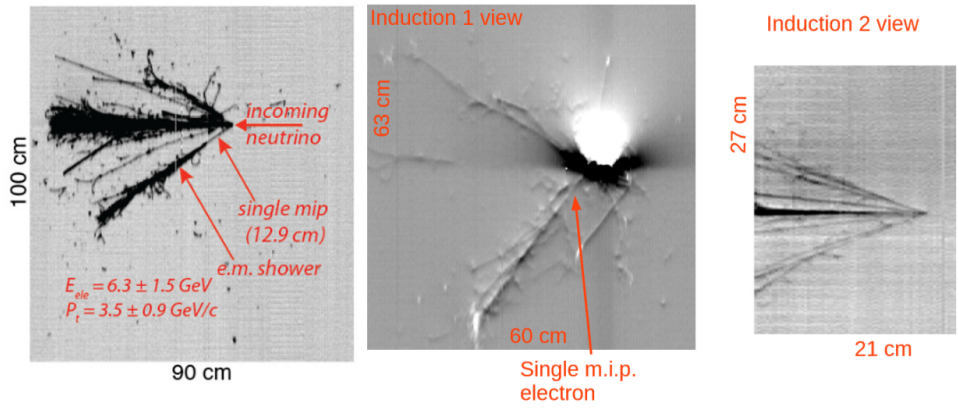

Figure 4.23: A CNGS ν_e event: Run 11731, event 4278 [109]. Collection (left), Induction 1 (middle) and 2 (right) views are shown.

4.4.3 The 2482 CNGS subsample data analysis

To be able to study various aspects of neutrino physics such as neutrino oscillation or ν_μ disappearance, one has to be sure about that the reconstruction of the collected data is correct. During the 2011–2012 runs the total number of 2482 neutrino interaction events were identified. For further analysis only 1403 muon-neutrino interactions were chosen (see Tab. 4.4), satisfying 2.5 m muon length requirement (∼3 hadronic interaction lengths in LAr). Among these events the subsample of ν_μCC events of stopping muons was used to validate the algorithm for muon momentum estimation from the Multiple Coulomb Scattering method [71]. Due to staggered boards, some of the events could not be properly reconstructed, which resulted in further reduction of events to 1285, corresponding to $6.73 \cdot 10^{19}$ pot. Careful visual scanning resulted in further reduction to 1191 events ($6.23 \cdot 10^{19}$ pot). The results presented in the following sections refer to these 1191 events. The events were divided into 3 groups: (1) "good" events, (2) "poor" and (3) "dimuon" events. The "good" events refer to the most clean and reliable, whereas in the "poor" ones there were detector hardware readout problems observed, resulting in problems in e.g. deposited energy reconstruction. The "dimoun" events contain at least two muon (or pion identified as muon) originated from neutrino interaction vertex. A few examples of muon-neutrino interactions are shown in Figs. 4.24 to 4.28.

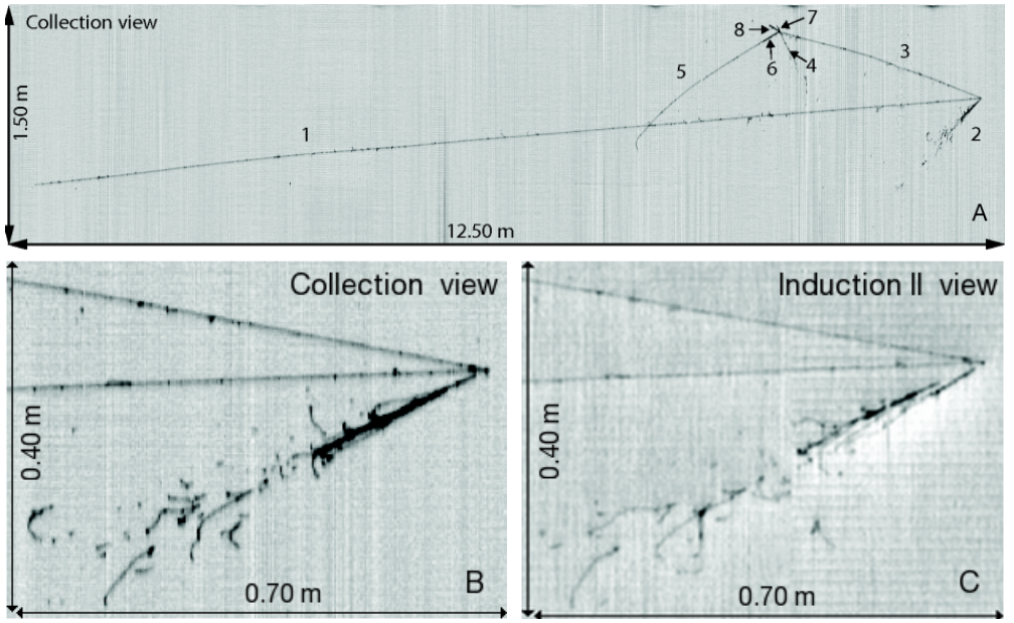

Figure 4.24: An example of ν_μCC interaction from the CNGS beam: (A) Collection view, (B) close-up view of the *primary* vertex and (C) Induction 2. The numbers in the Figure indicate particles originated from *primary* vertex: (1) μ, $E_{dep} = 2701$ MeV, (2) π^0, $E_{dep} = 521 \pm 16$ MeV, (3) π, $E_{dep} = 753 \pm 64$ MeV and particles from secondary vertex: (4) multiple tracks, (5) $\mu + e$ from 6, (6) K, (7) proton, (8) escaping [122].

During analysis, for each ν_μ interaction the following were identified: (1) the neutrino

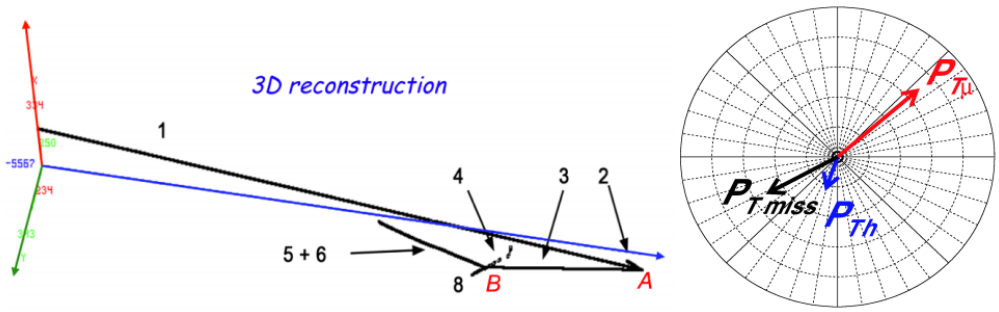

Figure 4.25: Left: 3D reconstruction of the event shown in Fig. 4.24. Right: Momentum reconstruction in the transverse plane for muon (p_{T_μ}), hadrons (p_{T_h}) and missing ($p_{T_{miss}}$); the neutrino direction is perpendicular to the page; the outermost circle corresponds to 500 MeV/c. Explanation of numbers can be found in Fig. 4.24 [122].

interaction vertex (*primary* vertex), (2) the place where muon is clearly separated from the hadronic jet (so called *beginning* vertex) and (3) the place where muon stopped or left the active volume of the detector. All this information was used by the procedure which determined muon momentum from MSC (section 4.4.1). In addition, it was checked and confirmed that the *primary* vertex is uniformly distributed inside the detector fiducial volume, for both CNGS data and FLUKA simulations (see Fig. 4.29). The deposited energy of the hadronic part was measured directly from the collected charge in the Collection wires, corrected for: (1) the quenching related to electrons recombination in LAr, (2) the attenuation due to the finite electrons lifetime and (3) for undetected (mostly due to neutrals) or not contained particles. The last case is set out in details in the following section.

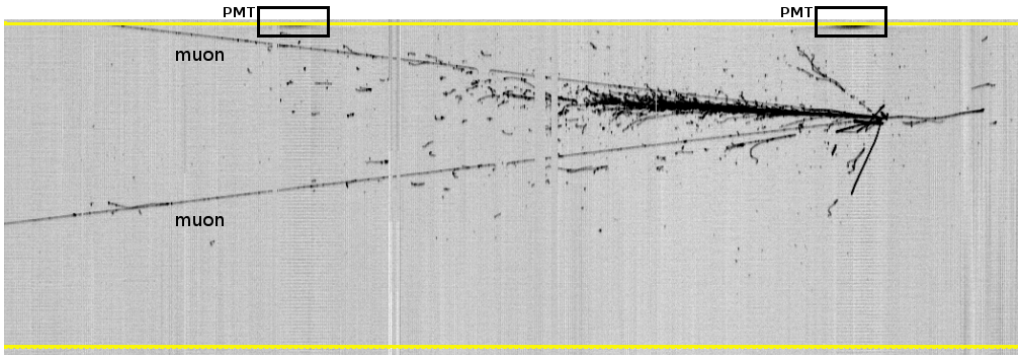

Figure 4.26: An example of CNGS ν_μCC interaction classified as "dimuon". Yellow lines: bottom - cathode, top - side wall of the module. The location of two PMTs is shown. Run 10542, event 80874.

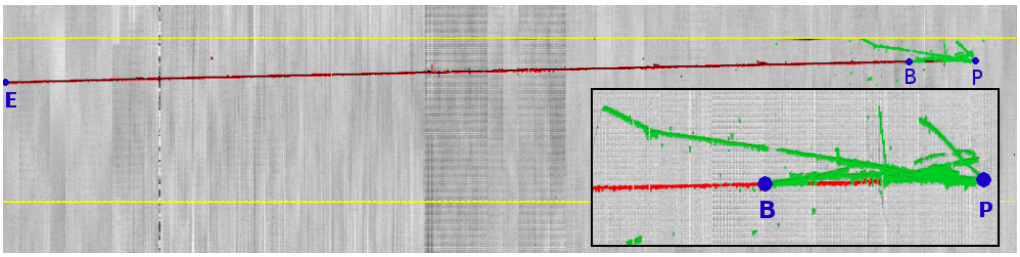

Figure 4.27: The example of CNGS ν_μCC event with denoted vertexes: (P) *primary*, (B) *beginning* and (E) *end*. Also the hadronic part of the event is shown (green color). Yellow lines: bottom - cathode, top - side wall of the module. Run 10489, event 11382.

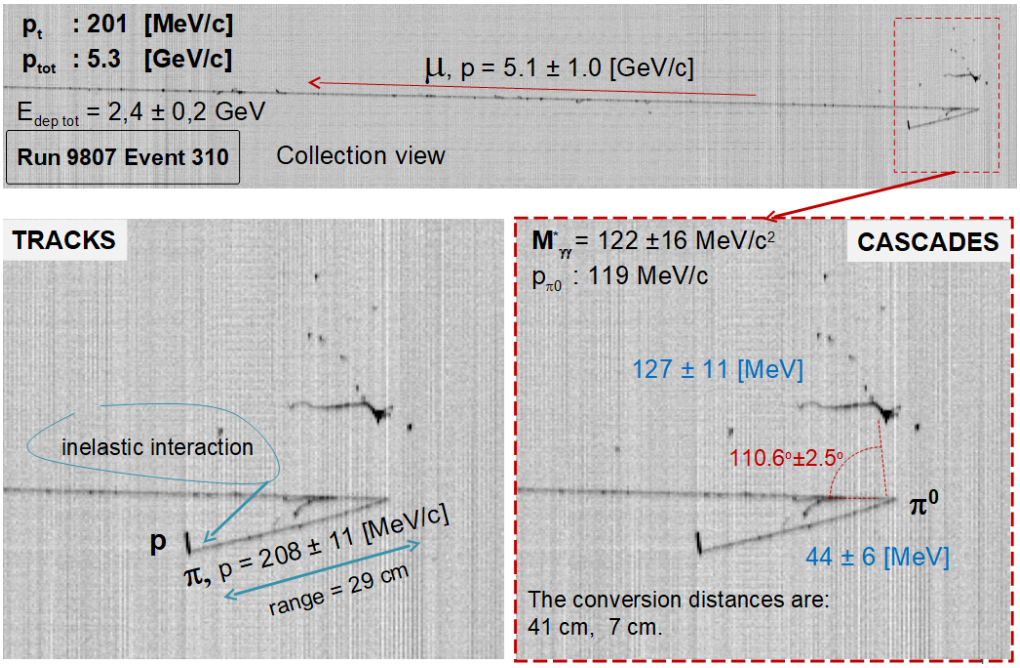

Figure 4.28: An example of fully reconstructed ν_μCC interaction from the CNGS beam, Run 9807, event 310.

4.4.4 Correction for undetected/non contained hadronic part

Neutrino interactions result in production of both, charged and neutral particles. To reconstruct the incoming neutrino energy, it is necessary to correct the measured energy deposited in the LAr-TPC by: (1) the not measured energy (not deposited) carried by the neutral particles and (2) for the not measured energy from particles leaving the fiducial volume of the detector. The correction was carried out only for the hadronic part of the events. The FLUKA simulation used was without muon propagation. To do

Table 4.6: Shell cuts and volume of individual shells. Colors correspond to the shell shown in Fig. 4.29. The cuts correspond to the distance between the shell and wall of the detector.

Shell number	cuts [cm]	volume with cathode cut [%]	volume without cathode cut [%]
1 (inner, blue)	upstream: 40 downstream: 100 side: 40	50.31	50.31
2 (middle, red)	upstream: 20 downstream: 60 side: 20	21.90	21.90
3 (outer, green)	upstream: 5 downstream: 15 side: 1.5	23.76	24.75
Sum		95.97	96.96

this each module of the detector was divided into three 3-dimensional shells, one inside the other (see Fig. 4.29), according to the cuts given in Tab. 4.6.

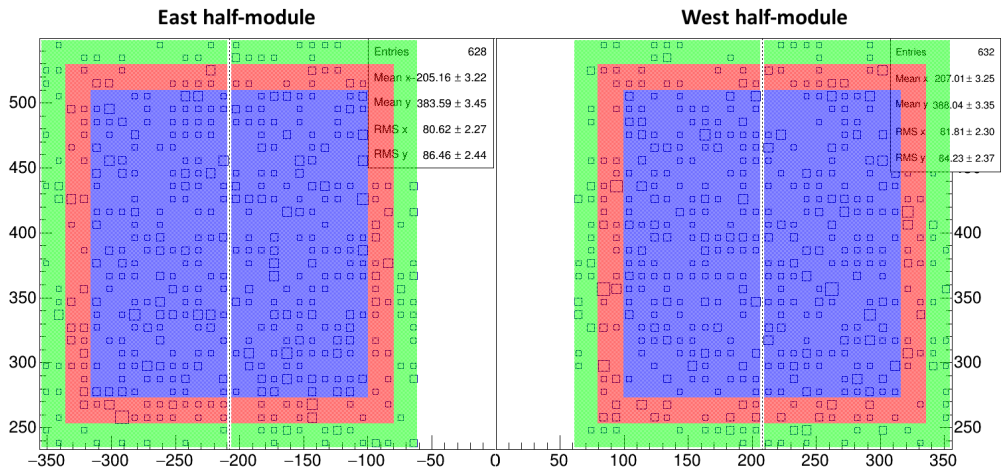

Figure 4.29: The scheme of the upstream ICARUS T600 detector view (XY plane, see Fig 2.7) with the three virtual shells, one inside the other. The shells are marked by colors: blue - the most inner one, red - middle and green - outer. The distribution of the *primary* vertexes of the CNGS ν_μCC events are also shown.

The correction factor (CF), for not measured (i.e. not deposited) energy, was calculated for each shell using ν_μCC events simulated with FLUKA package. The FLUKA simulation includes the detector geometry, necessary physical processes and ν_μ CNGS beam properties. The distribution of the CF is shown in Fig. 4.30. For each shell, a single value of CF was calculated, by taking the median or average value of the distribution. It was found that the median reflects correction better - long tail of CF distribution

significantly distorts the average CF value. Therefore it was decided that the median for CF will be used (see Tab. 4.7). The CF is defined as:

$$CF = \frac{E_{had}^{truth}}{E_{had}^{dep}}, \tag{4.8}$$

where:

E_{had}^{truth} - energy of the hadronic part of ν_μCC event obtained from FLUKA simulations i.e. muon-neutrino energy minus muon energy,

E_{had}^{dep} - reconstructed energy deposited by hadrons in the fiducial volume of the ICARUS T600 detector for ν_μCC FLUKA MC generated events.

Table 4.7: CF for three ICARUS T600 detector shells defined in Tab. 4.6. The number of CNGS ν_μ interactions inside each volume are shown as well.

Shell number	CF value	No. ν_μ
1 (inner)	1.68	771
2 (middle)	1.89	281
3 (outer)	2.36	206

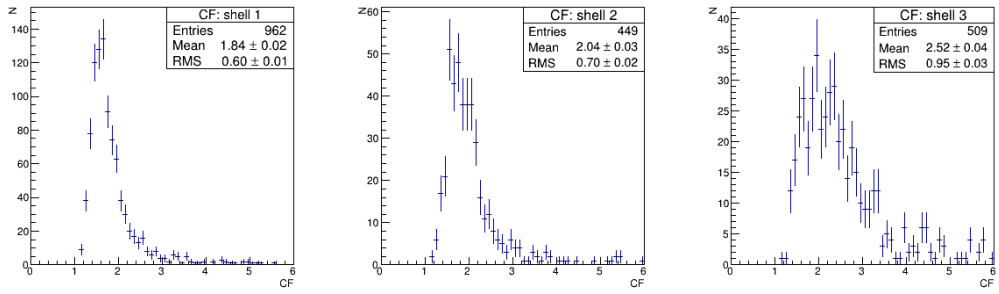

Figure 4.30: The MC correction factor distribution for individual shells.

The CFs were used to reproduce the deposited hadronic part of the energy spectrum of CNGS ν_μCC interactions. The energy of the hadronic part of an event E_{had} reconstructed from summed individual energy deposits in LAr was corrected according to Eq. 4.9 for: (1) deposited muon energy E_μ^{PB}, (2) charge attenuation (electron lifetime) and correction for charge quenching; average correction factor $R = 0.64$, from measurements on m.i.p., was used [125] and (3) non-contained hadronic jet. The comparison of the FLUKA and CNGS corrected hadron energy spectra is shown in Fig. 4.31. A good agreement between both distributions shows reliability of the applied approach.

$$E_{had}^{dep,\,corr} = \frac{E_{had}^{dep} - E_\mu^{PB}}{R} CF, \tag{4.9}$$

where:

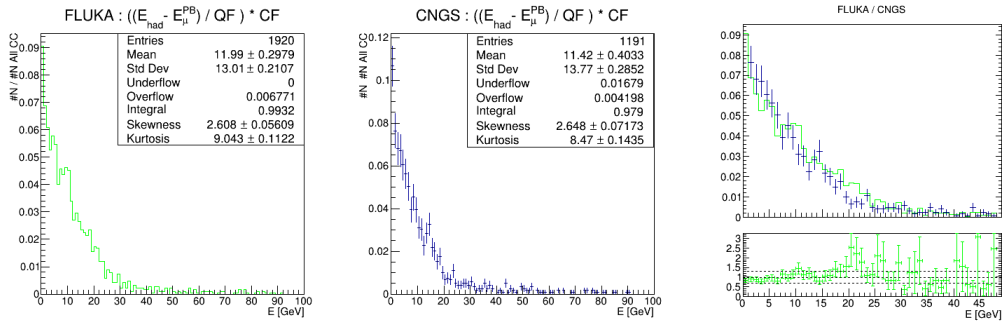

Figure 4.31: The hadron energy spectrum after corrections according to Eq. 4.9. The first and second (from left) Figures represent FLUKA and CNGS hadronic energy distributions, respectively. In the most right-top Figure the comparison between them is shown whereas the most right-bottom Figure represents the ratio plot between both distributions.

E_{had}^{dep} - hadronic energy; energy deposited by hadrons in LAr fiducial volume,

E_{μ}^{PB} - energy deposited by muon in the region where it was not possible to distinguish between a muon and the hadronic part of a ν_{μ}CC event, PB - distance between *primary* vertex and *beginning* vertex (see Fig. 4.27), E_{μ}^{PB} - energy deposited by a muon along its path from *primary* vertex to *beginning* vertex, calculated by taking into account the average energy loss per cm, equal to $\sim$2.1 MeV/cm for the μ in LAr,

R - quenching factor: charge attenuation and average correction for charge quenching,

CF - correction factor.

In addition, the length of a muon track from ν_{μ}CC CNGS interactions was measured. The corresponding distribution of the primary muon track's length (for $L_{\mu} > 2.5$ m) compared with the FLUKA Monte Carlo expectations is shown in Fig. 4.32. A very good agreement between the data and simulation is clearly visible. Both results were presented in the final ICARUS experiment reports to the CERN SPSC[8] [126] and LNGS Scientific Committee [127].

4.4.5 ν_{μ}CC vertex reconstruction

The visual scanning of CNGS data resulted, among others, in finding the neutrino interaction vertex (*primary* vertex). The precision of the vertex position reconstruction was validated by comparison between vertex position from FLUKA simulations and reconstructed coordinates from visual scanning (199 neutrino events from uniformly distributed Monte Carlo simulation were used). During the visual scanning the detection of vertexes from at least two views was required (Collection plane and at least one of the Induction views). On the basis of the visually selected vertex position in two views, the three dimensional reconstruction of the vertex position was performed. Such vertexes

[8] SPS and PS Experiments Committee.

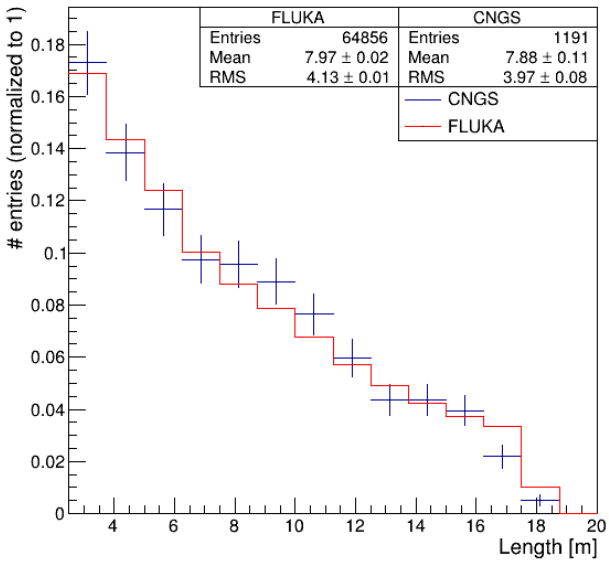

Figure 4.32: Reconstructed primary muon track length distributions: CNGS data and FLUKA simulation, normalized to 1, from ν_μ and $\overline{\nu}_\mu$CC interactions.

were compared with vertex coordinates from FLUKA simulation. On average, the true and scanned values differ by about 3.5 mm, showing high precision of applied procedure.

4.4.6 Reconstruction of the muon-neutrino energy E_{ν_μ}

In order to reconstruct muon-neutrino E_{ν_μ}, two components are required: (1) the energy of the hadronic part ($E_{had}^{dep,\,corr}$) and (2) the muon energy (E_μ) (Eq. 4.10). The same, as for the CF factor calculation, FLUKA Monte Carlo data were used.

$$E_{\nu_\mu} = E_{had}^{dep,\,corr} + E_\mu. \tag{4.10}$$

The corrected hadronic energy was obtained by using the method set out in section 4.4.4, whereas the muon energy was calculated by applying a gaussian smearing of 15% over the true muon momentum from MC. The results of the calculations and comparison with MC ν_μ energy spectrum are presented in Fig. 4.33. One can find good agreement between *true* (i.e. simulated) and reconstructed values. Unfortunately, the Multiple Coulomb Scattering algorithm prepared for determining the muon momentum (see section 4.4.1), was validated only for the muon momenta up to 4 GeV/c while the average muon energy from the CNGS beam is about 13.6 GeV (Fig. 4.34). Therefore, the gaussian smearing of MC μ momentum was used.

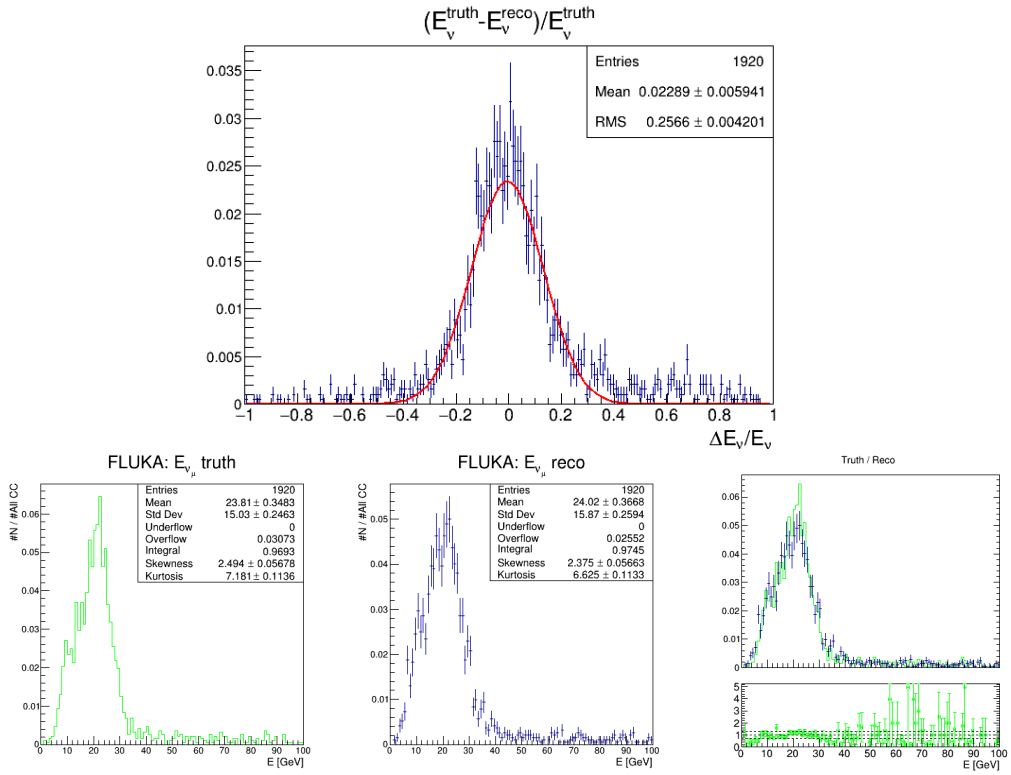

Figure 4.33: Simulated and reconstructed muon-neutrino energy distribution (E_{ν_μ}). Bottom: the first and second (from left) Figures represent simulated ('truth') and reconstructed (on the basis of simulated data; 'reco') E_{ν_μ} distributions, respectively. The most right-top and top Figures show comparison between them and in the most right-bottom Figure the ratio plot between both distributions is presented.

4.4.7 Search for ν_μ disappearance with the ICARUS T600 detector

The ICARUS T600 is investigating the disappearance of muon-neutrinos from ν_μ CNGS beam and application of the result to $|\Delta m^2_{32}|$ and $\sin^2(2\theta_{23})$ measurement. The disappearance of muon-neutrinos should manifest itself in the suppression of the total neutrino flux and the distortion of the neutrino spectrum measured in the ICARUS T600 detector. The CNGS beam is mainly composed of ν_μ with small ν_e ($\overline{\nu}_e$) contamination and negligible contamination of ν_τ (see chapter 3). The neutrinos can be distinguished, when they produce a charged lepton: (1) ν_μ produces a muon, (2) ν_e produces an electron and (3) ν_τ results in a tau production. In the ICARUS detector: (1) μ appears as a long almost straight track, (2) e from ν_e interaction is recognized by identification of particle originated from primary vertex which creates an electromagnetic cascade, while (3) τ is not observed. The τ which has a very short lifetime $(2.906(10) \pm 10^{-13}\,\mathrm{s})$ decays already after a few hundreds micrometers. Consequently, to observe the τ track a

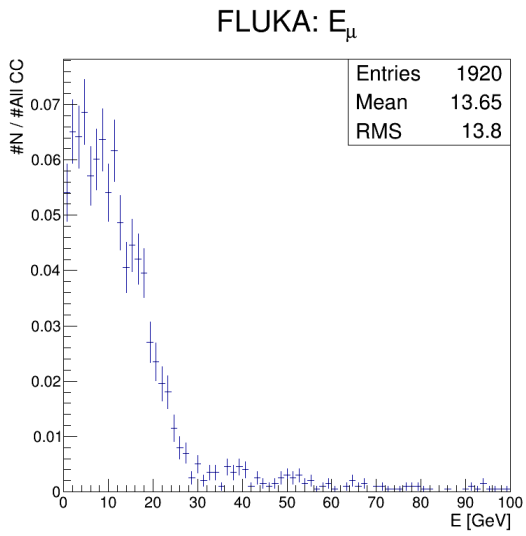

Figure 4.34: Simulated muon energy distribution (E_μ), normalized to 1, from ν_μCC interaction.

micrometer scale spatial resolution is necessary, something that only nuclear emulsions can provide. Therefore muon-neutrino disappearance can be explained by $\nu_\mu \rightarrow \nu_\tau$ oscillation phenomenon.

Neutrinos produced as ν_μ oscillate into ν_e and ν_τ neutrinos because the flavor eigenstates are superpositions of three mass eigenstates with different masses. Muon-neutrino disappearance depends on the survival probability which is given by [19, 128]:

$$\begin{aligned} P(\nu_\mu \rightarrow \nu_\mu) = 1 - 4\cos^2(\theta_{13})\sin^2(\theta_{23}) \\ [1 - \cos^2(\theta_{13})\sin^2(\theta_{23})] \\ \sin^2(1.27\Delta m^2_{32}\frac{L}{E_\nu}), \end{aligned} \tag{4.11}$$

where:

- E_ν - neutrino energy,
- L - neutrino propagation length i.e. the distance between the source and the detector,
- Δm^2_{32} - neutrino mass-squared difference $\Delta m^2_{32} = m^2_3 - m^2_2$ for normal hierarchy (NH),
- θ_{13}, θ_{23} - so-called neutrino mixing angles from Pontecorvo–Maki–Nakagawa–Sakata matrix [129, 130], defining how different the flavor states are from the mass states.

Using approximation for a two-flavor $\nu_\mu \rightarrow \nu_\tau$ oscillation, disappearance probability is given by:

$$P(\nu_\mu \to \nu_\mu) = 1 - \sin^2(2\theta_{23}) \sin^2(1.27\Delta m^2_{32} \frac{L}{E_\nu} [\text{eV}^2 \frac{\text{km}}{\text{GeV}}]) \quad \text{(SI unit), or}$$
$$P(\nu_\mu \to \nu_\mu) = 1 - \sin^2(2\theta_{23}) \sin^2(\Delta m^2_{32} \frac{L}{4E_\nu}) \quad \text{(natural units).} \tag{4.12}$$

These approximation is possible because the mixing angle θ_{13} is small and two of the mass states are very close in mass compared to the third.

In order to obtain the number of muon-neutrino events $N_{\nu_\mu \text{CC}}$ which should be observed inside the fiducial volume of the ICARUS T600 detector, the following has to be known:

- CNGS muon-neutrino flux Φ_{ν_μ} (Fig. 4.35 - top-left),
- ν_μCC-Ar cross section (currently due to lack of ν_μCC-Ar cross section the neutrino cross section per nucleon (for an isoscalar target) in further analysis was used (Fig. 4.35 - top-right)),
- integrated exposure accounting for the delivered beam ($6.23 \cdot 10^{19}$ for 2011–2012),
- two-neutrino survival probability (Eq. 4.12 and Fig. 4.35 - bottom-left),
- fiducial mass ($\langle 437.5 \rangle$ t: 433 t in 2011 and 442 t in 2012),
- estimated selection efficiency for the identification of ν_μCC events within the detector fiducial volume.

4.4.7.1 Expected ν_μ events

In this section a slightly different approach to getting the expected number of ν_μCC events than presented earlier from MC prediction, is shown. The expected number of ν_μCC events occurring inside the fiducial mass of LAr for the given number of pot can be obtained according to Eq. 4.13.

$$N_{\nu_\mu CC} = N_A m \int_{E_\nu^{min}}^{E_\nu^{max}} \Phi_{\nu_\mu} P_{surv}(E_\nu) \sigma_{\nu_\mu}(E_\nu) dE_\nu, \tag{4.13}$$

where:

N_A - Avogadro constant,
m - mass of the LAr in fiducial volume,
E_ν - neutrino energy,
E_ν^{min}, E_ν^{max} - minimal and maximal neutrino energy,
Φ_{ν_μ} - neutrino flux of the CNGS beam at Gran Sasso site,
P_{surv} - ν_μ survival probability,
σ_{ν_μ} - ν_μCC-nucleon cross section.

There are 4 sources of ν_μ: (1) "pure" ν_μ flux at GS from CNGS beam, (2) $\overline{\nu}_\mu$ ($\sim$13.3 events in the detector fiducial volume), (3) $\nu_e \to \nu_\mu$ ($\sim 2.98 \cdot 10^{-3}$) and (4) $\overline{\nu}_e \to \overline{\nu}_\mu$ ($\sim 2.1 \cdot 10^{-4}$). The values in (1–4) were calculated for the normal neutrino mass hierarchy. Total number of ν_μ has to be corrected for: (1) estimated selection efficiency for

the identification of ν_μCC events within the detector fiducial volume, (2) number of pot ($6.23 \cdot 10^{19}$), (3) percentage of the events satisfying $L_\mu > 2.5\,\text{m}$ (∼71%, see section 4.4) requirement and (4) NC contamination (∼10 events). The expected muon-neutrino spectrum (without $\overline{\nu}_\mu$, $\nu_e \to \nu_\mu$ and $\overline{\nu}_e \to \overline{\nu}_\mu$ contamination) calculated from Φ_{ν_μ} can be found in Fig. 4.35 - bottom-right. The total value of ν_μ events from various sources (ν_μ, $\overline{\nu}_\mu$, $\nu_e \to \nu_\mu$ and $\overline{\nu}_e \to \overline{\nu}_\mu$) in the energy range from 0 to 400 GeV is equal to 603.2, resulting after correction in about 1177 ν_μCC expected events whereas 1191 ν_μCC (corresponding to $6.23 \cdot 10^{19}$ pot) interactions inside the ICARUS T600 fiducial volume, were registered.

The results presented in sections 4.3 and 4.4.7 are preliminary and are still under analysis.

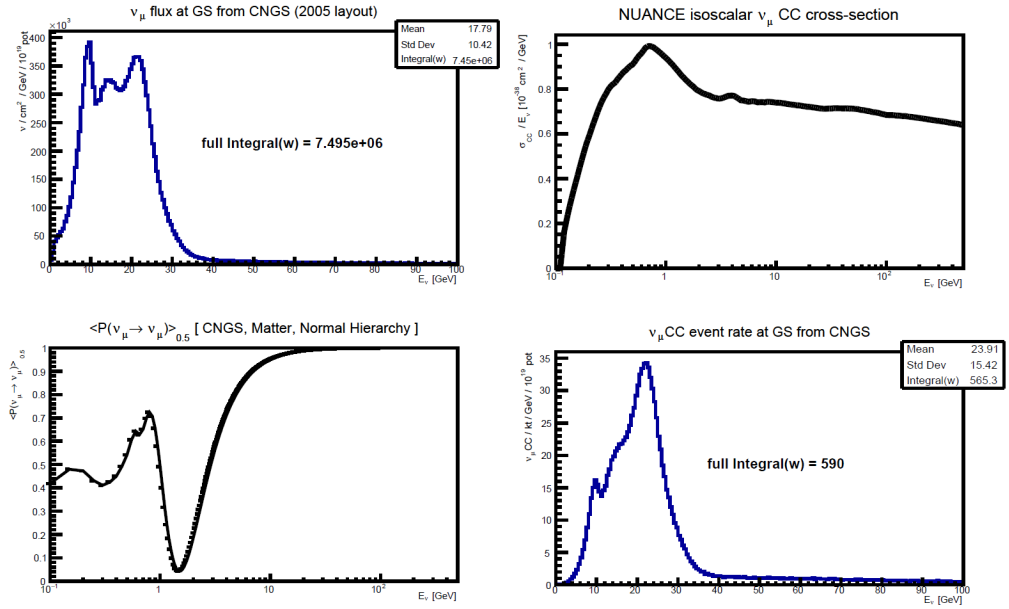

Figure 4.35: Top-left: Official neutrino flux at Gran Sasso site from CNGS (2005 layout) [10]. Bottom-left: $\langle P(\nu_\mu \to \nu_\mu)\rangle$ - ν_μ survival probability calculated with GLoBES [131, 132]. Top-right: neutrino cross section per nucleon (for an isoscalar target) divided by neutrino energy and plotted as a function of the energy obtained from the NUANCE generator [133]. The CNGS flux and ν_μ event rate are integrated over the full energy range (0–400 GeV). Bottom-right: CNGS ν_μCC event rate at GS for a mass of 1 kt and 10^{19} pot, obtained by multiplication of the flux by ν_μ survival probability and ν cross section.

Chapter 5

Current status of the ICARUS T600 detector

In 2014 the ICARUS T600 detector was moved to CERN for overhauling and refurbishing in the framework of the CENF platform for LAr-TPC development for short/long-baseline neutrino experiments (WA104 project, see section 2.6).

After completing the overhauling, in April 2017, the detector was transported to the Fermilab. The installation has begun in May 2017 whereas the detector commissioning is planned for 2018.

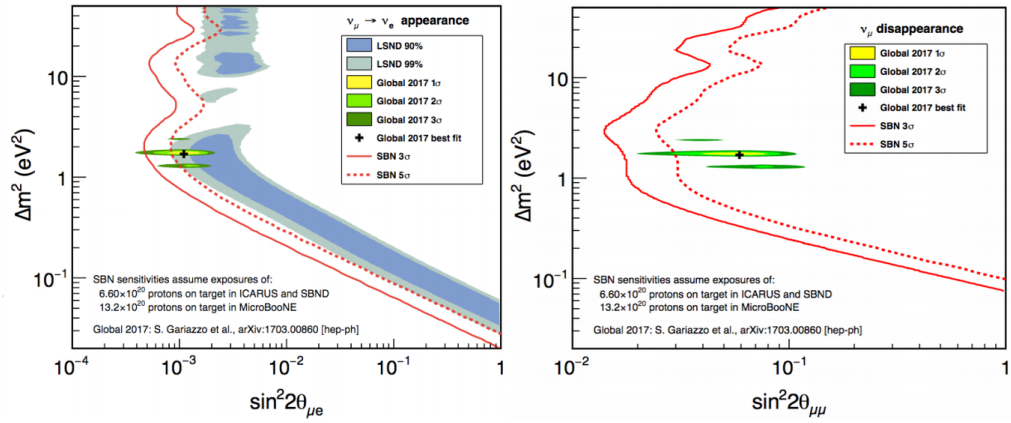

Figure 5.1: Left: Sensitivity in the ν_e appearance channel for three year combined data taking (plus three more years for MicroBooNE). Right: the same conditions but sensitivity achievable in the ν_μ disappearance channel [6].

The ICARUS T600 together with two other LAr-TPC detectors (SBND [11] and MicroBooNE [12]) will be a part of the Short-Baseline Neutrino Program at Fermilab (SBN [6]) which is a joint proposal of three collaborations exploiting the LAr-TPCs technique, to perform sensitive search and clarification of the LSND/MiniBooNE anomaly by precise and independent measurement of both ν_e appearance and ν_μ disappearance

oscillation channels exploiting the BNB. The expected ν_e appearance signal at each detector is shown in Fig. 5.3. BNB at FNAL is a ν_μ beam with ν_e and $\overline{\nu}_e$ contamination similar to the CNGS beam and at a level of 1% and the energy peaked at about 700 MeV, i.e. thus much lower than the CNGS one. In the case of absence of anomalies, which could be explained by the existence of the sterile flavor, signals from all three detectors should be a copy of each other. The assumed exposure, during three years of data taking, is about of $6.6 \cdot 10^{20}$ protons on target in ICARUS and SBND and $13.2 \cdot 10^{20}$ protons on target in MicroBooNE (so far more than $6.1 \cdot 10^{20}$ pot have been collected) [103, 134].

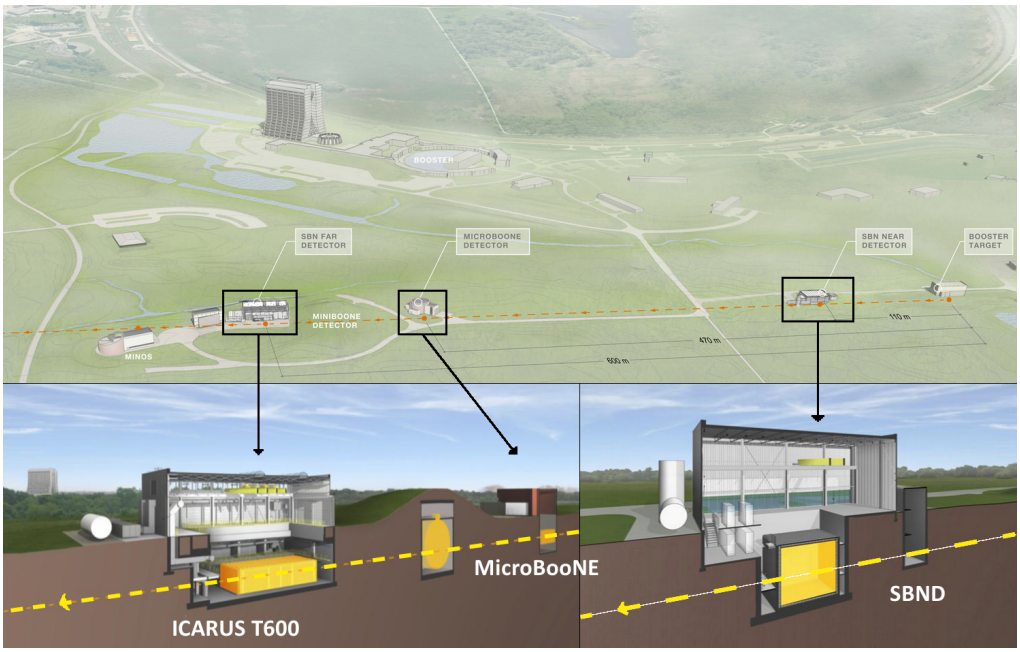

Figure 5.2: The location of three detectors (SBND, MicroBooNE and ICARUS) at FNAL site. The neutrino beam direction is indicated by the yellow/orange dashed lines [5].

The MC sensitivity simulations [6] demonstrate that the LSND 99% CL allowed region could be covered at 5σ level, in ν_e appearance mode. The SBN program will extend the sensitivity on ν_μ disappearance by a factor of ten, with respect to accelerator-based experiments. Fig. 5.1 presents the experimental sensitivity of the proposed Fermilab SBN program to $\nu_\mu \rightarrow \nu_e$ appearance signals in the $(\Delta m^2, \sin^2 2\theta)$ plane with a comparison to the original LSND allowed region [3].

The ICARUS T600 detector will serve as the last, farthest from the BNB target, detector placed at a distance of 600 m (Fig. 5.2). Description of individual detectors with their capabilities together with some information about the physical program can be also found in section 1.5.4 and chapter 2.

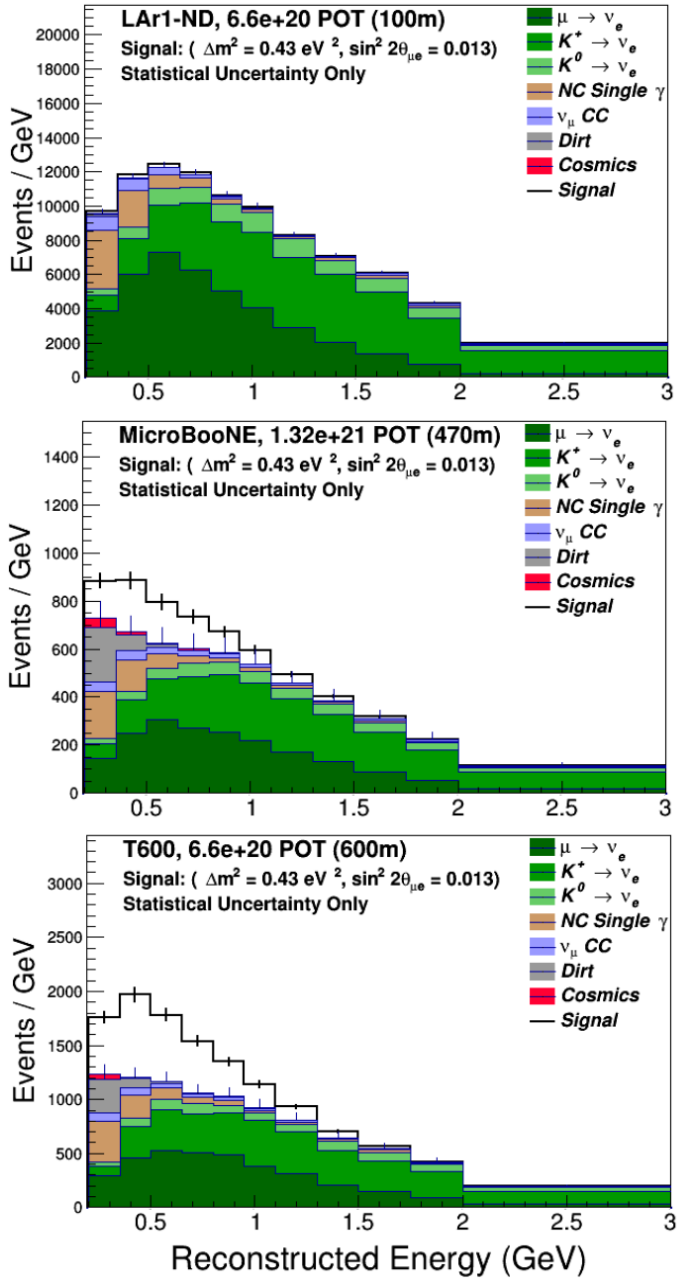

Figure 5.3: The SBN expected signal for $\nu_\mu \to \nu_e$ appearance at each of the detectors: SBND (top), MicroBooNE (middle) and ICARUS T600 (bottom). Oscillation signal events for the best-fit oscillation parameters from [135] are indicated by the white histogram on top in each distribution and demonstrates the expected signal enhancement with increasing baseline distance [6].

Conclusions

In previous chapters I presented the most important past, current and future experiments that use the LAr-TPC based detectors. I focused most on the ICARUS detector, whose potential and capabilities allowed for further investigation of a rare phenomena. This detector is a milestone towards the realization of future massive LAr detectors. Historically, imaging detectors have always played an important role in particle physics. In recent decades, successive detector generations have allowed to visualize the interaction of particles, in a completely new way, advancing the progress of science and the discovery of unpredicted phenomena, even on the basis of single fully reconstructed events.

The ICARUS T600 detector, installed underground at the LNGS laboratory, collected data from May 2010 to 2013. During its operation, the T600 detector proved that liquid argon technique is a really advancement. Its technical performance can be summarized as follows:

- unique 3D reconstruction capabilities ($1\,\mathrm{mm}^3$ spatial resolution in event topology), with accurate ionization measurement,
- good calorimetric energy resolution $\sigma(E)/E\,[\mathrm{GeV}]$ for: (1) hadronic showers ($\simeq 0.3/\sqrt{E}$), (2) electromagnetic showers ($\simeq 0.03/\sqrt{E}$) and (3) low energy electron ($\simeq 0.11/\sqrt{E} + 0.02$),
- good particle identification via dE/dx measurement,
- very good e/π_0 separation by means of dE/dx in the first part of the cascade and e/γ separation with 2% X_0 sampling ($X_0 = 14\,\mathrm{cm}$),
- momentum reconstruction of non fully contained muon via Multiple Scattering ($\Delta p/p \simeq 16\%$) in the 0.4–4 GeV/c momentum range of interest for the future short/long-baseline neutrino experiments,
- very long electron mobility (achievements in LAr purification, electron lifetime $\tau_e > 15\,\mathrm{ms}$) being a key feature in point of view of new larger mass LAr-TPCs.

Using LAr-TPC detector, all the above characteristics allow for better reconstruction and identification of the events with respect to the other neutrino experiments. Besides superior technical achievements the ICARUS has also pure physics accomplishments being the result of a wide physics program carried out by the Collaboration. The main goal was to (1) collect events from the ν_μ CNGS neutrinos beam to study the $\nu_\mu \to \nu_\tau$ oscillation, (2) study the solar and atmospheric neutrino, (3) search for LSND-like ν_e excess and (4) explore in a new way the nucleon stability, in particular channels beyond the present limits. Some of the results were described in detail in the previous chapters

and some are still under study. During 2013, after the definitive CNGS beam stop on December 3rd 2012, the ICARUS T600 detector continued its data taking with cosmic rays until June 26th, when the detector decommissioning started. The decommissioning procedure lasted throughout 2014 and resulted in transportation of both ICARUS cryostats to CERN in December 2014. The CERN was only a pit stop on the way to the Fermilab, where ICARUS will continue further research in the field of neutrino physics as it was mentioned in the last chapter.

The experience gained from the ICARUS experiment is of great value for the future research in these fields. The ICARUS showed that the LAr-TPCs offer really unique and magnificent imaging performance with excellent energy resolution and good background rejection power. Massive LAr-TPCs located underground are also capable of delivering compelling atmospheric neutrino detection, very sensitive proton decay search and astrophysical source study. Moreover it is complementary to long-baseline physics with beams. The worldwide neutrino scientific community should strive for a further generation of deep-underground several dozen kton or even more LAr-TPC detectors.

Appendix A

The Famous Pauli letter

The existence of neutrinos was postulated for the first time by Wolfgang Pauli in 1930 to explain how beta decay could conserve energy, momentum and angular momentum (spin). Wolfgang Pauli called it neutron. In 1931 Enrico Fermi renamed Pauli's "neutron" to neutrino. Pauli, in his now famous letter, suggested that this "neutron" was emitted during beta decay and had simply not yet been observed:

"Dear Radioactive Ladies and Gentlemen,

As the bearer of these lines, to whom I graciously ask you to listen, will explain to you in more detail, because of the "wrong" statistics of the N- and Li-6 nuclei and the continuous beta spectrum, I have hit upon a desperate remedy to save the "exchange theorem" (1) of statistics and the law of conservation of energy. Namely, the possibility that in the nuclei there could exist electrically neutral particles, which I will call neutrons, that have spin 1/2 and obey the exclusion principle and that further differ from light quanta in that they do not travel with the velocity of light. The mass of the neutrons should be of the same order of magnitude as the electron mass and in any event not larger than 0.01 proton mass. - The continuous beta spectrum would then make sense with the assumption that in beta decay, in addition to the electron, a neutron is emitted such that the sum of the energies of neutron and electron is constant.

Now it is also a question of which forces act upon neutrons. For me, the most likely model for the neutron seems to be, for wave-mechanical reasons (the bearer of these lines knows more), that the neutron at rest is a magnetic dipole with a certain moment μ. The experiments seem to require that the ionizing effect of such a neutron can not be bigger than the one of a gamma-ray and then μ is probably not allowed to be larger than $e \cdot (10^{-13}$ cm).

But so far I do not dare to publish anything about this idea and trustfully turn first to you, dear radioactive people, with the question of how likely it is to find experimental evidence for such a neutron if it would have the same or perhaps a 10 times larger ability to get through [material] than a gamma-ray. I admit that my remedy may seem almost

Original - Photocopie of PLC 0393

Abschrift/15.12.30 PM

Offener Brief an die Gruppe der Radioaktiven bei der Gauvereins-Tagung zu Tübingen.

Abschrift

Physikalisches Institut
der Eidg. Technischen Hochschule
Zürich

Zürich, 4. Dez. 1930
Gloriastrasse

Liebe Radioaktive Damen und Herren,

Wie der Ueberbringer dieser Zeilen, den ich huldvollst anzuhören bitte, Ihnen des näheren auseinandersetzen wird, bin ich angesichts der "falschen" Statistik der N- und Li-6 Kerne, sowie des kontinuierlichen beta-Spektrums auf einen verzweifelten Ausweg verfallen um den "Wechselsatz" (1) der Statistik und den Energiesatz zu retten. Nämlich die Möglichkeit, es könnten elektrisch neutrale Teilchen, die ich Neutronen nennen will, in den Kernen existieren, welche den Spin 1/2 haben und das Ausschliessungsprinzip befolgen und sich von Lichtquanten ausserdem noch dadurch unterscheiden, dass sie nicht mit Lichtgeschwindigkeit laufen. Die Masse der Neutronen müsste von derselben Grössenordnung wie die Elektronenmasse sein und jedenfalls nicht grösser als 0,01 Protonenmasse.- Das kontinuierliche beta- Spektrum wäre dann verständlich unter der Annahme, dass beim beta-Zerfall mit dem Elektron jeweils noch ein Neutron emittiert wird, derart, dass die Summe der Energien von Neutron und Elektron konstant ist.

Nun handelt es sich weiter darum, welche Kräfte auf die Neutronen wirken. Das wahrscheinlichste Modell für das Neutron scheint mir aus wellenmechanischen Gründen (näheres weiss der Ueberbringer dieser Zeilen) dieses zu sein, dass das ruhende Neutron ein magnetischer Dipol von einem gewissen Moment μ ist. Die Experimente verlangen wohl, dass die ionisierende Wirkung eines solchen Neutrons nicht grösser sein kann, als die eines gamma-Strahls und darf dann μ wohl nicht grösser sein als $e \cdot (10^{-13}$ cm).

Ich traue mich vorläufig aber nicht, etwas über diese Idee zu publizieren und wende mich erst vertrauensvoll an Euch, liebe Radioaktive, mit der Frage, wie es um den experimentellen Nachweis eines solchen Neutrons stände, wenn dieses ein ebensolches oder etwa 10mal grösseres Durchdringungsvermögen besitzen würde, wie ein gamma-Strahl.

Ich gebe zu, dass mein Ausweg vielleicht von vornherein wenig wahrscheinlich erscheinen wird, weil man die Neutronen, wenn sie existieren, wohl schon längst gesehen hätte. Aber nur wer wagt, gewinnt und der Ernst der Situation beim kontinuierliche beta-Spektrum wird durch einen Ausspruch meines verehrten Vorgängers im Amte, Herrn Debye, beleuchtet, der mir kürzlich in Brüssel gesagt hat: "O, daran soll man am besten gar nicht denken, sowie an die neuen Steuern." Darum soll man jeden Weg zur Rettung ernstlich diskutieren.- Also, liebe Radioaktive, prüfet, und richtet.- Leider kann ich nicht persönlich in Tübingen erscheinen, da ich infolge eines in der Nacht vom 6. zum 7 Dez. in Zürich stattfindenden Balles hier unabkömmlich bin.- Mit vielen Grüssen an Euch, sowie an Herrn Back, Euer untertänigster Diener

gez. W. Pauli

Figure A.1: Famous Pauli's letter suggesting existence of an additional particle: neutron [20].

improbable because one probably would have seen those neutrons, if they exist, for a long time. But nothing ventured, nothing gained and the seriousness of the situation, due to the continuous structure of the beta spectrum, is illuminated by a remark of my honored predecessor, Mr Debye, who told me recently in Bruxelles: "Oh, It's better not to think about this at all, like new taxes." Therefore one should seriously discuss every way of rescue. Thus, dear radioactive people, scrutinize and judge. - Unfortunately, I cannot personally appear in Tübingen since I am indispensable here in Zürich because of a ball on the night from December 6 to 7. With my best regards to you and also to Mr. Back, your humble servant

signed W. Pauli"

The Pauli's letter (Fig. A.1) and the translation taken from [20].

Appendix B

A new concept for ν detectors: LAr-TPC

The place and time where LAr-TPC detector's history began. The first page of the CERN report with a liquid argon detector proposal (Fig. B.1) [7] where Carlo Rubbia suggested to use LAr-TPC (originally LAPC) for neutrino detection.

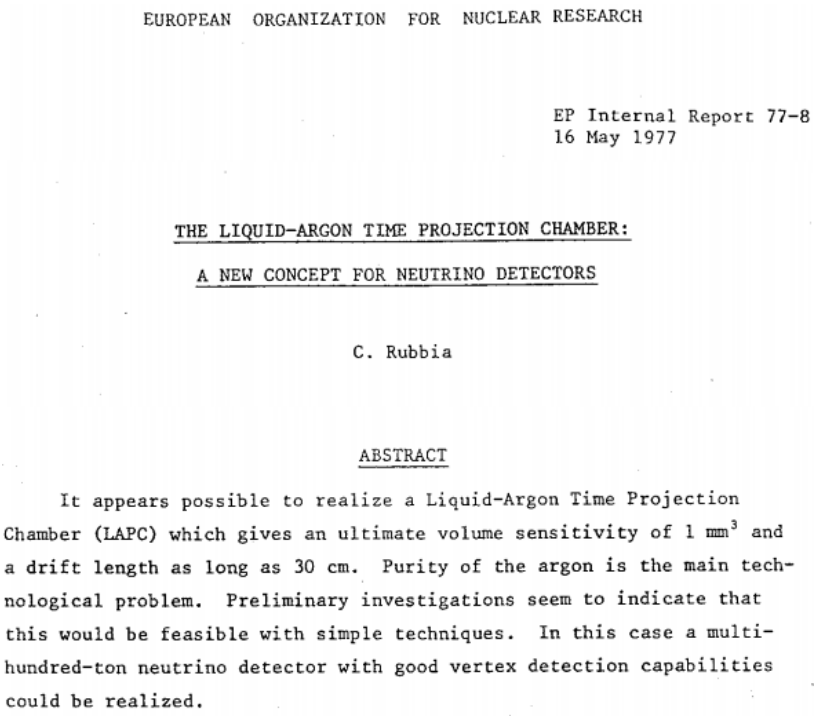

EUROPEAN ORGANIZATION FOR NUCLEAR RESEARCH

EP Internal Report 77-8
16 May 1977

THE LIQUID-ARGON TIME PROJECTION CHAMBER:

A NEW CONCEPT FOR NEUTRINO DETECTORS

C. Rubbia

ABSTRACT

It appears possible to realize a Liquid-Argon Time Projection Chamber (LAPC) which gives an ultimate volume sensitivity of 1 mm^3 and a drift length as long as 30 cm. Purity of the argon is the main technological problem. Preliminary investigations seem to indicate that this would be feasible with simple techniques. In this case a multi-hundred-ton neutrino detector with good vertex detection capabilities could be realized.

Figure B.1: The first page of the report with a liquid argon detector proposal [7].

Acknowledgements

People don't have to like or support you, so you always have to say thank you

Ruben Studdard, September 2003

Numerous people have been indispensable during the completion of this work and have given me valuable insights as the project progressed. I had the privilege to be supervised by great people, who offered me their trust and assistance in my works.

First of all I would like to express my gratitude to the leader of our Katowice ICARUS group Prof. Dr. Jan Kisiel for his criticisms, insights and suggestions while writing this monograph. I am grateful for his careful reading of the manuscript and many useful remarks.

I am deeply indebted to Jacek Holeczek for his criticism and biting comments about my work. He reminded me that sometimes it is better to stop running and to think first.

I owe great dept to my colleagues from Padova, Pavia and Kraków group: Daniele Gibin, Christian Farnese, Filippo Varanini, Alessandro Menegolli and Krzysztof Cieślik. Our weekly meetings and discussions on data analysis were extremely helpful during the implementation of my work.

I also thank Basia Mierzyńska, an English teacher, for reading the manuscript and for correcting the English language.

I would like to express my sincere gratitude to all who guided some aspects of my work and helped whenever I was in need, especially enriching my knowledge for their unique insight into the world of liquid argon technology. I would like to thank all those people who have contributed to the success of the ICARUS experiment over the years. Without their contribution, this work would have no basis to arise.

A really huge and special thanks go to my wife Basia and to my daughters, Tosia and Marysia, for their patience, endurence my moods, support me in the moments of fatigue and doubt, making every day special and for giving joy and will to lives.

At the end I would like to thank once more all those who made this work an enjoyable experience for me. This monograph would have never been possible without them.

Bibliography

[1] Official LNGS website, URL: https://www.lngs.infn.it, 2017, accessed: 2017-09-19.

[2] M. Buhler-Broglin *et al.*, (2000), CERN AC Note (2000-03).

[3] LSND Collaboration, A. Aguilar *et al.*, Physical Review D **64**, 112007 (2001), DOI: 10.1103/PhysRevD.64.112007.

[4] T. Adam *et al.*, Journal of High Energy Physics **2012**, 93 (2012), DOI: 10.1007/JHEP10(2012)093.

[5] Official Fermilab website, URL: http://www.fnal.gov, 2017, accessed: 2018-02-16.

[6] R. Acciarri *et al.*, (2015), arXiv:1503.01520.

[7] C. Rubbia, (1977), CERN Report No. CERN-EP-INT-77-8.

[8] S. Amerio *et al.*, Nuclear Instruments and Methods in Physics Research Section A **527**, 329 (2004), DOI: 10.1016/j.nima.2004.02.044.

[9] Official INFN website, URL: http://infn.it, 2017, accessed: 2018-02-16.

[10] Official CNGS project website, URL: http://proj-cngs.web.cern.ch/proj-cngs, 2017, accessed: 2017-09-19.

[11] Official SBND website, URL: http://sbn-nd.fnal.gov, 2017, accessed: 2017-11-07.

[12] B. J. P. Jones, (2011), arXiv:1110.1678.

[13] Official DUNE website, URL: http://www.dunescience.org, 2017, accessed: 2017-09-15.

[14] CERN Neutrino Platform, URL: http://cenf.web.cern.ch, 2017, accessed: 2017-09-18.

[15] ICARUS/WA104 Collaboration, M. Bonesini, Journal of Physics: Conference Series **650**, 012015 (2015), DOI: 10.1088/1742-6596/650/1/012015.

[16] C. L. Cowan *et al.*, Science **124**, 103 (1956), DOI: 10.1126/science.124.3212.103.

[17] G. Danby *et al.*, Physical Review Letter **9**, 36 (1962), DOI: 10.1103/PhysRevLett.9.36.

[18] K. Kodama *et al.*, Physics Letters B **504**, 218 (2001), DOI: 10.1016/S0370-2693(01)00307-0.

[19] S. Bilenky, *Introduction to the Physics of Massive and Mixed Neutrinos* (Springer Berlin Heidelberg, 2010), DOI: 10.1007/978-3-642-14043-3.

[20] C. Polly, Neutrino history 1927 - 1987, 2010, MicroBooNE-doc-953-v1.

[21] A. R. Clark *et al.*, PEP-PROPOSAL-004, SLAC (1976).

[22] T. Doke, Nuclear Instruments Methods **A327**, 113 (1993), DOI: 10.1016/0168-9002(93)91423-K.

[23] A. Rubbia, Nuclear Physics B - Proceedings Supplements **235-236**, 190 (2013), DOI: 10.1016/j.nuclphysbps.2013.04.010.

[24] W. J. Willis and V. Radeka, Nuclear Instruments and Methods **120**, 221 (1974), DOI: 10.1016/0029-554X(74)90039-1.

[25] N. Canci, Physics Procedia **37**, 1257 (2012), DOI: 10.1016/j.phpro.2012.02.466, Proceedings of the 2nd International Conference on Technology and Instrumentation in Particle Physics (TIPP 2011).

[26] R. Acciarri *et al.*, (2016), arXiv:1601.05471.

[27] Official Hyper-Kamiokande project website, URL: http://www.hyperk.org, 2017, accessed: 2017-12-29.

[28] CERN Gargamelle website, URL: https://home.cern/about/experiments/gargamelle, accessed: 2018-02-03.

[29] CERN library of archives of Gargamelle Bubble Chamber, CERN-ARCH-GGM-001 to CERN-ARCH-GGM-153, 2007.

[30] M. Antonello *et al.*, Journal of Instrumentation **9**, P12006 (2014), DOI: 10.1088/1748-0221/9/12/P12006.

[31] W. Walkowiak, Nuclear Instruments and Methods **A449**, 288 (2000), DOI: 10.1016/S0168-9002(99)01301-7.

[32] S. Amoruso *et al.*, Nuclear Instruments and Methods in Physics Research Section A **516**, 68 (2004), DOI: 10.1016/j.nima.2003.07.043.

[33] C. Zhang, X. Qian, and B. Viren, Wire-Cell - A 3D Reconstruction Package for LArTPC, URL: http://www.phy.bnl.gov/wire-cell, 2017, accessed: 2017-09-07.

[34] A. Rubbia, (2004), arXiv:hep-ph/0402110.

[35] Dual-Phase Liquid Argon Time Projection Chambers, URL: http://if-docdb.fnal.gov, 2017, accessed: 2017-09-16.

[36] A. Bubak, Acta Physica Polonica B **46**, 2387 (2015), DOI: 10.5506/APhysPolB.46.2387.

[37] L. A. Bella, Nuclear Instruments and Methods in Physics Research Section A **718**, 60 (2013), DOI: 10.1016/j.nima.2012.11.077, Proceedings of the 12$^{\text{th}}$ Pisa Meeting on Advanced Detectors.

[38] D. B. Cline *et al.*, Nuclear Instruments and Methods in Physics Research Section A **503**, 136 (2003), DOI: 10.1016/S0168-9002(03)00656-9, Proceedings of the 3$^{\text{rd}}$ International Workshop on Neutrino Factories based on Muon Storage Rings.

[39] C. Anderson *et al.*, Journal of Instrumentation **7**, P10019 (2012), DOI: 1748-0221/7/10/P10019.

[40] J. Paley *et al.*, (2014), arXiv:1406.5560.

[41] CAPTAIN Collaboration, H. Berns *et al.*, (2013), arXiv:1309.1740.

[42] O. Palamara, private communication, 2017.

[43] First Neutrino Events Candidates in MicroBooNE, URL: https://www-microboone.fnal.gov/first-neutrinos, 2017, accessed: 2017-09-13.

[44] Official VENu project website, URL: http://venu.physics.ox.ac.uk, 2018, accessed: 2018-02-04.

[45] B. Baibussinov *et al.*, Astroparticle Physics **29**, 174 (2008), DOI: 10.1016/j.astropartphys.2008.01.001.

[46] N. McConkey, (2017), EPS-HEP 2017.

[47] V. Papadimitriou *et al.*, (2017), arXiv:1704.04471.

[48] M. Nessi, European Neutrino Meeting LBNF/DUNE, 2016, URL: https://indico.cern.ch/event/493989/contributions/2005327.

[49] B. Abi *et al.*, (2017), arXiv:1706.07081.

[50] D. Autiero, ProtoDUNE dual-phase overview, URL: https://indico.cern.ch/event/617300, 2017, accessed: 2018-01-18.

[51] ArgonCube Collaboration, C. Amsler *et al.*, (2015), CERN Report No. CERN-SPSC-2015-009, SPSC-I-243.

[52] ArgonCube Collaboration, M. Auger, A. Ereditato, and J. Sinclair, (2017), CERN Report No. CERN-SPSC-2017-025, SPSC-I-246.

[53] M. B. Avanzini, Physics Procedia **61**, 524 (2015), DOI: j.phpro.2014.12.117, 13$^{\text{th}}$ International Conference on Topics in Astroparticle and Underground Physics (TAUP 2013).

[54] A. Cervera *et al.*, Nuclear Instruments and Methods in Physics Research Section A **624**, 601 (2010), DOI: 10.1016/j.nima.2010.09.049.

[55] S. Murphy, Physics Procedia **61**, 560 (2015), DOI: 10.1016/j.phpro.2014.12.053, 13th International Conference on Topics in Astroparticle and Underground Physics (TAUP 2013).

[56] A. Rubbia, Journal of Physics: Conference Series **171**, 012020 (2009), DOI: 10.1088/1742-6596/171/1/012020.

[57] A. Rubbia, Journal of Physics: Conference Series **375**, 042058 (2012), DOI: 10.1088/1742-6596/375/1/042058.

[58] A. Badertscher *et al.*, (2008), arXiv:0804.2111.

[59] Official ArDM project website, URL: http://darkmatter.ethz.ch, 2018, accessed: 2018-02-02.

[60] A. Marchionni *et al.*, Journal of Physics: Conference Series **308**, 012006 (2011), DOI: 10.1088/1742-6596/308/1/012006.

[61] T. Alexander *et al.*, Astroparticle Physics **49**, 44 (2013), DOI: 10.1016/j.astropartphys.2013.08.004.

[62] P. Agnes *et al.*, Physics Letters B **743**, 456 (2015), DOI: 10.1016/j.physletb.2015.03.012.

[63] S. Pandolfi, A 350-metre-tall tower to purify argon, URL: http://cds.cern.ch/record/2294969, 2017.

[64] C. E. Aalseth *et al.*, (2017), arXiv:1707.08145.

[65] R. Brunetti *et al.*, (2004), arXiv:astro-ph/0411491.

[66] L. Grandi, (2005), INSPIRE-705641, PhD thesis, Pavia University.

[67] A. Zani, Advances in High Energy Physics **2014**, 1 (2014), DOI: 10.1155/2014/205107.

[68] K. Mavrokoridis *et al.*, (2016), CERN Report No. CERN-SPSC-2016-008.

[69] D. B. Cline, Y. Seo, and F. Sergiampietri, (2003), arXiv:astro-ph/0301545.

[70] A. Ankowski *et al.*, Nuclear Instruments and Methods in Physics Research Section A **556**, 146 (2006), DOI: 10.1016/j.nima.2005.10.108.

[71] M. Antonello *et al.*, Journal of Instrumentation **12**, P04010 (2017), DOI: 10.1088/1748-0221/12/04/P04010.

[72] M. Antonello *et al.*, Journal of Instrumentation **10**, P12004 (2015), DOI: 10.1088/1748-0221/10/12/P12004.

[73] C. Vignoli, Physics Procedia **67**, 796 (2015), DOI: j.phpro.2015.06.13, Proceedings of the 25th International Cryogenic Engineering Conference and International Cryogenic Materials Conference 2014.

[74] J. Postel, STD6 RFC **768** (1980), DOI: 10.17487/rfc0768.

[75] P. Christensson, GPS Definiton, URL: https://techterms.com/definition/gps, 2006, accessed: 2018-02-04.

[76] M. Antonello *et al.*, Journal of Instrumentation **9**, P08003 (2014), DOI: 10.1088/1748-0221/9/08/P08003.

[77] B. Baibussinov *et al.*, Journal of Instrumentation **5**, P12006 (2010), DOI: 10.1088/1748-0221/5/12/P12006.

[78] Technical note: An Introduction to the Silicon Photomultiplier, URL: https://www.sensl.com, 2011, accessed: 2017-09-26.

[79] E. Gschwendtner, p. 4 (2006), CERN-AB-2007-005, revised version submitted on 2007-02-14 08:38:23.

[80] G. Giacomelli, Journal of Physics: Conference Series **116**, 012004 (2008), DOI: 10.1088/1742-6596/116/1/012004.

[81] G. Giacomelli, AIP Conference Proceedings 972:412-420, 2008 (2007), arXiv:0712.2126.

[82] Particle Data Group, C. Patrignani *et al.*, Chin. Phys. **C40**, 100001 (2016), DOI: 10.1088/1674-1137/40/10/100001.

[83] A. Ferrari *et al.*, (2007), CERN-AB-Note-038.

[84] A. Ferrari, A. Guglielmi, and P. Sala, Nuclear Physics B - Proceedings Supplements **168**, 169 (2007), DOI: 10.1016/j.nuclphysbps.2007.02.073, Proceedings of the Neutrino Oscillation Workshop.

[85] N. Nosengo, Nature **485**, 435 (2012), DOI: 10.1038/485435a.

[86] A. G. Cohen and S. L. Glashow, Physical Review Letter **107**, 181803 (2011), DOI: 10.1103/PhysRevLett.107.181803.

[87] M. Antonello *et al.*, Physics Letters B **711**, 270 (2012), DOI: 10.1016/j.physletb.2012.04.014.

[88] M. J. Longo, Physical Review D **36**, 3276 (1987), DOI: 10.1103/PhysRevD.36.3276.

[89] A. Habig, (2005), arXiv:astro-ph/0507051.

[90] K. Abe *et al.*, The Astrophysical Journal **652**, 198 (2006), DOI: 10.1086/508016.

[91] Y. Huo *et al.*, Phys. Rev. D **85**, 034022 (2012), DOI: 10.1103/PhysRevD.85.034022.

[92] F. W. Stecker and S. T. Scully, Phys. Rev. D **90**, 043012 (2014), DOI: 10.1103/PhysRevD.90.043012.

[93] M. Antonello *et al.*, Physics Letters B **713**, 17 (2012), DOI: 10.1016/j.physletb.2012.05.033.

[94] P. A. Sanchez *et al.*, Physics Letters B **716**, 401 (2012), DOI: 10.1016/j.physletb.2012.08.052.

[95] LVD Collaboration, N. Y. Agafonova *et al.*, Physical Review Letter **109**, 070801 (2012), DOI: 10.1103/PhysRevLett.109.070801.

[96] M. Antonello *et al.*, Journal of High Energy Physics **11**, 049 (2012), DOI: 10.1007/JHEP11(2012)049.

[97] P. Alvarez and J. Seranno, (2011), CERN BE-CO-HT Internal Note.

[98] ESAT company webpage, 2017, URL: www.esat.it, accessed: 2017-11-07.

[99] N. Ashby, Living Reviews in Relativity **6**, 1 (2003), DOI: 10.12942/lrr-2003-1.

[100] D. Dequal, PHD thesis, URL: http://paduaresearch.cab.unipd.it/5959/, 2013.

[101] B. Pontecorvo, Sov. Phys. Journal of Experimental and Theoretical Physics (JETP, Zh. Eksp. Teor. Fiz.) **53** (1967), URL: http://www.jetp.ac.ru/cgi-bin/dn/e_026_05_0984.pdf.

[102] S. Bilenky, Nuclear Physics B **908**, 2 (2016), DOI: 10.1016/j.nuclphysb.2016.01.025, Neutrino Oscillations: Celebrating the Nobel Prize in Physics 2015.

[103] O. Palamara, The Short-Baseline Neutrino Oscillation Program in the Fermilab Booster Neutrino Beam, Erice Workshop on Nuclear Physics, 2017, 2017, 39th Erice Workshop on Nuclear Physics, 2017.

[104] MiniBooNE Collaboration, A. A. Aguilar-Arevalo *et al.*, Physical Review Letter **110**, 161801 (2013), DOI: 10.1103/PhysRevLett.110.161801.

[105] G. Mention *et al.*, Physical Review D **83**, 073006 (2011), DOI: 10.1103/PhysRevD.83.073006.

[106] SAGE Collaboration, J. N. Abdurashitov *et al.*, Physical Review C **80**, 015807 (2009), DOI: 10.1103/PhysRevC.80.015807.

[107] F. Kaether *et al.*, Physics Letters B **685**, 47 (2010), DOI: 10.1016/j.physletb.2010.01.030.

[108] M. Antonello *et al.*, The European Physical Journal C **73**, 2345 (2013), DOI: 10.1140/epjc/s10052-013-2345-6.

[109] M. Antonello *et al.*, The European Physical Journal C **73**, 2599 (2013), DOI: 10.1140/epjc/s10052-013-2599-z.

[110] F. Capozzi *et al.*, Physical Review D **89**, 093018 (2014), DOI: 10.1103/PhysRevD.89.093018.

[111] F. Boffelli *et al.*, Final update of 2010-2012 CNGS data processing, Report ICARUS-TM 15-01 (unpublished), 2015.

[112] C. Farnese, AIP Conference Proceedings **1666**, 110020 (2015), DOI: 10.1063/1.4915574.

[113] MiniBooNE Collaboration, A. A. Aguilar-Arevalo *et al.*, Phys. Rev. Lett. **110**, 161801 (2013), DOI: 10.1103/PhysRevLett.110.161801.

[114] KARMEN Collaboration, B. Armbruster *et al.*, Physical Review D **65**, 112001 (2002), DOI: 10.1103/PhysRevD.65.112001.

[115] P. Astier *et al.*, Physics Letters B **570**, 19 (2003), DOI: 10.1016/j.physletb.2003.07.029.

[116] S. Avvakumov *et al.*, Physical Review Letter **89**, 011804 (2002), DOI: 10.1103/PhysRevLett.89.011804.

[117] OPERA Collaboration, N. Agafonova *et al.*, Journal of High Energy Physics **07**, 004 (2013), arXiv:1303.3953, [Addendum: JHEP07,085(2013)].

[118] T. Bohlen *et al.*, Nuclear Data Sheets **120**, 211 (2014), DOI: 10.1016/j.nds.2014.07.049.

[119] A. Ferrari *et al.*, *FLUKA: A multi-particle transport code (program version 2005)* CERN Yellow Reports: Monographs (CERN, Geneva, 2005), DOI: 10.5170/CERN-2005-010.

[120] F. Arneodo, (2001), arXiv:hep-ex/0103008.

[121] ICARUS Collaboration, M. Antonello *et al.*, (2015), CERN Report No. CERN-SPSC-2015-024; SPSC-SR-163.

[122] C. Rubbia *et al.*, Journal of Instrumentation **6**, P07011 (2011), DOI: 10.1088/1748-0221/6/07/P07011.

[123] A. Cesana *et al.*, Status report of the 2010-2011 CNGS data processing, Report ICARUS-TM 12-07 (unpublished), 2012.

[124] M. Antonello *et al.*, Advances in High Energy Physics **2013**, 1 (2013), DOI: 10.1155/2013/260820.

[125] S. Amoruso *et al.*, Nuclear Instruments and Methods in Physics Research Section A **523**, 275 (2004), DOI: 10.1016/j.nima.2003.11.423.

[126] ICARUS Collaboration, M. Antonello *et al.*, (2017), ICARUS Report No. CERN-SPSC-2017-021; SPSC-SR-214.

[127] Official LNGS Scientific Committee website, URL: https://www.lngs.infn.it/en/scientific-committee, 2018, accessed: 2018-02-01.

[128] T2K Collaboration, K. Abe *et al.*, Physical Review D **85**, 031103 (2012), DOI: 10.1103/PhysRevD.85.031103.

[129] B. Pontecorvo, Sov. Phys. JETP **6**, 429 (1957), URL: SPHJA,6,429, [Zh. Eksp. Teor. Fiz.33,549(1957)].

[130] Z. Maki, M. Nakagawa, and S. Sakata, Progress of Theoretical Physics **28**, 870 (1962), DOI: 10.1143/ptp.28.870.

[131] P. Huber, M. Lindner, and W. Winter, Computer Physics Communications **167**, 195 (2005), DOI: 10.1016/j.cpc.2005.01.003.

[132] P. Huber *et al.*, Computer Physics Communications **177**, 432 (2007), DOI: 10.1016/j.cpc.2007.05.004.

[133] D. Casper, Nuclear Physics B - Proceedings Supplements **112**, 161 (2002), DOI: 10.1016/S0920-5632(02)01756-5.

[134] S. Tufanli, (2017), EPS-HEP 2017.

[135] J. Kopp *et al.*, Journal of High Energy Physics **2013**, 50 (2013), DOI: 10.1007/JHEP05(2013)050.